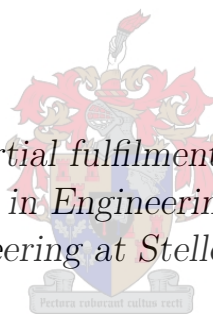


Latent Heat Thermal Energy Storage for Solar Water Heating using Flat Heat Pipes and Aluminium Fins as Heat Transfer Enhancers

by

Daniël Johannes Malan

*Thesis presented in partial fulfilment of the requirements for
the degree of Master in Engineering (Mechanical) in the
Faculty of Engineering at Stellenbosch University*



Supervisor: Mr. R.T. Dobson

December 2014

Declaration

By submitting this thesis electronically, I declare that the entirety of the work contained therein is my own, original work, that I am the sole author thereof (save to the extent explicitly otherwise stated), that reproduction and publication thereof by Stellenbosch University will not infringe any third party rights and that I have not previously in its entirety or in part submitted it for obtaining any qualification.

Date: November 21, 2014

Copyright © 2014 Stellenbosch University
All rights reserved.

Abstract

Solar energy is a time dependent, high-temperature radiant energy resource. The utility of a solar thermal energy system increases if the hot temperature source is available when it is needed most. This is realized by the thermal storage of the solar energy. Thermal storage gives greater versatility to a solar energy system by decoupling the heat source from the heat sink. A large quantity of energy may be stored during the melting process in a phase change material (PCM) within a small temperature range. This molten PCM can then deliver its absorbed heat at a constant temperature in a heating application. In this study a phase change storage system (PCS) is developed and proposed for a solar water heating application. This PCS system stores more heat per unit mass than would be possible with water across the same temperature range. The heat transfer rate in and out of many PCMs is slow because of the low thermal conductivity of the PCM. However, heat transfer enhancers (HTE), such as heat pipes and fins may be added to enhance heat absorption and heat removal rates. Heat pipes have the inherent capability to transfer heat at high rates across large distances, even where the temperature difference is small.

In this thesis a description is given of a PCS system consisting of paraffin wax as the PCM and which uses rectangular heat pipes in conjunction with aluminium fins to enhance heat transfer. The storage design is modular and each module has the characteristic that enhanced heat transfer in and out of the PCM is possible when the module is heated or cooled. It also has the capability to quickly absorb or alternatively to supply heat at a nearly constant temperature during the phase change of the module.

A rectangular module was designed and built. The module was then analysed under controlled heat absorption and heat removal cycles. The heat up experiment involved an electrical kettle as the hot temperature source. The heat sink was a mains water heat exchanger. The experimental results were compared to those of a transient numerical model, which calculates theoretically how the module will perform thermally under the given test conditions. The numerical model of the experimental set-up was validated when it was found that the numerical model results resemble the experimental results. The numerical model was then adapted to simulate a novel solar water heater (SWH) with an additional PCS container. The improvement over previous designs is that

the additional storage container can be heated to a higher temperature than the allowable geyser temperature. The system also heats up and cools down at a faster rate than would be possible without the HTEs. From the numerical simulation the size and performance of such a system is determined. This numerical analysis indicated that a phase change storage system in a SWH application will increase the hot water delivered by a given solar collector and geyser by increasing the storage capacity and by heating up the geyser overnight for early morning hot water use.

Keywords: Experimental comparative measurements, heat transfer enhancers, numerical modelling, phase change material, rectangular heat pipe, solar water heating.

Uittreksel

Son energie is 'n tyd afhanklike, hoë temperatuur radiasie energiebron. Die bruikbaarheid van 'n sontermiese energie sisteem verhoog indien die hoë temperatuur bron beskikbaar is wanneer dit die meeste benodig word. Dit kan verwesenlik word deur die sonenergie termies te stoor. Termiese storing bied groter veelsydigheid aan 'n sontermiese stelsel deur effektief die hittebron te ontkoppel van die hitte sink. 'n Groot hoeveelheid energie kan, gedurende die smeltingsproses in 'n faseveranderingsmateriaal binne 'n nou temperatuurband gestoor word. Hierdie gesmelte materiaal kan weer op sy beurt in die waterverhittingstoepassing, die geabsorbeerde hitte teen 'n konstante temperatuur oordra. In hierdie studie word 'n sonwaterverwarmer stelsel wat aangepas is deur 'n addisionele latente hittestoor daaraan te heg, voorgestel. Hierdie faseverandering hittestoor kan meer hitte stoor as wat water in dieselfde temperatuur band sou kon. Die hitteoordrag tempo na en van baie van die faseveranderingsmateriale (FVM) is egter as gevolg van die lae termiese geleidingskoëfisient, stadig. Hierdie eienskap kan gelukkig verbeter word deur hittepype en hitteoordrag verhogings materiaal soos vinne by te voeg. Hittepype het die inherente eienskap om hitte teen 'n hoë tempo oor groot afstande, oor te dra, selfs oor 'n klein temperatuurverskil.

In hierdie tesis word 'n ondersoek rakende 'n faseverandering storingsstelsel wat bestaan uit paraffien was as die FVM en reghoekige hittepype wat te same met aluminium finne gebruik word om die hitteoordragtempo te verhoog, beskryf. Die stoorontwerp is modulêr en elke module het die kenmerk van hoë hitteoordrag na en van die FVM. Die module het verder ook die eienskap om vining hitte te absorbeer of hitte af te gee. Dit gebeur teen 'n konstante temperatuur gedurende die faseverandering van die FVM.

Presies so 'n reghoekige module is ontwerp en gebou en onder beheerde hitte absorbering- en hitte verwyderingsiklusse analiseer. Tydens die verhittings eksperiment is 'n elektriese ketel van gebruik gemaak wat gedien het as die hoë temperatuur bron. Die hitte sink was 'n hiteruiler wat kraanwater van 'n konstante hoogte tenk ontvang het. Die resultate van die volledige toets is met die resultate van tydafhanklike numeriese model vergelyk. Hierdie numeriese model bereken teoreties wat die module se storing verrigting onder gegewe toets omstandighede sal wees. Die numeriese model se resultate het goed

vergelyk met die resultate van die eksperimente. Die numeriese model van die module is toe aangepas om 'n sonwaterverwarmer met addisionele stoortenk wat fase verandering materiaal gebruik, te simuleer. Hierdie ontwerp is anders as vorige ontwerpe in die sin dat hoër temperature as wat die warmwatertoestel kan hanteer, in die faseverandering storingstank, bereik kan word. Die sisteem kan ook as gevolg van die hitteoordrag verhoging materiaal, vinniger verhit of afkoel en teen 'n vinniger tempo. Die simulاسie van die sonwaterverwarmer met FVM word gebruik om die grootte en verrigting van die sisteem te bepaal. Hierdie numeriese model toon aan dat wanneer 'n addisionele faseverandering storingstelsel in 'n sonwaterverwarmer toepassing gebruik word, die warm water wat die verbruiker uit die sisteem kan verkry, kan verhoog. Die rede hiervoor is dat meer hitte gestoor kan word, wat beskikbaar gemaak word aan die warm water tank.

Sleutelwoorde: Eksperimentele vergelykende metings, hitte oordrag versnellers, numeriese modellering, faseveranderingsmateriaal, reghoekige hittepyp, sonwaterverwarming.

Acknowledgements

I thank my God and Saviour Jesus Christ. Through the loving power of your Holy Spirit I am blessed to know You, especially with regards to this thesis. I would also like to thank Annemarie de Kock for her loving support and encouragement. Also my parents and sisters for always looking out for my total well-being, and for their fervent prayers.

I thank my supervisor Mr. R.T. Dobson for giving me the freedom to explore the wonderful world of heat transfer and especially the field of solar thermal energy storage.

I thank the staff at the mechanical workshop of the Mechanical Engineering Faculty for their technical expertise, especially with regard to the welding and sealing of the flat aluminium heat pipes.

My sincere appreciation also goes to those at Cape Heat Exchangers who gave me the great opportunity to manufacture a scaled version of the integral collector and thermal storage model.

I thank the solar thermal energy research group (STERG) for the measuring equipment and for creating a platform to engage and pitch our ideas and explain our work in progress.

I thank Mr. Cobus Zietsman and Mr. Julian Stanfliet for your help in the laboratories.

I also thank the developers of all the open software programs that I was privileged to use. God willing I will continue to do so in future. The programs used are Code Blocks, used for developing the C++ numerical models, Gnuplot, used for plotting graphs, Inkscape for graphics development and L^AT_EX for typesetting the thesis.

Contents

	Page
Declaration	i
List of Figures	xi
List of Tables	xvi
Nomenclature	xx
1 Introduction	1
1.1 Sensible solar water heater background	1
1.2 Latent solar water heater background	2
1.3 The objectives of the thesis project	4
1.4 The design objectives of the PCS system	5
1.5 A background to previous phase change storage systems (PCS) . .	7
1.6 Concept development of the PCS system	9
1.6.1 Materials used in the design concept	11
1.6.2 Components used in the design concept	11
1.7 The motivation for developing and analysing PCS systems	12
1.8 Chapter divisions of the thesis	14
1.9 Conclusion of introductory chapter	14
2 Literature study	15
2.1 Introduction of literature study	15
2.2 Numerical analysis of PCS systems	15
2.3 Possible applications of the PCS systems	16
2.4 The use of a phase change material in a latent heat storage system	17
2.5 The use of heat transfer enhancers (HTEs) with phase change material embedded in between	21
2.5.1 The use of heat pipes as heat transfer enhancers	22

2.5.2	The use of fins as heat transfer enhancers	25
2.5.3	The use of form stable expanded graphite matrix as a heat transfer enhancer	27
2.5.4	The use of metal foam as heat transfer enhancer	27
2.6	Conclusion of literature study	28
3	The numerical thermal simulation model	29
3.1	Overview of the thermal simulation model	29
3.2	Test conditions that were applied on the numerical and experimental model	31
3.3	Discretization of the test module with HTE	33
3.4	Initial values and input conditions of the test module with HTE	34
3.5	The numerical modelling of the heat absorption heat pipes evaporator wall control volume	34
3.6	The numerical modelling of the heat pipe calculation	40
3.7	The numerical modelling of the main fin in the PCS system calculation	41
3.8	The numerical modelling of the inner fin in the PCS system calculation	42
3.9	The numerical modelling of the wax control volumes in the PCS system	44
3.10	The numerical modelling of the PCS-SWH system	47
3.11	Conclusion of numerical model	51
4	The experimental set-ups, testing and analysis of the designed thermal storage module	53
4.1	The modular set up rationale for using rectangular test section, paraffin wax, heat pipes and an aluminium fin matrix	53
4.2	Indoor test set-up of the heat pipe	54
4.3	Indoor testing of the wax only PCS module	55
4.4	Indoor testing of the PCS module with fins as HTE	59
4.5	Methodology of analysing the absorbed heat in the the storage section of the numerical and experimental modules	60
4.6	Observations of flow phenomena during the experiments conducted	61
4.7	Sensors and instrumentation	61
4.8	Health and safety	63

4.9 Conclusion of experimental set-ups	64
5 The numerical and experimental results	65
5.1 The results of the tests done with the experimental wax only PCS module	65
5.2 The results of the tests done with the experimental and numerical PCS module with HTE	69
5.3 The results of tests on the numerical PCS SWH system with HTE	79
5.4 Discussion of the results	82
6 Discussion and conclusions	86
6.1 The contribution of the heat pipes and wax experiments to the experimental analysis	87
6.2 The contribution of the PCS system comparison with and without fins to the experimental analysis	88
6.3 The contribution of the simulation of the PCS system with HTE fins to the numerical analysis	90
6.4 The benefit of comparing the numerical and experimental results to the numerical model validation	90
6.5 The potential of an additional latent heat storage tank in a solar water heating application	91
6.6 Main conclusions and contributions of the thesis	92
7 Recommendations for future work	94
Appendix A Calibration and error analysis of the thermocouples used in the experiments	96
Appendix B In depth experimental results	100
B.1 Analysis of the heat flow characteristics conducted for the kettle and the heat pipe	100
B.1.1 The heat pipe characteristic test	100
B.1.2 The kettle characteristic test	101
B.2 Analysis of the PCS module with HTE fins	103
B.2.1 The temperature variations in the PCS system	103
B.2.2 The power transferred through the heat pipes during heat absorption and heat removal modes	106
B.2.3 The total energy and power absorbed and extracted during a heat up and a cool down test	112
B.2.4 The total energy in each segment of the PCS system	114

Appendix C Solar angle calculation and heat transfer coefficients determination for the SWH system.	123
C.1 Calculation of the solar angles.	123
C.2 Calculation of the ambient air and the sky temperature.	127
References	130

List of Figures

	Page
1.1 a)The layout of a typical direct sensible SWH system as well as b)a SWH system with an additional PCS system.	3
1.2 The internal energy of water compared to paraffin wax with a melting temperature T_m of 59°C.	5
1.3 The cross section of an integral solar water heater developed by Mettawee and Assassa (2006), dimensions in mm.	8
1.4 The cross section of the cylindrical water tank with added polyethylene bottles filled with PCM. Dimensions in mm. (Canbazoglu <i>et al.</i> , 2005).	10
1.5 The concept design of the laboratory set-up latent heat thermal storage system.	13
2.1 The different kinds of thermal storage materials and their advantages and disadvantages.	19
2.2 The cross sections of the PCS systems of Liu <i>et al.</i> (2006a).	24
2.3 Schematic diagram of Robak <i>et al.</i> (2011a) experimental set-up.	25
2.4 Photographs of Robak <i>et al.</i> (2011a) experimental results during heat removal at a)t=60 min, b)t=120 min, c)t=180 min and d)t=240 min.	26
3.1 A simplified model of the PCS systems test module indicating the heat absorption HP1, the test section with a PCM and HTE control volume and the extracting heat pipe.	35
3.2 A thermal resistive diagram cross section of the PCS systems test module as viewed from the side.	36
3.3 a)The PCS module cross section, b)The simplified cross section used in the numerical simulation, c) The thermal resistance diagram cross section of the PCS module viewed from the top.	37

3.4	The general flow diagram of the main numerical simulation program.	38
3.5	The in depth flow diagram of the numerical simulation program. . .	39
3.6	The numerical analysis of a wax control volume during heating and melting and cooling and solidifying.	45
3.7	The control volumes of the PCM SWH used in the system simulation.	48
4.1	The test set-up for the indoor heat pipe characteristic tests.	55
4.2	The diagram of the test set-up of the indoor experiment depicting the thermocouple names.	56
4.3	The diagram of the test set-up of the indoor experiment depicting the important dimensions in mm.	57
4.4	The photograph of the test set-up of the indoor experiment. Dimensions in mm.	58
4.5	The solidification of the wax during the heat removal cycle.	62
4.6	The final state of the wax after a complete heat removal cycle.	63
5.1	The melt front development during a heat absorption cycle of the control PCS module.	66
5.2	The heat front development during a heat removal cycle of the control PCS module.	67
5.3	Temperature comparison between the PCS module with and without fins during a typical heat absorption cycle.	68
5.4	Temperature comparison between the PCS module with and without fins during a typical heat removal cycle.	68
5.5	Power and energy comparison between the PCS module with and without fins during a typical heat removal cycle.	70
5.6	Temperature response during a heat absorption cycle of the experimental and numerical module.	72
5.7	Temperature response during the heat removal of the experimental and numerical module.	72
5.8	The numerically determined temperature variations and the melt fraction of the PCS module as viewed from the top during heat absorption only from the heat absorption side.	74
5.9	The numerically determined temperature variations and the melt fraction of the PCS module as viewed from the top during cool down only from the heat removal side.	75

5.10	Heat transfer rates during a heat absorption cycle of the experimental and numerical module.	77
5.11	The heat transfer rates during heat removal of the experimental and numerical module.	77
5.12	The energy absorbed during heat absorption of the experimental and numerical module.	78
5.13	The energy extracted during heat removal of the experimental and numerical module.	79
5.14	The temperatures that the solar collector, PCS system and geyser reach during two typical sunny days during the summer solstice. . .	80
5.15	The total energy incident on the solar collector, as well as the total energy absorbed by the solar collector and extracted from the PCS system to the solar geyser as well as the total energy used by the consumer.	81
5.16	The absorbed energy in the PCS system and specifically the wax as well as the energy in the geyser during two consecutive days of operation.	81
5.17	The finned PCS system cross section as seen from the top which was developed by Laing <i>et al.</i> (2013).	85
A.1	The calibration test set-up of 9 thermocouple wires with a resistance thermometer.	97
A.2	The calibration of the thermocouples in the range of 0 °C to 150 °C.	98
A.3	The error of the thermocouples when compared to the resistance thermometer in the range of 0 °C to 100 °C.	99
B.1	a)The characteristic of heat transfer rates of the heat pipe for various $T_h - T_{cold(avg)}$ temperatures, and b)the least squares regression fits through the initial mode of heat transfer rates.	102
B.2	The initial mode of the characteristic heat pipe heat transferr performance with a linear curve fit.	103
B.3	The heat transfer coefficient of the evaporator side of the heat pipe during characteristic test.	104
B.4	The loss to the environment from the kettle averaged over 400 seconds and a linear regression fit	105

B.5	The temperatures measured at the top of the PCS system, the middle of the PCS system and the bottom of the PCS system and the heat pipes during the heat up test	107
B.6	The temperatures measured at the top of the PCS system, the middle of the PCS system and the bottom of the PCS system and the heat pipes during the cool down test	108
B.7	The temperatures measured at the left, the middle and the right side of the PCS system during the heat up test.	109
B.8	The temperatures measured at the left, the middle and the right side of the PCS system during the cool down test.	110
B.9	The power transferred through the heat absorption HP1 during the heat absorption cycle.	111
B.10	The power transferred through the heat removal HP2 during heat removal.	111
B.11	The total energy in the kettle and the total energy flows into and out of the kettle measured and calculated	112
B.12	The power absorbed in the wax during heat up according to measurements	113
B.13	The power transferred into the water of the heat exchanger from the heat removal HP2 and the total energy absorbed in the water and removed from the PCS module.	115
B.14	The total energy in each segment of wax during heat up indicating instantaneous melting in the measuring point	116
B.15	The total energy in each segment of wax during cool down indicating instantaneous solidification in the measuring point	116
B.16	The total energy loss to the environment calculated from the energy PCS system sides	117
B.17	The temperature of the wax during a heat up test and the instantaneous rate of temperature change as well as the average rate during the test.	118
B.18	The averaged rates of temperature change for the middle horizontal level of thermocouples during heat absorption mode.	119
B.19	The averaged rates of temperature change for the 9 sections during heat absorption mode.	120

B.20	The averaged rates of temperature change for the middle horizontal level of thermocouples during heat removal mode.	120
B.21	The heat transfer coefficient of the heat absorption HP1 evaporator section.	121
B.22	The heat transfer coefficient of the heat removal HP2 evaporator section.	121
B.23	The heat transfer coefficient of the heat removal HP2 condensor section.	122
C.1	The solar angles for two consecutive days that relates to the solar irradiance intensity determination.	127
C.2	The solar irradiance components for two consecutive days.	128

List of Tables

	Page
1.1 Comparison of various heat storage media; $\Delta T = 15^\circ\text{C}$ (Hasnain, 1998)	4
C.1 The input conditions for the PCS SWH system analysis.	124

Nomenclature

a	Clear sky coefficient
amb	Ambient
B	Date factor, °
b	Breadth, m
c_p	Specific heat at constant pressure, J/kg K
E	Energy, J
\dot{G}	Incident solar irradiance, W/m ²
Gr	Grashof number
h	Latent heat of fusion, J/kg, heat transfer coefficient, W/m ² K
I	Irradiance intensity, W/m ²
k	Thermal conductivity, W/m K
\dot{m}	Mass flow rate, kg/s
$nett$	Netto
Nu	Nusselt number
P	Pressure, Pa
Q	Energy, J
\dot{Q}	Power, W
R	Resistance, °C/W
Ra	Raleigh number
Re	Reynolds number
T	Temperature, °C

t	Thickness, m
V	Volume, m ³
X	Fraction factor
x	The width of the PCS system, m
y	the depth of the PCS system, m
z	The height of the PCS system, m

Greek Symbols

α	Altitude angle, ° thermal diffusivity (m ² /s)
β	Thermal expansion coefficient, K ⁻¹
δ	Declination angle, °
γ	Azimuth angle, °
ι	Incidence angle, °
λ	Longitude, °
ν	Kinematic viscosity, m ² /s
ω	Hour angle, °
ρ	Density, kg/m ³
σ	latitude angle, °
θ_z	Zenith angle, °

Superscripts

t	Time, s
Δt	The change in time, s

Subscripts

Al	Aluminium
avg	Average
c	Condenser, corrected, cold
$column$	Number of PCM compartments
cv	Convection

<i>d</i>	Diffuse
<i>E</i>	Experimental module
<i>e</i>	Evaporator, effective
<i>f</i>	Fin
<i>h</i>	Hot
<i>hp</i>	Heat pipe
<i>i</i>	Inside, inner, inlet
<i>in</i>	In
<i>j</i>	Counter
<i>k</i>	Counter
<i>l</i>	Liquid, left
<i>M</i>	Mass, kg
<i>m</i>	Main, melt, middle
<i>mix</i>	Mixture
<i>N</i>	Numerical module
<i>n</i>	Normal
<i>o</i>	Outside
<i>out</i>	Out
<i>r</i>	Right
<i>rel</i>	Relative
<i>S</i>	PCS module
<i>s</i>	Solid
<i>sc</i>	Solar collector
<i>sl</i>	Fusion
<i>surr</i>	Surroundings
<i>T</i>	Total
<i>V</i>	Volume, m ³

v Vapour

w Wall

wax Wax

Abbreviations

EoT Equation of time

GMT Greenwich Mean Time

HP Heat Pipe

HTE Heat Transfer Enhancers

LST Local solar time

LSTM Local solar time mean

PCM Phase Change Material

PCS Phase Change Storage

SASOL South African Synthetic Oil Limited

SWH Solar Water Heater

TC Time correction

Chapter 1

Introduction

In the light of increasing electricity prices in South Africa, solar water heaters (SWH) has attracted renewed attention from consumers and industry alike. The reason being that electric water heating accounts for between 30%-50% of the domestic energy sector (Eskom, s.a.). Solar water heaters are becoming a common sight in South Africa, since Eskom, the electricity supplier in South Africa, gave a rebate on 38 000 high pressure and 84 000 low pressure systems between 2008 and 2011, resulting in energy savings of approximately 60 GWh/annum and in 54.9 kt/annum savings of CO₂ emissions (Eskom, s.a.).

1.1 Sensible solar water heater background

Solar water heaters are composed of a solar collector to absorb the solar energy and convert it to heat, and a hot water container, also called a geyser, to store the heat in a sensible form. Thus the more heat collected, the hotter the water in the geyser will become. Some pressurised solar geysers have the capability of storing water at high temperatures, which increases the amount of energy that can be stored in the geyser. These geysers are connected to a tempering valve that prohibits flashing to steam or delivering too hot water at the outlet. Low pressure geysers do not have this advantage since the water boils at a lower temperature and therefore less energy can be stored in such geysers. It is inherently safer to keep the water in the geyser below a temperature of 76 °C to prohibit the risk of scalding the end user at the outlet.

The limiting parameters of a sensible SWH are the size and the operating pressure of the geyser, and the type and size of the solar collector, which limit how much energy can be absorbed and stored in the geyser. The outlet geyser water only needs to be heated to a temperature of 40 °C when used by the end user. It is required to store the absorbed solar thermal energy because of the relatively slow solar heating that occurs during the course of the day, compared to the quick rate of hot water use, which occur mostly at night or early morning.

1.2 Latent solar water heater background

Another possible method to store some of the collected heat is to store it in latent form. This means that a phase change material (PCM), for example, paraffin wax, is used as the intermediate thermal storage material. The advantages of using such an intermediate storage material are that more energy may be stored per unit mass of storage material and it can be stored at a lower temperature than the same mass of water would require. The sensible SWH system and the proposed SWH system with additional phase change storage (PCS) is indicated in Figure 1.1. The PCS system is placed above the solar collector to ensure that heat can only be transferred from the collector to the PCS system. A pump is used to transfer heat from the PCS system to the geyser when required. In this set-up the PCS may be heated to very high temperatures (synthetic wax can be heated up to 250 °C without thermal degradation), thereby storing more energy in the PCM that may be transferred to the geyser at a later time. The internal energy comparison between water and paraffin wax is shown graphically in Figure 1.2. The wax can store four times more energy (400 kJ/kg in the wax versus 100 kJ/kg in the water) than water in a typical SWH application. This is deduced from the assumption that the water is set by the thermostat in the geyser to a maximum temperature of 65 °C and the wax in an unpressurised container is heated to 140 °C. Of course the water can also be stored at 140 °C at which temperature the material's internal energy is the same, taking 45 °C as reference, but then the water would be required to be stored in a pressure vessel and there is the added risk that the water can flash to steam at the outlet. The advantage is that the wax can be stored in an unpressurised container at a much hotter temperature than would be the case with the same amount of water. Another advantage is that the PCM stores most of its energy at a constant temperature, which will result in a constant heat removal rate during the heat removal cycle. This is a very sought after property in thermal energy storage systems. Therefore, there is inherent potential in using phase change materials in solar thermal heating applications. They are capable of storing additional energy at the required intermediate storage temperature in solar heating systems. This additional energy should however be stored and released at a sufficient rate. In the SWH application the final test of how well this system works must in some way be related to how much hot water (above 35 °C) is delivered to the end user compared to the cost of the system. Then this can be compared with the case of present sensible systems.

The PCS system should be composed of an inherently safe phase change container, which is in some way connected directly or indirectly to the solar collector and the geyser. This system must be able to exchange heat at a sufficient rate to heat up the hot water tank quickly enough. This must be done shortly after hot water has been extracted from the geyser by the end

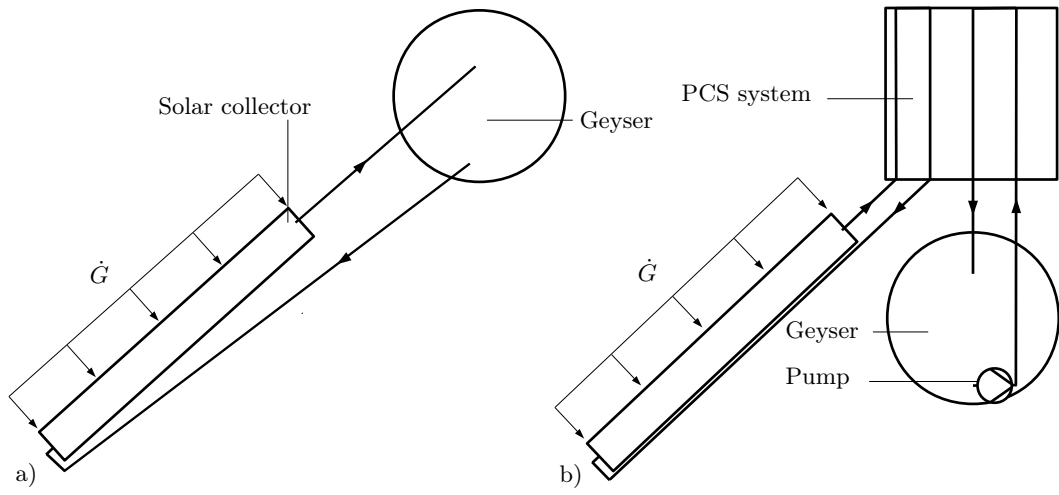


Figure 1.1. a) The layout of a typical direct sensible SWH system as well as b) a SWH system with an additional PCS system.

user. During a shower, for example, cold water flows into the geyser and the backup electric power supply is then normally switched on to heat this cold mains water, especially if the hot water is used in the early morning or late in the evening, which is usually the case. But if there is an additional latent heat store, this can be utilised to heat up the geyser. This means less electric energy will be used because the backup electric element needs to be switched on for a shorter period of time. This system holds the potential to decrease the electricity used during peak electricity use periods, by using the PCS system to heat up the water during peak periods, while increasing the hot water that can be delivered by the solar thermal system.

The review conducted by Hasnain (1998) and summarised in Table 1.1 compared materials that either store heat in a sensible or in a latent form on a volume and mass basis. He found that it is advantageous to use a PCM as a thermal heat storage material. The good physical properties of the organic PCMs make them preferable to inorganic PCMs. The reasons include their latent heat of fusion being very high and close to that of inorganic PCMs. Also only 25% more mass will be required to obtain the same amount of storage. Furthermore, no extra precautions, such as adding nucleating agents, need to be taken and congruent melting can be achieved for many cycles without thermal degradation. Organic PCMs are also non-corrosive to metals. The organic PCM is therefore very suitable for thermal storage at low temperatures.

Research has already been conducted, which is further described in Section 1.5, on various systems that incorporate a PCM as latent heat thermal storage. The characteristics of the heat transfer systems can be controlled to a certain extent by designing them to have sufficient heat exchanger area exposed to the

PCM and by choosing a suitable phase change material. A suitable PCM is chosen by considering different PCMs melting temperature T_m , specific heat coefficient c_p , latent heat of fusion h_{sl} , thermal conductivity k and density change between phases ρ_s and ρ_l .

In the design of a PCS system the components considered are the PCM described in Section 2.4 and the heat transfer enhancers (HTE), described in Section 2.5. The main parameters to consider in the material selection and geometry of the system are a phase change material with a reasonable melting point (high enough to sufficiently heat the cold incoming water) and to choose a geometry comprising of PCM and HTEs that will ensure that the heat is absorbed at a sufficient rate and that it can be extracted at a sufficient rate in order to be useful in a solar water heating application. Numerical analysis will be used in modelling the set-up. The numerical model will calculate the rate of heat transfer into and from a latent heat thermal storage unit. The model will take into account the intricate fin geometry, heat pipes and PCM that change phase during heat absorption and heat removal cycles. An analytical approach would be too limited to capture the physical phenomena that occur during the transient heat transfer processes accurately enough.

To achieve the main objective of designing a viable PCS system, the system needs to be analysed numerically in order make it possible to grasp the inner workings of the system during operation. Such a theoretical model is set up and described in Chapter 3 which uses the components chosen in the concept design described in Section 1.6.

1.3 The objectives of the thesis project

The objectives of the thesis are set out as follows:

Table 1.1. Comparison of various heat storage media; $\Delta T = 15^\circ\text{C}$ (Hasnain, 1998)

Property	Heat Storage Material			
	Sensible Heat Storage		PCS	
	Rock	Water	Organic	Inorganic
Latent heat of fusion (kJ/kg)	-	-	190	230
Specific heat (kJ/kg K)	1.0	4.2	2	2
Density (kg/m ³)	2240	1000	800	1600
Mass for storing 300 kWh (kg)	67000	16000	5300	4350
Relative mass	15	4	1.25	1
Volume for storing 300 kWh (m ³)	30	16	6.6	2.7
Relative volume	11	6	2.5	1

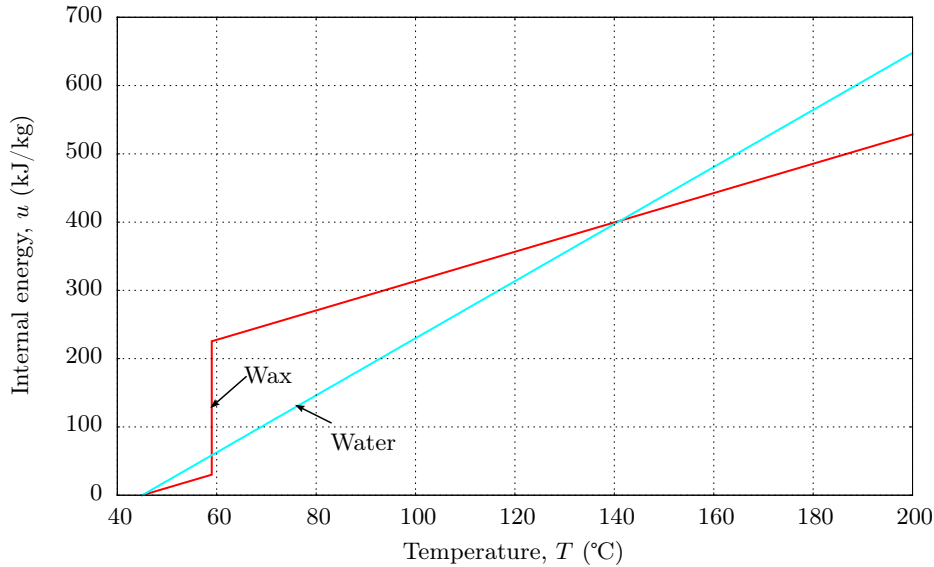


Figure 1.2. The internal energy of water compared to paraffin wax with a melting temperature T_m of 59°C .

1. To describe the work already undertaken in the field of solar-powered latent heat storage systems. See Section 1.5 and Chapter 2;
2. Using the existing designs as a point of departure, a novel design will be suggested in Section 1.6;
3. To describe the development and manufacturing of a PCS module and how it was analysed numerically. This is done in Chapters 3 and 4 to convey the design of the modular PCS system and the analysis undertaken to quantify its performance;
4. To analyse the results obtained from the experimental and numerical analysis and to compare the experimental results to the numerical results. These results will be described fully in Chapter 5;
5. To conduct a numerical system analysis of a solar collector, solar geyser and additional PCS system (described in Section 3.10) to quantify how well such a system will work to make a solar collector system deliver more hot water while using less electric energy. The results of this numerical system analysis is given in Section 5.3.

1.4 The design objectives of the PCS system

The design objectives are to design a modular thermal storage unit and calculate its thermal response numerically. The heat transfer to and from the PCS module must be enhanced to such a degree that the application, where many

modules are incorporated into a PCS system, can be extended to either solar water heating, or to other applications at higher operating temperatures and thereby using different fin materials and higher melting PCM where thermal storage and enhanced heat transfer is required for successful operation.

The main objective is to develop a solar water heating system that incorporates additional PCS material to improve the hot water output from a given solar geyser and collector system. The designed system must be able to extract heat at a sufficient rate, because the natural tendency in these systems is for the heat transfer rate to decrease as a solid layer of PCM develops on the piping and fins during the heat removal phase, as noted from the experimental analysis conducted by Mettawee and Assassa (2006). Their integral PCS SWH is further described in Section 1.5. The designed system must also agree with the theoretical simulation model to the extent that the main heat transfer mechanisms agree. In the case of the melting or otherwise solidification of the phase change material, the natural convection currents must be suppressed sufficiently so that the robust conduction model may be utilised for the transient analysis of the system. To achieve this main objective the following sub-objectives have been set:

1. Set up experimental PCS modules and test their performance for certain input conditions and load cases.
2. Set up a simulation model that calculates the thermal performance under similar conditions to those experienced during the experimental test set-ups.
3. Use both the experimental and numerical results to compare and verify that the numerical simulation is calculating reasonable results.
4. Use the numerical simulation model and adapt it to describe a solar thermal system that heats water to above 40 °C. Calculate how much hot water will be made available to the consumer by the PCS SWH system will be when installed in Stellenbosch, and the solar collector is positioned to face North, tilted at 45 ° with respect to the horizontal and the system experiences typical environmental input conditions, such as solar irradiation, and the heated system experiences convection and radiation losses to the environment.

From an experimental measurement perspective the test set-up's measuring points must fully capture the transient test cases. These cases include the heating up and melting of the PCM during the heat absorption phase, and the cooling down and solidification during the heat removal phase of the PCM. Finally, from a simulation and future design perspective the numerical

simulation model of the test module must characterise the heat transfer to and from the PCS module. The optimum parameters of the PCS section will be determined from a sensitivity analysis point of view. A scaled-up version composed of sufficient PCS modules of the correct size will then be analysed in terms of total heat capacity and heat transfer rate to and from the PCS system.

When the numerical simulation has been compared and sub-objective 3 (to verify the numerical model) has been reached, it will be adapted to calculate the performance of a PCS system in a typical solar water heating application and the system will be sized for a given load case and location. Different options exist, such as collector types, fin geometry, collector size, PCS size and geyser size, which make the PCS SWH truly adaptable, capable of being tailor-designed for a given residential use pattern in a specific location.

1.5 A background to previous phase change storage systems (PCS)

Previous solar water heater designs included integral systems, for example, the system of Mettawee and Assassa (2006) depicted in Figure 1.3, where the PCS is inside the solar collector. A single water pipe is placed in the solar collector, before the wax is melted into the solar collector. With only wax and no HTEs, the time to melt all the wax on a sunny summer day was longer than 7 hours. The heat transferred into the water passing through the one metre long pipe started at 350 W when all the wax was still liquid and after 3 hours it had dropped to merely 50 W in a more or less linear fashion. This is a low rate of heat removal and only a small part of the wax solidified in the three hours of heat removal. In a test with aluminium powder embedded in the PCM, the melting period was decreased to 70% of that of the control test case (5 hours with HTE to complete melting, compared to 7 hours without HTE with an average of 750 W/m² solar irradiation during the heat absorption period). The heat removal rate for the same flow rate started at 425 W and after a half hour it dropped to 250 W. Thereafter it decreased more or less linearly to 125 W after 4 hours. The total energy extracted was 27% more than with the wax only test case for four hours of hot water draw off. This is an early practical example showing that heat transfer enhancers can greatly improve the heat transfer rate during heat absorption and heat removal of a PCS system. In a practical integral solar water heater it is suggested that more pipes be passed through the wax container to extract the available heat from the integral collector at a faster rate.

In a review by Sharma *et al.* (2009) a box design for evening and morning hot water is described. The water is contained inside the box and the double walled container contains the paraffin wax. The melting point of the phase

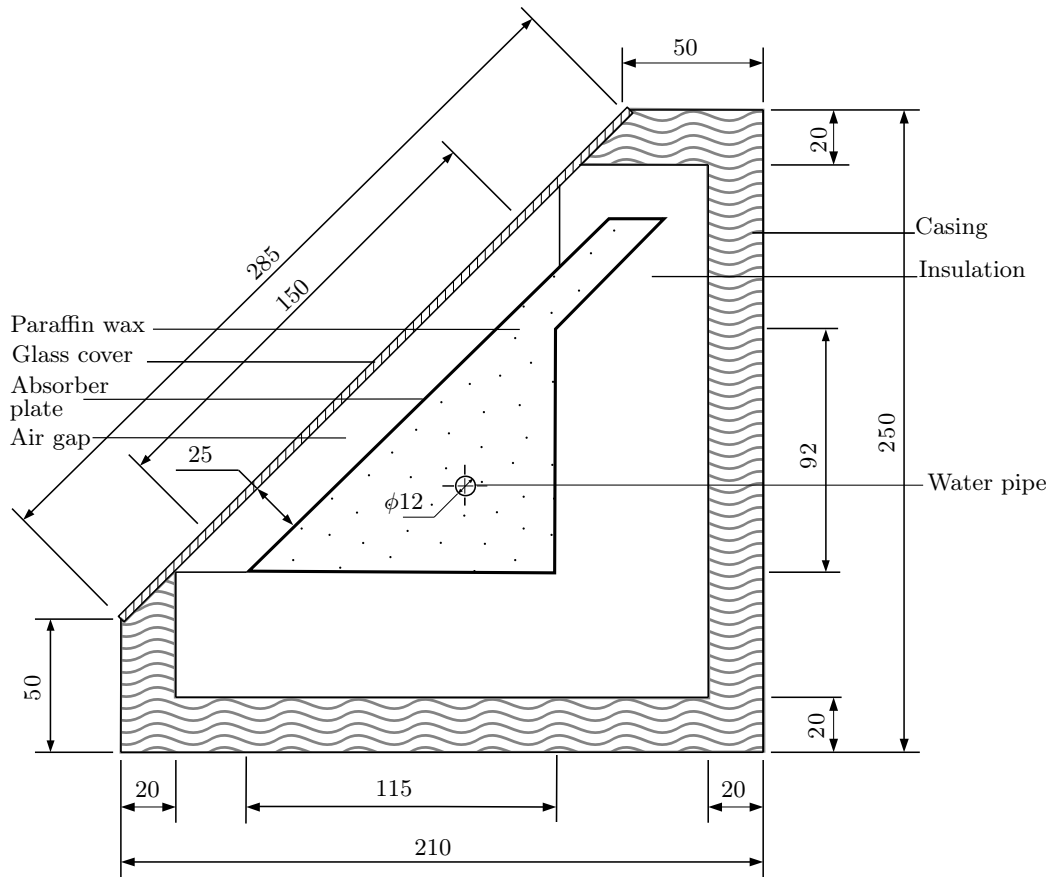


Figure 1.3. The cross section of an integral solar water heater developed by Mettawee and Assassa (2006), dimensions in mm.

change material is $T_m = 54^\circ\text{C}$. It is noted by the author that the system is effective in getting the water to the specified hot temperature after transferring heat to the water throughout the night. In the work conducted by Trp (2005) another design was analysed theoretically, this time an indirect system where the PCS is separate from the collector. A shell and tube PCS tank is described in which the water pipes pass through a cylindrical PCM tank. Trp (2005) used in her analysis an implicit enthalpy tracking method, where each control volume's internal energy is calculated at each time step and used to keep track of the heat transfer process. The author analysed and documented the way in which the unit melts and solidifies: The melt front is not uniform in the radial direction, but the hotter molten fluid collects at the top, while solid pieces drop to the bottom during melting. In the paper it is described how the PCM starts heating up, first in a conduction only mode, and as the molten wax layer thickens, it changes to a convection dominant heat transfer. During the heat removal phase the heat transfer starts off initially as convection dominant, but very soon the solid layer of wax that forms on the cold pipes forces the heat transfer mode to become conduction dominant.

This design of a shell and tube heat exchanger system found practical application in the solar water heater designs of Cabeza *et al.* (2006) and those of Canbazoglu *et al.* (2005). Cabeza *et al.* (2006) put PCM bottles inside a vertical cylindrical hot water container and found that such a system performs better in actual conditions than one without the PCM containers. This will result in requiring a smaller hot water tank for the same overall hot water delivered by the system, or a higher hot water potential for the same size tank. In the design of Canbazoglu *et al.* (2005) many PCM filled bottles were used in the adapted hot water tank, as depicted in Figure 1.4. The hot water tank, with PCM bottles placed inside, delivered 2.59 to 3.45 times more hot water during outdoor conditions and normal draw off conditions than a tank with only water. The main mode of operation in the design of Mettawee and Assassa (2006), shown in Figure 1.3, requires cold water to be circulated through the pipes that are embedded in the PCM for a few hours. In the other designs the cold water that enters the water tank containing PCM bottles, heats up overnight by heat transfer from the PCM bottles to the water. The cold inlet water is slowly heated throughout the night by the slightly hotter PCM that transfers its latent heat at a near constant temperature to the initially cold water in the tank.

The shortcomings of PCS systems for low temperature applications according to Sharma *et al.* (2009) are high cost, bulky systems, and high environmental losses during nighttime such as was the case for all integral systems where the PCM was in the collector. In the PCS concept design further described in Section 1.6, the author recommends that the heat absorbed in the collector be transferred away from the collector to a PCS system which is insulated so that the thermal heat may be stored for longer periods of time until it is required by the end user.

1.6 Concept development of the PCS system

The main objective of the design concept is to deliver hot water when it is required by the end user and reduce the electric backup energy use. This is achieved by utilising solar energy incident on the end user's roof. The sub objectives are to store the heat in a storage material, such as water or phase change material, because the solar irradiation is intermittent, and a lot of hot water may be required in a very short time. It therefore makes sense to store some of the absorbed heat in the geyser until it is required. It was decided to use a PCM as intermediate storage material, because of its superior energy storage capability at a lower temperature compared to water in the operating range of 45 °C to 90 °C. The PCS system can be configured to heat the cold water in the geyser after the hot water has been utilised during the evening. The choice of which PCM to use depends on what temperatures it must be able

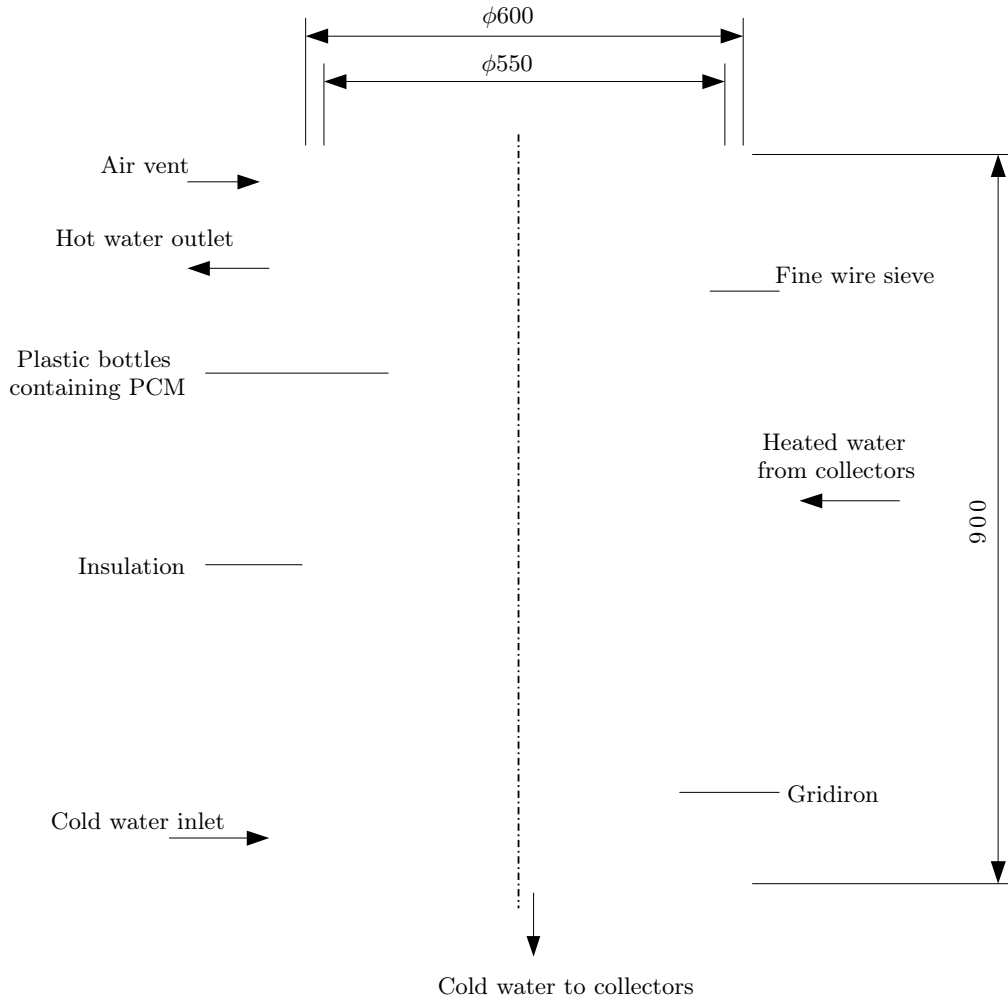


Figure 1.4. The cross section of the cylindrical water tank with added polyethelene bottles filled with PCM. Dimensions in mm. (Canbazoglu *et al.*, 2005).

to withstand, and the temperature to which the hot water must be heated. For a glazed flat plate collector with black painted fins the maximum temperature will not be higher than $140\text{ }^{\circ}\text{C}$ and the water must be heated by the wax to at least $45\text{ }^{\circ}\text{C}$. Paraffin wax melting at $59\text{ }^{\circ}\text{C}$ was selected for the laboratory tests, since cold water was used to cool it, and a kettle able to achieve $95\text{ }^{\circ}\text{C}$ to melt it. For an evacuated tube solar collector a synthetic wax with a higher melting point of at least $80\text{ }^{\circ}\text{C}$ or even at $100\text{ }^{\circ}\text{C}$ and having a very high flash point must be used. The heat must be transferred into the PCS system from the solar collector, and this is achieved by the heat absorption heat pipes. From the PCS system the heat needs to be transferred to the water that is circulated from the geyser, and this is achieved by pumping the water through the heat exchanger.

The transfer of heat through the system is another aspect that needs to be

considered. Following the design philosophy of passive design that incorporates naturally occurring phenomena to transport the heat, heat pipes are selected by the author in the laboratory test module. Natural circulation thermosyphons or pumped systems can also be used, but the author decided to analyse a heat pipe system. The decision regarding what heat exchanger material, heat pipes and PCS geometry to use is another design consideration. In the lab test module rectangular multichannel aluminium heat pipes were selected to transfer heat to and from the PCM because of their excellent heat transfer capabilities (see Section B.1), and the good heat transfer distribution throughout the entire heat transfer surface. Aluminium fins were chosen to create heat paths into the phase change material. The numerical simulation model is based on this geometry and is described in Section 3.

Using the previous designs described in Section 1.5 and mentioned in Chapter 2 as a point of departure, a novel design is developed. The designed solar water heater system uses components with good heat transfer rates by adding a fins as HTE to the PCM and passive operation by using heat pipes to transfer the heat away from the collector and into a PCS system. By adapting the previous designs to meet such criteria, the concept developed is indicated in Figure 1.5. To arrive at the correct sizing and operation for a given solar irradiation site and end user hot water requirements, the components need to be modelled correctly and accurately enough. It is necessary to calculate the thermal response of the concept so that the hot water that can be obtained from the system, can be determined. Also the final geometry and amount of HTE required to achieve a fully working prototype, needs to be determined.

1.6.1 Materials used in the design concept

To model the system the thermal properties of the components must be known. In this design paraffin wax, acquired from SASOL, was used. Its properties were as follows. $T_m = 59^\circ\text{C}$, $h_{sl} = 200 \text{ kJ/kg}$, $c_{p(wax)} = 2.15 \text{ kJ/kg K}$, $\rho_{wax(l)} = 790 \text{ kg/m}^3$, $\rho_{wax(s)} = 910 \text{ kg/m}^3$, $k_{wax} = 0.21 \text{ W/m K}$. The thermal conductivity of the heat transfer enhancer must be high enough to greatly enhance the rate of heat transfer into and from the wax material when it is embedded in it. The properties of the aluminium fins are $c_{p(al)} = 0.903 \text{ kJ/kg K}$, $\rho_{Al} = 2700 \text{ kg/m}^3$, $k_{Al} = 237 \text{ W/m K}$. It is a lightweight material and since the fins are bought per mass this greatly improves the total volume that can be bought for the same price.

1.6.2 Components used in the design concept

In the solar water heater design heat pipes are used to transfer the heat into and out of the PCS system that contains the fins and the paraffin wax. The advantages are that during nighttime small losses to the environment result

because the heat pipe acts as a thermal diode. This thermal diode only transfers heat from the lower to the higher end of the heat pipe through boiling of the liquid at the bottom and condensate forming and flowing down to the bottom, thereby transferring heat at a high rate from the lower hot section to the higher cooler section. But when the collector cools down during nighttime the less dense hot vapour stays at the top, and the cool liquid stays at the bottom. During the nighttime the hot PCS does not transfer heat to the solar collector, except through conduction along the thin-walled heat pipe. When the sun is incident on the solar collector during the daytime, high heat transfer coefficients result because of the boiling in the evaporator and the condensation in the condenser. In this way the latent heat of vapourisation acts as the heat carrier across a small temperature difference.

1.7 The motivation for developing and analysing PCS systems

The intention of the designed concept is to incorporate useful material properties, such as those of good thermal conductors, and incorporating passive heat transfer components, like heat pipes, that operate with boiling and condensation, and a PCM, that stores heat when melting and delivers heat when solidifying. In a passive solar heated thermal storing system design, all the main heat transfer phenomena need to be taken into account and to combine the components into a useful product. In this case the product needs to absorb, transport and store heat until it is required and then heat must be extracted to heat up the geyser water.

Although there is an obvious advantage in the use of PCM for thermal storage purposes, per se, from a thermal performance point of view it is also important that the PCS system must be able to absorb or release heat quickly enough. It is thus expedient to develop a transient numerical system simulation model in order to evaluate the thermal response of the system for both heat addition and heat removal operating conditions. The effect that the components will have on the heat transfer performance may be analysed with such a numerical model. The design of the model will take into account the geometry of the system, the inherent component capabilities, the material specifications and the heat transfer mechanisms involved in the system. This simulation may then be adapted to test different set-up configurations and for different solar heat PCS applications.

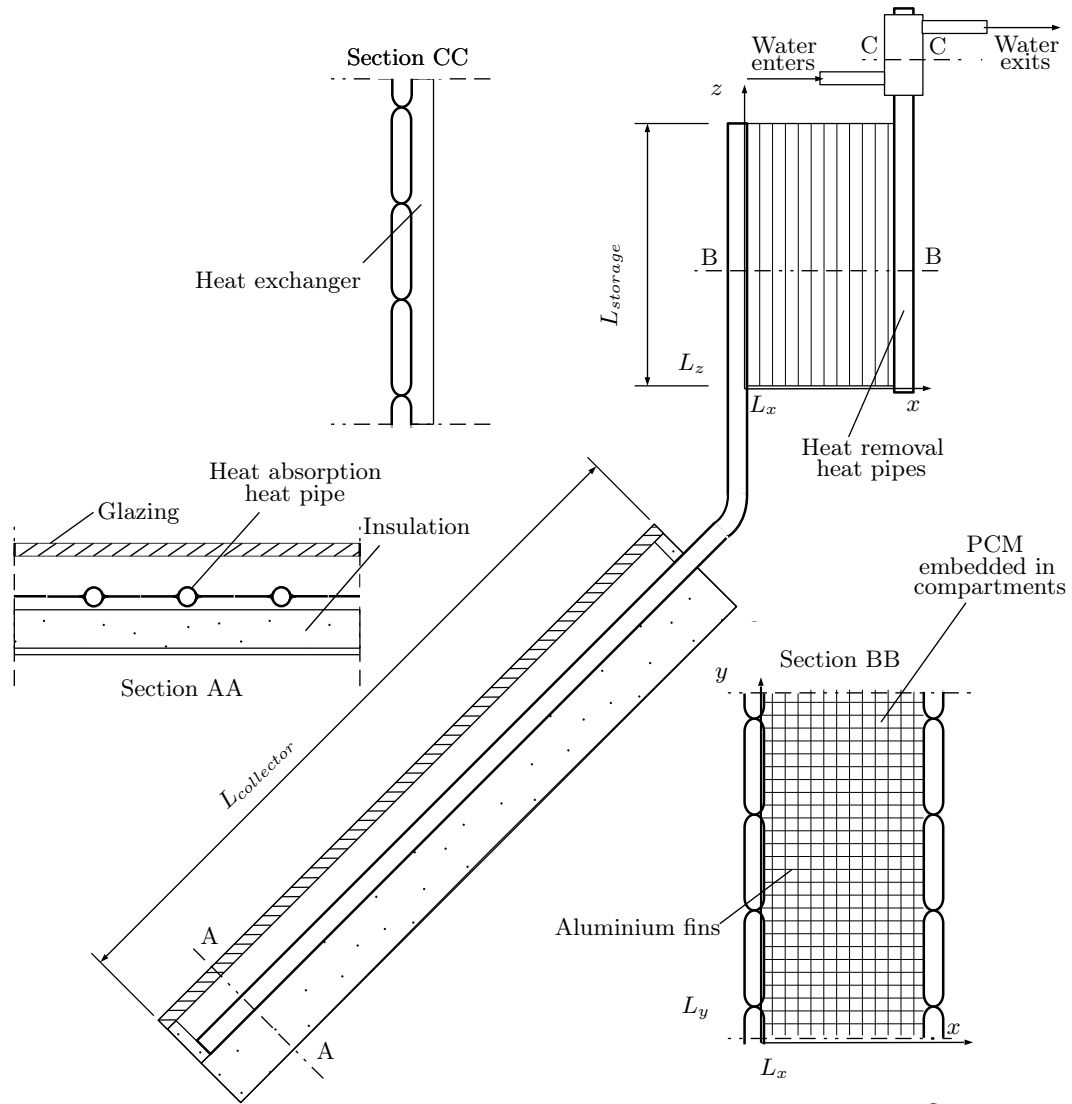


Figure 1.5. The concept design of the laboratory set-up latent heat thermal storage system.

1.8 Chapter divisions of the thesis

In Chapter 2 the literature study will be further discussed and alternative options for analysis of the PCS system, possible applications and different HTEs that may be used to improve the thermal properties of the PCS system will be examined. Then in Chapter 3 the numerical model used to analyse the experimental setup will be described. Particular attention will be given to how the phase change of each control volume is modelled and calculated with a special purpose computer program. In Chapter 4 the different experimental setups are described. The results are given in Chapter 5 where the results of both the numerical and theoretical results are given and compared. In Chapter 6 a conclusion and discussion of the important results follow.

1.9 Conclusion of introductory chapter

The introduction laboured to introduce the topic of solar water heating in Section 1.1 and in Section 1.2 it is suggested that PCM as additional heat store should be considered to improve the hot water utility that may be extracted from a PCS-SWH system. The objectives were set out of both the thesis and the design concept in Sections 1.3 and 1.4. A pre-literature study was conducted in Section 1.5. Then using the existing designs as a point of departure a novel SWH with PCS is suggested in Section 1.6 which aim to combine the advantages of an additional PCS unit that is well insulated and that may be charged to high temperatures, which is connected to the geyser by means of a pumped loop which will be switched on when the storage is hotter than the geyser and if the geyser is colder than the maximum allowed water temperature.

Chapter 2

Literature study

Some designs have already been mentioned in Section 1.5. This gave a general overview of the type of designs that have been investigated that are specifically relevant to SWH research with PCS to improve storage capabilities. This literature study aims to expand the scope of previous designs already mentioned. The different ways of analysing the system's thermal response numerically are looked into in Section 2.2. Also more application possibilities are examined in Section 2.3. The different PCMs available will be described in Section 2.4 and the potential HTEs is further investigated in Section 2.5. A short summary will conclude this chapter.

2.1 Introduction of literature study

The work conducted on phase change materials, especially on low temperature PCMs, their application in solar water heating and the available ways to improve their performance are extensive. A few reviews cite relevant work as far back as the 1970s up till the present, such as the work of Shukla *et al.* (2009) that was focused on SWH applications with PCM. Also the reviews of Sharma *et al.* (2009) are good guidelines for PCS systems from a system and applications perspective.

The analysis and recommendations made by the different researchers, such as the cost of each system, the heat transfer characteristics and the resulting heat capacity after the HTE has been added, are taken into account in the current design.

2.2 Numerical analysis of PCS systems

In the work of Verma and Singal (2008) the mathematical analysis complexities are discussed. The authors note that the moving boundary in the PCM during latent heat absorption and removal is particularly tricky to model mathematically and especially analytically. Verma and Singal (2008) make the distinction between models based on the first law of thermodynamics, which include models such as the enthalpy tracking method based on the energy equation, as well as the momentum and mass equations that form the conservation law equations, and models that calculate the entropy generation

and the exergy destruction that conform to the irreversibility law equations during heat transfer processes. Different authors who conducted numerical calculations on their designs are listed, as well as the assumptions that they made during their analyses. One of the authors listed is Trp (2005) who analysed a shell and tube heat exchanger. The transient numerical work conducted by her was experimentally verified and this shows the acceptability of this method, but the limitations of this energy analysis method must be realised. Energy analysis does not take into account the time heat is supplied and the thermodynamic efficiency of the system. The authors recommend that further work be done based on the second law of thermodynamics because of the insight this can give into system performance. This may lead to it becoming a more acceptable form of modelling. Exergy analysis of PCS systems was conducted by Li *et al.* (2012) and by Shabgard *et al.* (2012) and they show the potential of this method to develop, for example, cascaded PCS systems and to employ systems with good all round thermal efficiency. In this initial analysis of a novel concept design for a SWH application the first law of thermodynamics is incorporated as the analysis method.

In applying the conservation of energy at each time step, and for each control volume, it is important to decide whether natural convection should be taken into account, or whether it can be assumed that the PCM melts and solidifies mostly by conduction. The work where convection was taken into consideration such as the work of Shatikian *et al.* (2005) and Shatikian *et al.* (2008), they model a very small flow field under steady input conditions. This method of analysis is computationally intensive. It would be quite an extensive work to model a whole PCS systems with natural convection in three dimensions, and to use this as a design tool would require a lot of expertise. On the other hand if only conduction is considered the main operation modes may be captured accurately enough to model a whole system to a reasonable degree. This assumption is validated as Shatikian *et al.* (2005) noted that during melting of the PCM in a narrow compartment the convection currents are negligible, and during solidification the convection currents are also very weak and as the solid layer of wax grows the main mode of heat transfer is conduction. If this is insufficient and more accuracy is required then the work of Wang *et al.* (2010) is suggested, because they look in depth at natural convection on a chamber under certain boundary conditions, but that is still worlds away from developing a PCS system that takes natural convection into account with the complex geometry formed by the HTEs and the embedded PCM.

2.3 Possible applications of the PCS systems

The work conducted by Sharma (2005) indicates that PCS systems can be used very effectively to cook food in the evening when they are connected to

an evacuated tube solar collector. It was shown that a PCM, with a melting point of between 80 °C and 120 °C, is suitable for various cooking needs, and the researchers used Erythritol ($T_m = 118$ °C and $h_{sl} = 339.8$ kJ/kg) as PCM material. During summer time in Japan they could cook at noon and again in the evening and the system can potentially be used for community cooking.

With regard to high temperature PCS systems for power generation applications the work of Robak *et al.* (2011a) and Robak *et al.* (2011b) is very insightful. They show the potential of a PCS system that incorporates heat pipes as HTEs to utilise their excellent heat transfer characteristics and to move away from many thin-walled small diameter pipes that would cause too great a pressure drop if used to extract the heat from a large PCS system for power generation. Their design shows particular potential as a PCS system for high temperature application and it offers flexible operating conditions, since one heat pipe is used to transfer heat to the PCM and to the cold stream either directly or after it has been stored for a while. In the current design two heat pipes are used, instead of one multipurpose heat pipe, since the heat absorption HP1 will be exposed to the cold atmosphere during nighttime and it will cause the heat transfer rate to the cold stream to be too low. Two modes of operation are used by the PCS system, either heating from the lower end (evaporator section) of the heat absorption HP1, or cooling from the higher end (condenser section) of the heat removal HP2. This set-up is more suitable for the SWH application and it is easier to detect and replace a faulty heat pipe.

2.4 The use of a phase change material in a latent heat storage system

PCMs are materials that undergo a phase change of solid-solid, solid-liquid or liquid-gas. Of these the solid-liquid transition materials are considered to be the most usable as thermal storage mediums because of the availability of materials in the range of temperatures required and the low volume change during phase change. Of the phase change materials paraffins seem to be very suitable with a melting temperature of between 20 °C at the lower temperature range, which is very useful for passive building temperature control and wax melting up to 120 °C at the higher temperature range for use in storing energy for industrial heating purposes and the range between 50 °C to 80 °C for water heating. Salt hydrates are also good, but have some disadvantages as indicated in Figure 2.1 which make them a bit more tricky to use effectively as a thermal heat store.

Much experimental work has been conducted by phase change material suppliers to categorise their products. For example the work of van Dorp *et al.*

(2004) documents single and multiple rectangular PCM packs experimentally. The aim of the experiment was to analyse a virtually one dimensional flow of heat vertically through the PCM contained in square aluminium foil pouches of 0.4m in length and breadth and 0.005 m in height. It is suggested by van Dorp *et al.* (2004) that future temperature measurements be in direct contact with the PCM inside the PCM packs. Although the heat transfer through the packs was not accurately captured, much was learned of a possible method to test the PCM in a certain geometry in a transient manner.

Using PCMs to store heat is not as simple as a liquid storage system such as water that can easily be pumped through the solar collector. The reason being that the PCM solidifies to a solid medium during the phase change. Therefore the PCM is usually contained in a static container and the heat is transferred to and from it by means of a pump or by making use of heat pipes. There also exist some alternative possibilities to make use of a dynamic system by either micro-encapsulating of the PCM and passing it through the heat exchanger in a slurry. Delgado *et al.* (2013) tested such a slurry and found that a 10% micro-encapsulated PCM and water slurry improves the energy density across a $\Delta T = 3^\circ\text{C}$ was 75% higher than water. Alternatively there is a double screw heat exchanger under development by Zipf *et al.* (2013) that granulates the PCM as it solidifies and passes the granules to a containment section. This system effectively decouples the storage size from the heat exchanger size and is a very promising technology for large systems. These cutting edge technologies are thus able to decouple the heat exchanger size from the storage size. The heat exchanger is also steady in operation, which greatly simplifies heat exchanger design. Unfortunately such systems are not yet available for low cost low temperature SWH applications, but its development is looked to closely as further improvements and tests are done.

The convection in the liquid PCM may be used to increase melting and solidification rates. For example heating PCM from below, where heat transfer occurs mostly by convection in the liquid PCM, which is much faster than heating from above, where heat transfer occurs mostly by conduction. The difference in heat transfer rates into the PCM can be seen in the following equations where conduction across a surface A and the heat is transferred across a distance Δx where a finite temperature difference ΔT exist between the hotter surface and the cooler solid PCM.

$$\dot{Q}_{cd} = \frac{k_{wax} A \Delta T}{\Delta x} \quad (2.1)$$

Where $k_{wax} = 0.2 \text{ W/m K}$ which is very low when compared to a fin material such as aluminium with a thermal conductivity of $k_{Al} = 237 \text{ W/m K}$. The convection heat transfer that occurs in the liquid PCM section is dependent

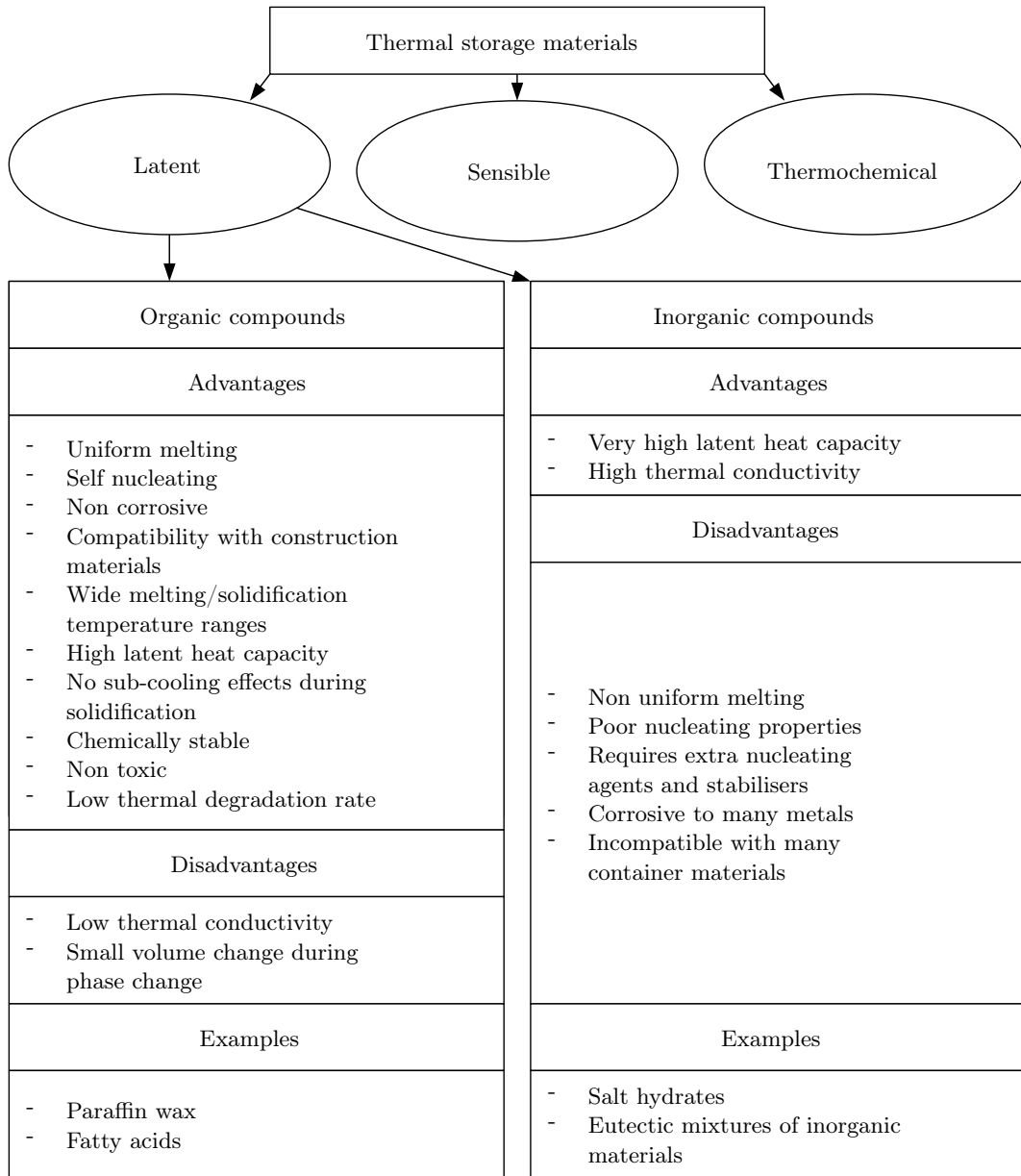


Figure 2.1. The different kinds of thermal storage materials and their advantages and disadvantages.

on the geometry, area, temperature difference and size of the liquid layer. The governing equation of natural convection of rectangular enclosures heated from the side is given by the following relations given by Bejan (2004):

$$\dot{Q}_{cv} = h_{wax} A \Delta T \quad (2.2)$$

Where the convective heat transfer coefficient is related to the Raleigh number in the case when the Raleigh number is larger than the following relation:

$$Ra^{1/4} > H/L \quad (2.3)$$

Where H is the height of the liquid section, and L is the width of the liquid section. The Raleigh number is calculated from the following relation:

$$Ra = \frac{g\beta\Delta TH^3}{\nu\alpha} \quad (2.4)$$

The convective heat transfer coefficient is dependent on the Nusselt number that is given by the following relation.

$$Nu = 0.364 \frac{L}{H} Ra^{1/4} \quad (2.5)$$

The convective heat transfer coefficient may be calculated to be as follows:

$$h_{wax} = \frac{Nuk_{wax}}{L} \quad (2.6)$$

The natural convection in the liquid PCM will be different if it is heated from the side, or if it is tilted or heated from the bottom because of buoyancy effects. Melting periods may be shortened even more if the solid layer is allowed to drop onto the hot contact surface as more and more wax is melted. This is known as contact melting and equations are given for these geometries by Bejan (2004). The problem of increasing solidification periods remain however, because the solid layer sticks onto the cooling pipes and the thickness increases as more liquid wax solidifies onto the pipes and less and less heat is absorbed in the water in the heat exchanger.

The convection in the storage can be increased by circulating the liquid and thereby causing forced convection in the liquid part of the PCM as done by Tay *et al.* (2013) which found a 33% to 89% decrease in melting time could be achieved in their initial tests of the circulating liquid PCM concept.

A good understanding of the heat transfer mechanisms during melting and

solidification opens up the possibilities to apply these mechanisms to develop novel heat storage concepts. The complexity of operation and the costs involved by adding heat transfer enhancing components which are discussed in the following sections.

2.5 The use of heat transfer enhancers (HTEs) with phase change material embedded in between

The low thermal conductivity of the paraffin waxes and other PCMs has resulted in many studies to combine a highly conductive material in a particular form, such as foam or shavings, with a PCM embedded in between. Velraj *et al.* (1999) utilise radial fins and Lessing rings to improve the heat absorption/removal cycle versus the heat stored per volume. The different options available to the designer of a PCS system are discussed in more detail in Subsections 2.5.4 to 2.5.4. The reason why HTEs are useful in PCS systems is that the low thermal conductivity of the PCMs limit the effective use in many heat storage applications. The problem is most visible during the heat removal cycle of a PCM. This was seen in the work of Mettawee and Assassa (2006) where most of the wax is still liquid but almost no heat is transferred after four hours of trying to extract the heat from PCS system. If no HTE is used the cold water is initially heated up very well because of the large temperature difference between the hot molten wax and the cold water stream, but as the solid layer of wax grows around the cold water pipe the heat needs to be conducted through the cool solid layer of wax. This results in very low heat transfer rates even though most of the wax is still very hot and high latent heat is still available. The insulating effect of the solidifying PCM must be effectively countered by either having many pipes running through the PCM compartment, which will increase the cost of piping and lessen the total volume of storage material, or by adding HTEs such as fins around each pipe, thereby reducing the amount of pipes required. The challenges with many of the HTE materials used are the uncertainty of the heat paths, as well as the non-isotropic behaviour of the resulting mixtures. This complicates the numerical analysis of the PCS system, because in many cases the resulting heat paths are at random and it is difficult to analyse whether conduction or convection or both take place in the molten wax, and the complex phase change boundary becomes difficult to calculate and experimentally measure.

2.5.1 The use of heat pipes as heat transfer enhancers

Heat pipes are used in evacuated tube solar collectors and they are effective heat transporters from the solar collector section to the water that cycles from the heat exchanger and the geyser (Riffat and Zhao, 2004). Heat pipes in the form of meso and micro channels are described in detail by Cheng and Wu (2006) as devices that can transfer heat very effectively, they are more compact and lighter in weight than other devices would be, hence their use in electronics and space applications. The lab experiments described in Chapter 4 uses such micro channel heat pipes. The advantage is not only high heat transfer rates to and from the PCS system, but the uniformity in temperature inside the heat pipe helps to achieve a congruent melt front that takes a vertical shape.

The improved heat transfer mechanisms such as can be found in heat pipes lead to their being considered for use in PCS systems design. The use of heat pipes in the design of PCS systems are taken into consideration in the work of Sharifi *et al.* (2012) where a solid rod, a hollow tube and a heat pipe are compared to an isothermal surface as a base case in the simulation thereof. The heat pipe melted the entire region much more quickly than the other materials. According to Sharifi *et al.* (2012) the total material that the heat pipes use is much less than the rods and this gives the heat pipes an economic advantage. Sharifi *et al.* (2012) therefore recommended heat pipes as the preferred option to enhance heat transfer to and from the PCM. Sharifi *et al.* (2012) made the argument that heat pipes are superior to thick long rods of the same outer dimensions of that of the heat pipes. With this statement there is full agreement. However, heat can be effectively transferred to the outer surface of the heat pipes, but then there is a bottleneck because the PCM has a very low thermal diffusivity. This results in low heat transfer rates between the wax control volumes to the extent that during solidification the solid PCM that form on the heat pipe surfaces insulates the wax that is still liquid and therefore contains high internal energy from the cool heat pipe. So how can this be circumnavigated? Well theoretically the heat pipe could be made into an intricate shape that will increase its effective area, or many heat pipes may be used, but these heat pipes will increase the cost of the system and make the system more intricate. Another possibility is to add fins to each heat pipe. This would not greatly increase the cost, and the surfaces are extended to such an extent that the heat does not need to be transferred across a large distance through the wax, but rather through the fins that has a much higher thermal diffusivity as described in the equations below: The thermal diffusivity is a ratio between the heat conduction rate and the heat stored. Therefore it gives an indication of how fast heat can propagate through the medium. For solid paraffin wax the thermal diffusivity $\alpha_{w(s)}$ is given as follows:

$$\alpha_{w(s)} = \frac{k_{w(s)}}{\rho_w C_{p(w(s))}} \quad (2.7)$$

$$\alpha_{w(s)} = \frac{0.2 \text{ W/m K}}{910 \text{ kg/m}^3 2150 \text{ J/kg K}} \quad (2.8)$$

$$\alpha_{w(s)} = 102.210^{-9} \quad (2.9)$$

For aluminium the thermal diffusivity is given as follows:

$$\alpha_{Al} = \frac{k_{Al}}{\rho_w c_{p(Al)}} \quad (2.10)$$

$$\alpha_{Al} = \frac{237 \text{ W/m K}}{2702 \text{ kg/m}^3 903 \text{ J/kg K}} \quad (2.11)$$

$$\alpha_{Al} = 97.1310^{-6} \quad (2.12)$$

$$\frac{\alpha_{Al}}{\alpha_{w(s)}} = 868 \quad (2.13)$$

This indicates the difference in thermal properties of the wax and the aluminium even when neglecting the phase change of the wax (when considered the wax has 100 times lower thermal diffusivity during phase change if a one degree temperature difference is considered as the phase change temperature). It makes sense therefore to use the fins as heat transfer conduits to extend the heat pipe surfaces, and to use the wax as thermal storage material.

Experimental analysis of a PCS system with the aid of heat pipes for different modes of operation was conducted and described by Liu *et al.* (2006a) and by Liu *et al.* (2006b) and their design is shown in Figure 2.2. Five heat pipes were used in the prototype and in the heating only mode it was shown that in the vertical direction there was not even a 3 °C temperature difference between the lower and the higher measuring points in the PCS system. This difference can also be ascribed to the additional heating that results as the hot stream heats the PCM from below. The whole unit heated up and melted very effectively with the aid of the heat pipes with the extended fin surfaces. The researchers showed that the hot inlet temperature had a bigger effect than the flow rate. No observations were noted by Liu *et al.* (2006a), neither was an energy balance of the system done although this information would have led to a better understanding of the heat transfer in the system and the PCM fluid flow expansion and contraction of the wax in the PCM container.

In another design by Shabgard *et al.* (2010) short heat pipes are incorporated to enhance heat transfer and to extract the heat from either the PCM tubes or from the PCM shell. The more heat pipes were added the more effectively

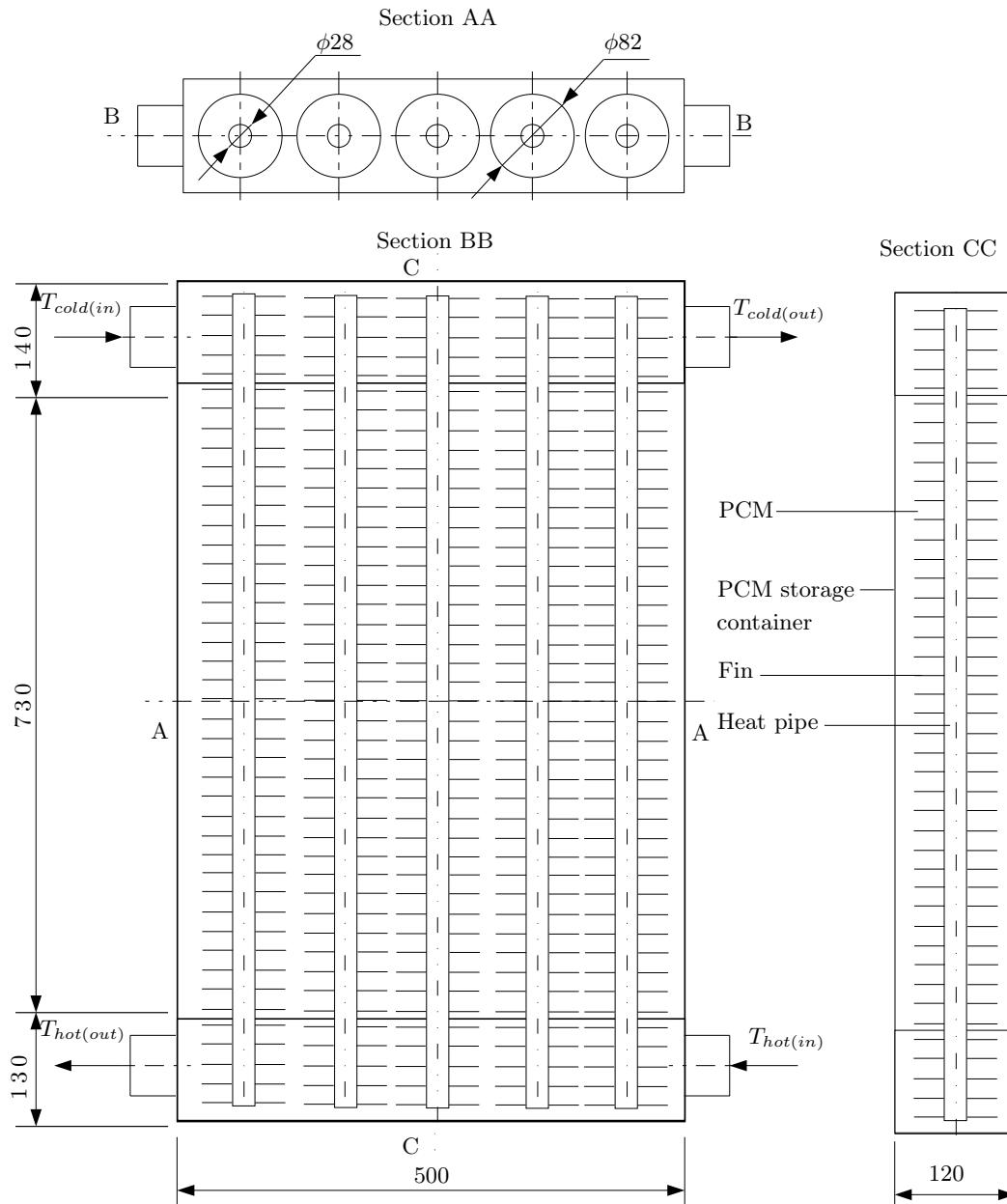


Figure 2.2. The cross sections of the PCS systems of Liu *et al.* (2006a).

the heat was extracted from the system, which indicates that the heat pipes effectively enlarge the total surface that is exposed to the cold stream. Robak *et al.* (2011a) realised the need to build small scale tests and to photographically capture the heat absorption and heat removal cycles of their tests. These tests were composed of a test case, where the PCS system was filled only with wax and also compared this test to a test with heat pipes as well as a test with solid rods. His experimental set-up is shown in Figure 2.3. The results show that the heat pipes melt the wax much faster than both the metal rods and the wax only cases. About 70% of the wax was melted in the test case when all the wax was melted by the heat pipes. Also during the heat removal cycle only 30% was solidified in the wax only case and with the rods about 45% by the time the heat pipes totally solidified the test section. This is shown in the photographs in Figure 2.4. This is a very important experiment, because it experimentally shows that heat pipes can work well to extract the heat from the PCS system by effectively enlarging the surface area exposed to the cold stream.

2.5.2 The use of fins as heat transfer enhancers

The use of vertical fins in a rectangular arrangement for geometries of a few millimetres, 10 mm in height and 4 mm in breadth, was investigated by Shatikian *et al.* (2005). The authors used in their simulation the convective phenomenon and determined that for the largest section the Raleigh number

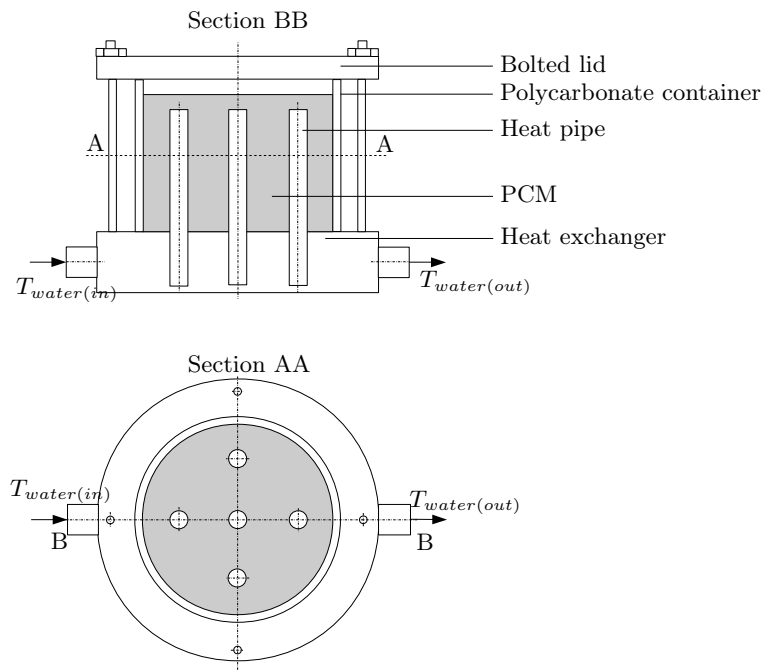


Figure 2.3. Schematic diagram of Robak *et al.* (2011a) experimental set-up.

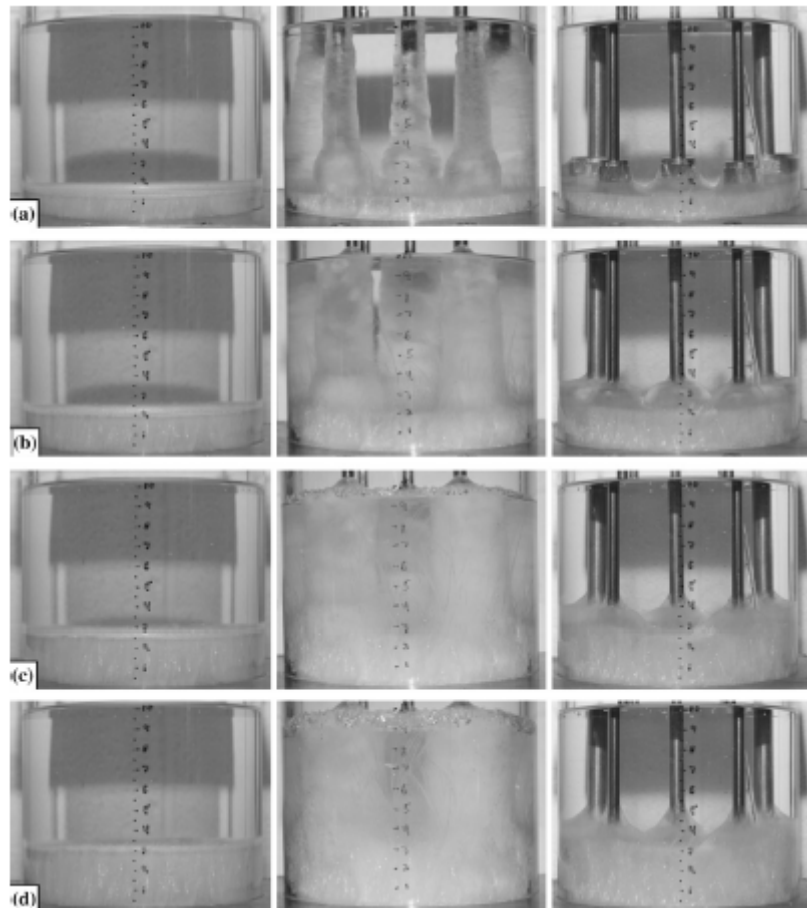


Figure 2.4. Photographs of Robak *et al.* (2011a) experimental results during heat removal at a) $t=60$ min, b) $t=120$ min, c) $t=180$ min and d) $t=240$ min.

was used to generate a generalised form. This generalisation showed that for large temperature differences between the fin and the PCM, convection currents in the molten PCM start to play a more dominant role in heat transfer. The test case was one small compartment of wax and to simulate a lot of small containers to such an in depth level is complicated and would take a lot of computing power. It is therefore suggested that the PCM is contained by the HTE to such a degree that convective currents do not become strong. In such a case a conduction dominant calculation will be sufficient.

The enhancement of PCM melting in enclosures with horizontally finned surfaces was analysed by Sharifi *et al.* (2011). They found that the melting rate is significantly improved by adding fins in their numerical simulation. It was found that the horizontal fins reduce melting and solidification periods. This study indicates that the heat absorption/removal period of a volume of PCM can be enhanced to a significant degree by adding fins as HTE.

2.5.3 The use of form stable expanded graphite matrix as a heat transfer enhancer

There are advantages to using form stable expanded graphite as a matrix material with the PCM embedded in between. These advantages include that the thermal conductivity can be greatly improved depending on the graphite percentage and orientation of the graphite particles in the matrix. Sari and Karaipekli (2007) specify that the mass fraction of the expanded graphite increases almost linearly from 0.4 W/m K for 2% mass fraction of expanded graphite and this rises to 0.8 W/m K for 10% of mass fraction of expanded graphite. The other advantage is that at 10% of expanded graphite a form stable mixture is achieved, that is to say that no wax leaks out from the expanded graphite mixture. The melting times of the matrix decreased in accordance with an increase in thermal conductivity. The authors suggest 10% expanded graphite mass fraction as the most promising combination, since the form stable property results in not having to have a container around it. Zhao and Wu (2011) compared porous metal foams to expanded graphite and found the metal foams performed better in terms of shortening melting and solidification processes, but they noted that high temperature applications with salts results in a corrosion issue. Luckily the expanded graphite does not degrade when used with salt as PCM. Another method was researched in South Africa. Mhike *et al.* (2012) conducted experiments on wax blended with LDPE plastic and exfoliated graphite. It was found that 10% exfoliated graphite increased the thermal conductivity to 1.2 W/m K and it is also a form stable product. In their research Zhang *et al.* (2012) noted that encapsulating or using holding tanks to contain the wax as it changes phase increases the cost and they therefore suggest a clay and graphite material matrix to form a form stable PCM composite. This can be prepared either by encapsulating the PCM into for example high-density polyethylene or it can be formed by embedding it into clay that was mixed with graphite. The authors suggest the clay and graphite as material matrix because of the form stable property and lower manufacturing cost. 5% graphite was introduced in the clay and a mass ratio of up to 65%/30%/5% paraffin/clay/graphite mixture was tested. It significantly reduces the latent heat of fusion from 174 kJ/kg to 105 kJ/kg which is quite a significant reduction, but the added safety of the material such as no spillage being possible from the material matrix makes it a very reasonable compromise. The 5% graphite helped to decrease melting and solidification times by 61% and 72% respectively. It is a very promising material, but maybe just more so for higher temperature applications.

2.5.4 The use of metal foam as heat transfer enhancer

Yet another way of increasing the thermal conductivity of the PCM is the use of metal foams. Vadwala (2011) used 95% porous copper foam which only

reduces the storage volume by 5% and noted that foams are also available in graphite, aluminium or nickel and it can have a very high thermal conductivity. In the study it was found that the metal foam increased the effective thermal conductivity from 0.21 W/m K to 3.8 W/m K. The melting time of the test section was 36% that of the pure wax test. The expanded metal foams are still a bit pricy though. For example one 1 m² of 20 mm thickness cost R2 000.00. As the cost of manufacturing these foams comes down the use in low temperature HTE applications will become a more viable option.

2.6 Conclusion of literature study

In this chapter the literature is examined in more depth, paying special attention to how PCS systems may be modelled theoretically as described in Section 2.2. It is decided to develop a special purpose code to numerically calculate the temperature and phase of the PCS system's control volumes in a transient response model. This model is described in Chapter 3. Different possible applications that exist are mentioned in Section 2.3 which mentions the possibility of using this work to assist PCS system developers to gain insight of their specific application. The different available PCMs are mentioned and compared in Section 2.4.

Then in Section 2.5 different HTE methods are described. From the research already conducted it is clear that there are various methods of increasing the thermal conductivity of a PCS system. One way to to achieve enhanced heat transfer is to add highly conductive materials to the PCM to improve the resulting thermal conductivity or to connect heat pipes between the PCM and heat exchanger to effectively extend the heat transfer surfaces. Or one can use more piping throughout the PCM. In order to compare different PCS systems with different HTE components the cost versus their thermal performance need to be taken into consideration in full thermal response simulations to determine when to use a certain HTE with a certain PCS application.

Chapter 3

The numerical thermal simulation model

In the previous chapter the literature was reviewed and numerical analysis was mentioned as a more precise calculation method than any available analytical methods can achieve. The reason for this is because when using HTEs the geometry is intricate and the melt front progresses in a non linear fashion because of the phase change process. This chapter introduces the numerical analysis method that was solved with a special purpose built C++ computer program that numerically calculates the state of each control volume and the heat transfer rates across the boundaries for each time step. It also keeps track of how the control volumes heat up, melt and expand, cools down, solidify and contract. Firstly an overview of the thermal simulation model is given in Section 3.1, then the test conditions are given in Section 3.2. The discretization of the finned test module which is described in Section 4.4 is given in Section 3.3. The numerical modelling governing equations for various control volumes are given in Sections 3.5 to 3.9. In Section 3.9 a description is given how the phase change was modelled in the numerical model. Finally a description is given how the theoretical SWH-PCS was modelled in Section 3.10.

3.1 Overview of the thermal simulation model

The numerical model of the test module uses the measured geometry of the experimental module. The heat transfer coefficients of the heat pipes are not calculated theoretically, but rather the average heat transfer coefficients of the heat pipes at both the evaporator and condenser sides are calculated from the temperature measurements experimentally during normal operation conditions. In the work of Stumpf *et al.* (2001) a similar approach was followed to characterise the heat pipe operation for their numerical model. The comparative tests between the experimental measurements and numerical calculations are therefore comparable in terms of how fast the whole system heats up or cools down. The physical experimental test module is modelled by discretising it into small control volumes. At any given time period each control volume exists at a certain temperature, density and phase. As heat is transferred into the control volumes the wax may heat up or melt and this needs to be accurately modelled to follow the model's thermal response during heat absorption and heat removal cycles. As the control volume absorbs heat and melts, or cools

down and solidifies, the temperature, density, phase and internal energy of the control volume changes.

In the numeric analysis it is required to keep track of whether the PCM control volume is solid, a mixture of solid and liquid or completely liquid. The rate of change of each control volume during each time step is calculated by applying an energy balance to each control volume. By choosing a relatively fine grid size and by running tests at different time step sizes a stable time step was obtained that was sufficiently small, but still large enough to overcome the round off errors experienced by the computer. The transient thermal response is found to be stable when 64 control volumes were taken in the width, one in the height and three control volumes in the depth. The time step became stable at values $\Delta t \leq 1$ ms. The discrete numerical model which takes into account the intricate geometry is a more precise representation of the system than any analytic model can calculate.

When developing a numerical thermal response model, the melting in the wax control volumes needs to be modelled. As the wax melts, the internal energy changes, the density also changes during the phase change and therefore the volume of the control volume needs to be adapted. In the tested case the wax is encased in long vertical compartments. When the wax changes phase and expands or contracts, the length of the control volume is adapted. The energy absorbed and the rate of heat transfer to and from the PCS system are two of the main macroscopic parameters of the storage module. In the transient analysis the total energy absorbed in the module, as well as the total rate of heat absorption and heat removal is kept account of.

The sensible heat absorbed in the fin compartments, and the sensible and latent heat in the phase change material are calculated from the temperature of the control volume, and in the case of liquid PCM the latent heat of fusion is taken into account.

The rate of energy transfer through conduction into the storage control volumes are given in Equation 3.1. It is equal to the temperature difference divided by the resistance between the temperature control volumes. The rate at which energy crosses the boundary of control volume is calculated with the old time step, and the enthalpy of the control volume is calculated with the newly calculated temperature and melt fraction properties.

$$\dot{Q}_{cd} = \frac{T_h - T_S}{R_{cd(h)} + R_{cd(s)}} \quad (3.1)$$

Where the resistances are calculated by the following relation:

$$R_{cd} = \frac{\Delta x}{kA} \quad (3.2)$$

Where Δx is the distance that heat is transferred through the control volume, and k is the thermal conductivity and A is the surface cross section that the heat is transferred through.

The general work which the numerical model performs is to calculate how a PCS module heats up and melts the PCM inside it and how it is cooled down until it ultimately solidifies during cool down. The program gives an overall indication of how the time dependent melting and solidification occurs. It keeps track of both the temperatures and the state either solid or liquid of all the control volumes during a heat absorption and heat removal cycle.

3.2 Test conditions that were applied on the numerical and experimental model

In all numerical models the precision of the calculation must be weighed up against the effort to include the different non linear phenomena in an increasingly computationally intensive program. The model must also be checked during critical changes such as the phase change during heat absorption and heat removal.

Another aspect to consider in the modelling of the PCM, is whether the PCM is pure and has a clear melting point, or whether it is a mixture which results in a mushy region during melting or solidification. When modelling the experimental results, only a few thermocouples were used to capture the cooling or heating of the PCS section comprising the fins and the wax embedded in between. To calculate what the whole storage response is, the storage is discretised into five control volumes. Each temperature reading represents its respective control volume's state. This was found to model more precisely the thermal response by linking the temperature to the energy in the control volume. The melt fraction of the wax $X_{M(wax)}$, which is embedded in between the fins, starts at zero at 45 °C and increases linearly to one at 59 °C. On the numerical modelling side it was deemed more accurate to model the wax as a clear melting point. The reason being that the wax section is divided into a lot of control volumes and each control volume is modelled at a specific state. This can fully capture the mushy region phenomena where multiple control volumes are in various melting fraction states.

The following test conditions were assumed during the calculation of the PCS module's heat absorption and heat removal cycles. The geometry of the module

and the known flow phenomena that are likely to occur and the material properties give leverage to apply the test conditions on the numerical model with a higher level of confidence.

1. The initial temperature of the latent heat storage unit is uniform and the PCM is in the solid phase for melting or in the liquid phase for solidification;
2. The heating and cooling water is incompressible and it can be considered as a Newtonian fluid;
3. The PCM is homogeneous and isotropic;
4. An adiabatic outer wall is assumed;
5. Inlet velocity and inlet temperature of the cooling water are kept constant with the aid of the constant head tank;
6. The natural convection in the liquid phase of PCM has been ignored;
7. The expansion of the wax control volumes are taken into account during the liquefying and solidifying cycle by assuming that the melting wax control volume will expand in the vertical direction z in a linear fashion to the melt fraction $X_{M(l)}$. It is also assumed that there is no mass transfer between the different wax control volumes, and mass and momentum transfer is not taken into account. This is deemed a reasonable assumption, because the narrow vertical wax control volumes are physically limited in their flow from one compartment to the next during their liquid state;
8. It is assumed that the wax of control volume will stay in that control volume and that no convection will take place between the wax control volumes. The in depth analysis of two and three dimensional flow fields is computationally heavy, and besides the overall effect of heat absorption and heat removal need to be analysed, not the in depth flow phenomena in each wax compartment as Shatikian *et al.* (2005) have already done;
9. It is also assumed that the temperature within the heat pipe during normal heating mode is uniform and that saturation conditions exist within the heat pipe. It is also assumed that the heat pipe is not operated in the dry-out limit where a very large temperature difference exists and where lower heat transfer rates are achieved.
10. It is assumed that the heat transfer area between the wax and the fin alongside it increases as the wax expands to take up a larger volume. Similarly during solidification this area decreases as the wax volume decreases and forms voids. This is equivalent to using different thermal conductivity for the two phases of the wax, but in keeping with the

assumption of negligible natural convection in narrow long containers the thermal conductivity of both solid and liquid state k_s and k_l stays the same;

11. It is also assumed that along the height L_z of the PCS module there is no significant difference in temperature distribution and that during the discretisation described in Section 3.3 there is only one control volume along the height L_z of the PCS system. This assumption flows forth also from the heat pipe that handles a reasonably uniform temperature distribution along its length. This assumption will be tested in Section 4.6 where there are measurements taken at three depths and repeated three times in the breadth of the PCS module.

3.3 Discretization of the test module with HTE

The thermal simulation model numerically calculates what the thermal response of the experimental module would be. The simulation model models the PCS module comprising wax embedded in between fins and sandwiched between the heat absorption and heat removal heat pipes. In Figure 3.1 a simplified test module is depicted that indicates the main layout of the PCS system. In Figure 3.2 the resistive diagram is drawn as viewed from the side. Only two PCM control volumes are drawn, but in the real module the PCS system is discretised accurately as depicted in Figure 3.3. It shows the PCS module as viewed from the top. The control volumes are discretised as follows. One hot kettle water control volume at temperature T_h . The rectangular heat pipes' insides are described as one control volume having a single temperature at saturated conditions for the inside temperatures T_{hp1i} and T_{hp2i} , and having wall control volumes corresponding in number to the control volumes alongside them at both the evaporation and condensation sides T_{hp1wc} and T_{hp1we} . Each control volume of the wax, main fin and inner fin material is discretised to have a single temperature and state each: $T_{wax(j)(k)}$, $T_{mf(2j)}$, $T_{if(j)(k)}$ and at a solid $X_{M(l)(j)(k)}$ or liquid state $X_{M(l)(j)(k)}$.

The difference between the wax control volumes and one of the inner fin control volumes is the difference in geometry m^2 , thermal conductivity k_{Al} and k_{wax} and internal energy Q_{Al} and Q_{wax} respectively. The large difference between these control volumes makes smaller time steps in the explicit calculation of the transient heat absorption and heat removal cycle necessary, and it is more computationally intensive than if they were more similar. The control volumes are drawn in a plane viewed from the top as indicated in Figure 3.3 and a single control volume is taken in the height of the PCS system. This approximation of long rectangular control volumes will be scrutinised experimentally in Section 4.6. Only one thirteenth of the PCS system is simulated, this may be done because of the thermal symmetry that arises from the thermal geometry of the

system. As the PCS system is heated or cooled the temperature distribution in the breadth y direction is assumed to be uniform. The calculation excludes losses to the sides, and the magnitude of this effect is also scrutinised in Section 4.6 on page 61.

3.4 Initial values and input conditions of the test module with HTE

The temperature of all the control volumes described in Section ?? are initialised at 14°C. The reason being that the tests were conducted at the end of July and early in the morning it was found that the whole system was quite cold before testing commenced. This startup temperature can be seen at the start of the test indicated in Figure 5.3. All the wax control volumes are in the solid state. The hot water input temperature T_h is then increased linearly over five minutes to 84°C, and it is kept at this temperature until steady state is reached. This is the heat absorption phase. The temperature of T_h is then lowered to 14 degrees over five minutes to emulate the removal of the hot water out of the kettle in the real experiment. The heat exchanger flow rate is then abruptly set to 0.641 g/s, and the inlet temperature is quickly lowered from 84°C to 15°C. The reason is not to abruptly shock the system, but still give reasonable input conditions, which closely simulate the experimental set-up and testing procedure. The results of this analysis will be further described in Section 5.2 on page 69.

3.5 The numerical modelling of the heat absorption heat pipes evaporator wall control volume

As the control volumes absorb heat or cool down the temperature and density of these control volumes change. The rate of change of each control volume is calculated by applying an energy balance to each control volume.

$$\Sigma E_{in}^t - \Sigma E_{out}^t = \frac{E^{t+\Delta t} - E^t}{\Delta t} \quad (3.3)$$

By using the Euler method described by Çengel and Ghajar (2011) the properties at the new time step for the heat pipe evaporator wall control volume

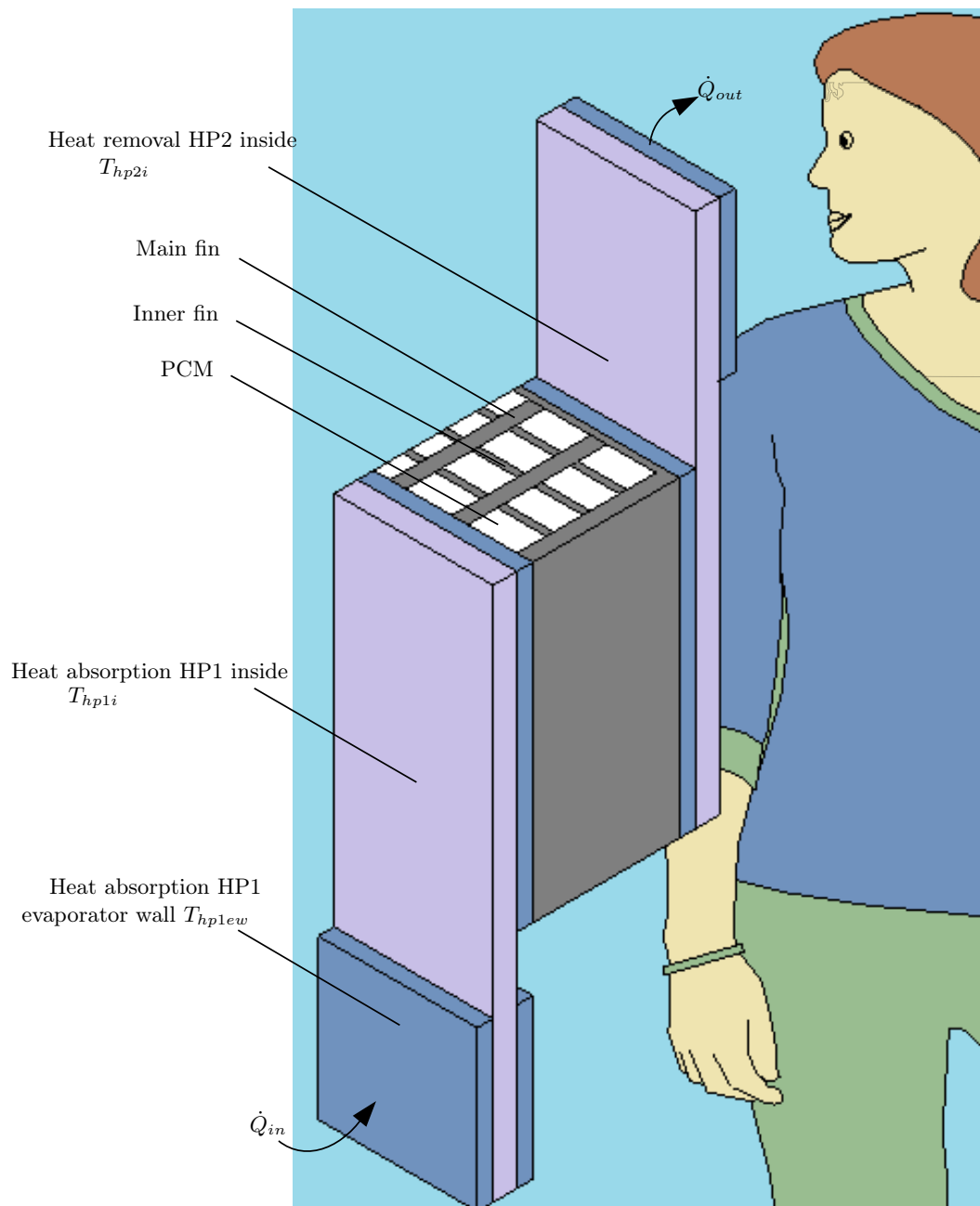


Figure 3.1. A simplified model of the PCS systems test module indicating the heat absorption HP1, the test section with a PCM and HTE control volume and the extracting heat pipe.

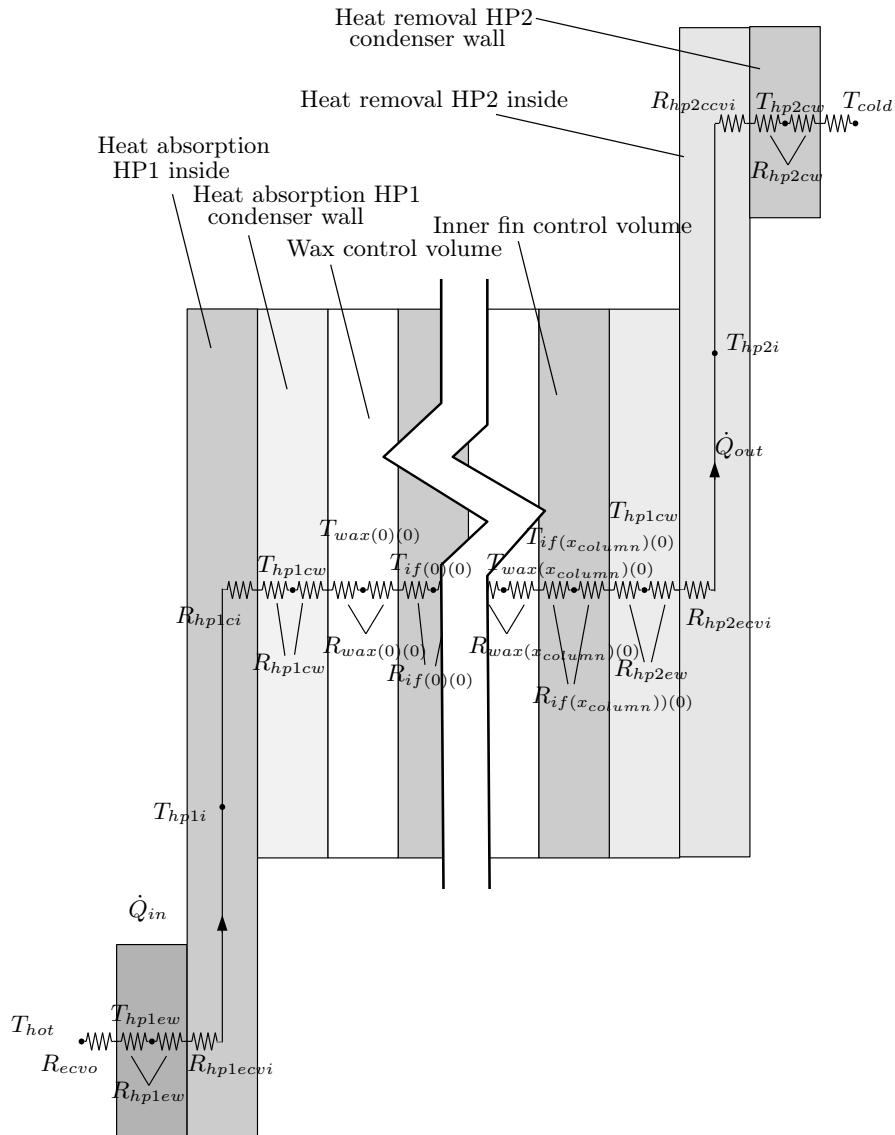


Figure 3.2. A thermal resistive diagram cross section of the PCS systems test module as viewed from the side.

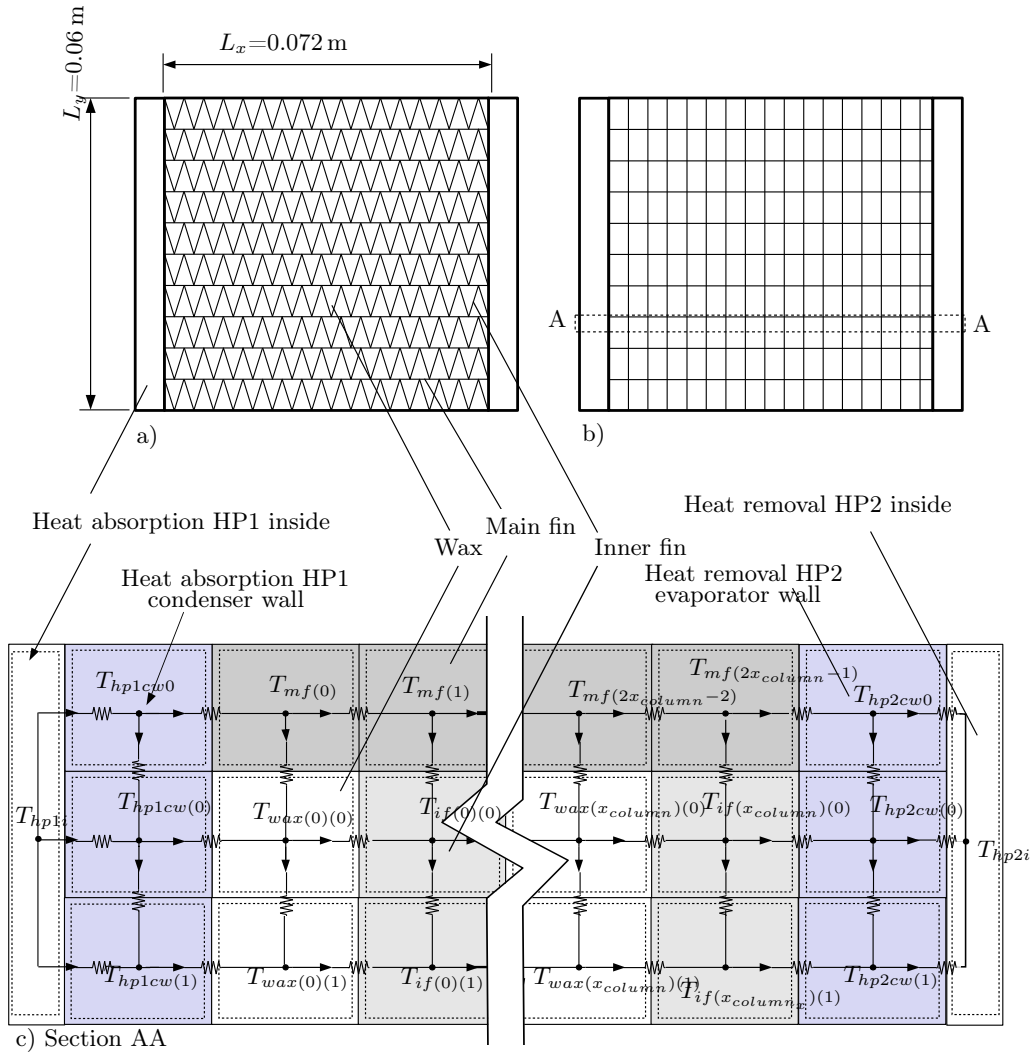


Figure 3.3. a) The PCS module cross section, b) The simplified cross section used in the numerical simulation, c) The thermal resistance diagram cross section of the PCS module viewed from the top.

are calculated explicitly:

$$\begin{aligned} \dot{Q}_{ecv(o)} - \dot{Q}_{ecv(i)} \\ = \frac{m_{ew} c_{p(al)} (T_{hp1ew}^{t+\Delta t} - T_{hp1ew}^t)}{\Delta t} \end{aligned} \quad (3.4)$$

Rearranging Equation 3.4 to calculate the new evaporator wall temperature:

$$T_{hp1ew}^{t+\Delta t} = T_{hp1ew}^t + \frac{\Delta t}{m_{ew} c_{p(al)}} (\dot{Q}_{ecvo} - \dot{Q}_{ecvi}) \quad (3.5)$$

Where the power entering the evaporator wall is calculated by:

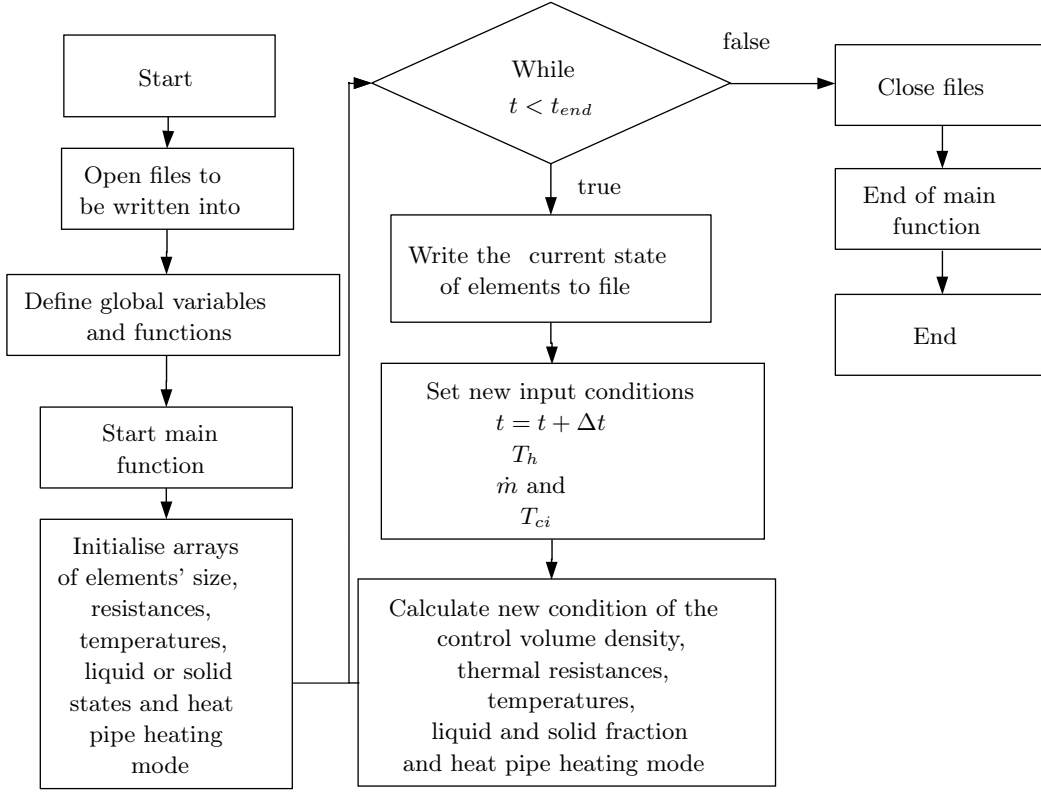


Figure 3.4. The general flow diagram of the main numerical simulation program.

$$\dot{Q}_{ecvo} = \frac{T_h^{t+\Delta t} - T_{hp1ew}^t}{R_{hp1ecv} + R_{hp1ew}} \quad (3.6)$$

and where the power transferred into the heat transfer fluid of the heat pipe is calculated by:

$$\dot{Q}_{ecvi} = \frac{T_{hp1ew}^t - T_{hp1ei}^t}{R_{hp1ew} + R_{hp1ei}} \quad (3.7)$$

The resistances at the evaporator side comprise the following entities:

$$R_{hp1ecvo} = \frac{1}{h_{hp1eo} 2L_y / 13L_{z_{hp1e}}} \quad (3.8)$$

$$R_{hp1ew} = \frac{x_w}{k_{Al} L_y / 13L_{z_{hp1e}}} \quad (3.9)$$

$$R_{hp1ecvi} = \frac{1}{h_{hp1ei} 2L_y / 13L_{z_{hp1e}}} \quad (3.10)$$

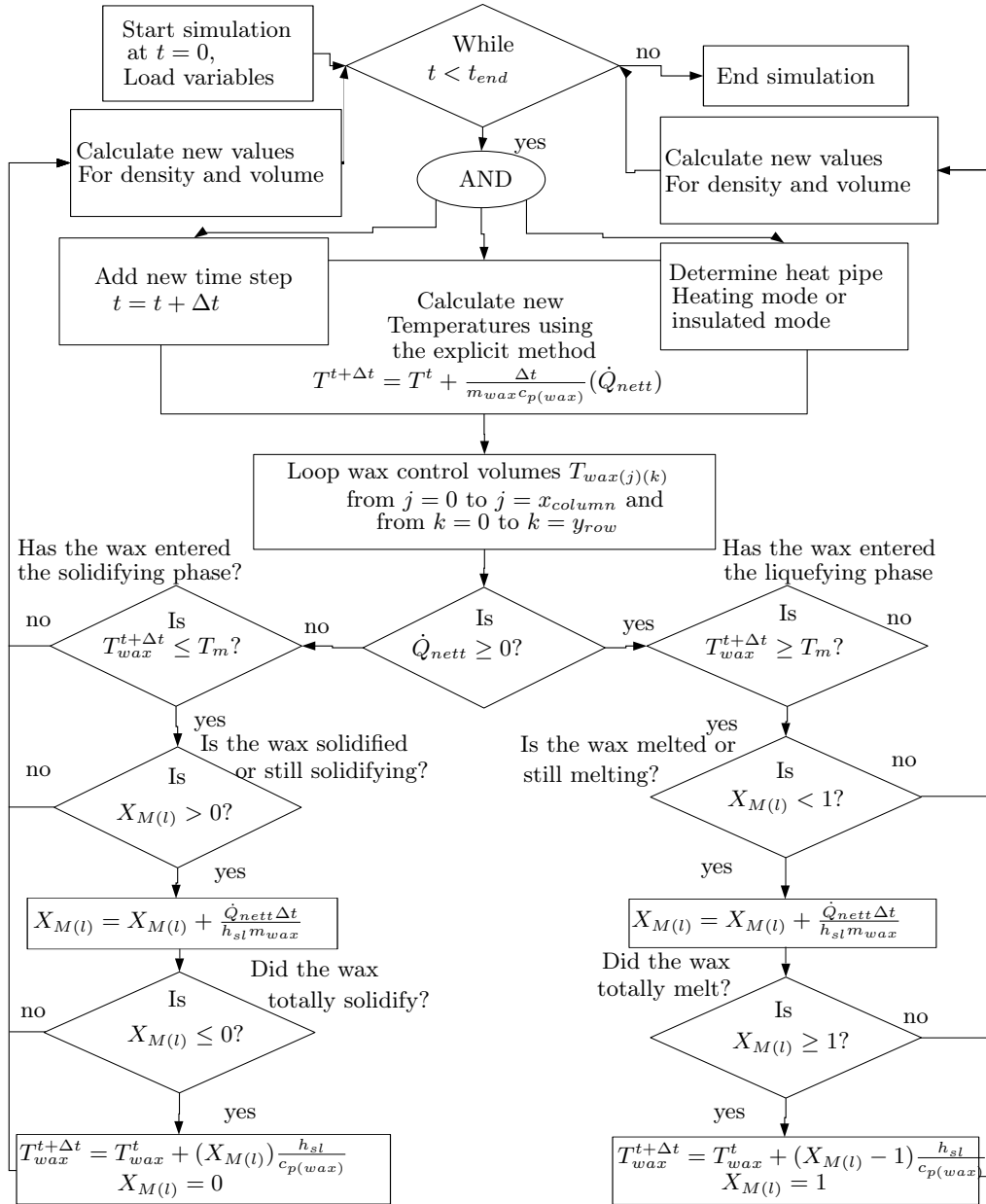


Figure 3.5. The in depth flow diagram of the numerical simulation program.

The value of the wall thickness $x_w = 0.5$ mm, the breadth of the heat pipe $L_y = 60$ mm, the sliver breadth used to calculate the numerical model of length $L_y/13 = 4.615$ mm and height $L_{z_{hp1e}} = 150$ mm. The values of the heat transfer coefficients of both h_{hp1eo} and h_{hp1ei} used in Equation 3.8 and in Equation 3.10 are measured experimentally during the heat transfer characteristic tests of the rectangular heat pipe, and it is compared to the calculated values involved natural circulation on the outside, and involved in boiling on the inside of the heat pipe.

3.6 The numerical modelling of the heat pipe calculation

The heat transfer coefficients on the insides of both heat pipes are quite high, because of the large value of the latent heat of vaporisation and condensation, this occurs even at low temperature differences. The inside temperature of the heat absorption HP1 acts as a superconductor of heat, and the negligible temperature difference between the inside evaporator and condenser effectively links the hot kettle source T_h with the colder fin and paraffin wax control volumes next to the heat pipe T_{mf0} and $\sum_{k=0}^{y_{row}} T_{wax(0)(k)}$. The energy equation of the inside heat pipe control volume T_{hp1i} is given by:

$$\dot{Q}_{in} = \dot{Q}_{out} + \overbrace{\dot{Q}_{loss}}^{\approx 0} \quad (3.11)$$

The value of \dot{Q}_{loss} is taken to be insignificant, because the adiabatic middle section is insulated and it is assumed that the friction loss between the vapour and liquid is negligible. Equation 3.11 is further described as the following:

$$\frac{T_h^{t+\Delta t} - T_{hp1i}^{t+\Delta t}}{R_{hp1ecvo} + 2R_{hp1ew} + R_{hp1ei}} = \frac{T_{hp1i}^{t+\Delta t} - T_{mf(0)(0)}^t}{R_{hp1ci} + 2R_{hp1cw} + R_{mf(0)}} + \sum_{k=0}^{y_{row}} \frac{T_{hp1i}^{t+\Delta t} - T_{wax(0)(k)}^t}{R_{hp1ci} + 2R_{hp1cw} + R_{wax(0)(k)}} \quad (3.12)$$

Equation 3.12 is now rewritten to calculate $T_{hp1i}^{t+\Delta t}$.

$$\begin{aligned}
 T_{hp1i}^{t+\Delta t} = & \left(\frac{T_h^{t+\Delta t}}{R_{hp1ecvo} + 2R_{hp1ew} + R_{hp1ei}} \right. \\
 & + \frac{T_{mf(0)(0)}^t}{R_{hp1ci} + 2R_{hp1cw} + R_{mf(0)}} \\
 & + \left. \sum_{k=0}^{y_{row}} \frac{T_{wax(0)(k)}^t}{R_{hp1ci} + 2R_{hp1cw} + R_{wax(0)(k)}} \right) \\
 & \cdot \left(\frac{1}{R_{hp1ecvo} + 2R_{hp1ew} + R_{hp1ei}} \right. \\
 & + \frac{1}{R_{hp1ci} + 2R_{hp1cw} + R_{mf(0)}} \\
 & + \left. \sum_{k=0}^{y_{row}} \frac{1}{R_{hp1ci} + 2R_{hp1cw} + R_{wax(0)(k)}} \right)^{-1} \quad (3.13)
 \end{aligned}$$

The values of the resistances at the condenser side $R_{hp1ccvi}$, R_{hp1cw} and $R_{hp1ccvo}$ comprise the following:

$$R_{hp1ccvi} = \frac{1}{h_{hp1ci} L_y / 13 L_{z_{hp1c}}} \quad (3.14)$$

$$R_{hp1cw} = \frac{x_w}{k_{Al} L_y / 13 L_{z_{hp1c}}} \quad (3.15)$$

$$R_{wax(0)(k)} = \frac{x_{wax}}{k_{wax_x} L_y / 13 L_{z_{hp1c}}} \quad (3.16)$$

The value of the wall thickness $x_w = 0.5$ mm, the breadth of the heat pipe $L_y = 60$ mm and the sliver calculated in the numerical model $L_y / 13 = 4.615$ mm and height $L_{z_{hp1c}} = 300$ mm. The heat transfer coefficient h_{hp1ci} is determined experimentally from temperature measurements.

3.7 The numerical modelling of the main fin in the PCS system calculation

The PCS control volumes are composed of main fins in the xz -plane, small inner fins in the yz -plane and embedded PCM in between the fins. The calculation of the first main fin control volume is as follows.

$$T_{mf(0)}^{t+\Delta t} = T_{mf(0)}^t + \frac{\Delta t}{m_{mf} C_{p(al)}} (\dot{Q}_{mf(0)netto}) \quad (3.17)$$

Where the netto power entering into the first main fin control volume is calculated by:

$$\begin{aligned} \dot{Q}_{mf(0)netto} = & \frac{T_{hp1i}^{t+\Delta t} - T_{mf(0)}^t}{R_{hp1ci} + 2R_{hp1cw} + R_{mf-mf(0)}} \\ & + \frac{T_{mf(1)}^t - T_{mf(0)}^t}{R_{mf-mf(0)} + R_{mf-mf(1)}} \\ & + \frac{T_{wax(0)(0)}^t - T_{mf(0)}^t}{R_{mf-wax(0)} + R_{waxy(0)(0)}} \end{aligned} \quad (3.18)$$

for symbols, second letter A is for romAn symbols

Where the resistances $R_{waxy(0)(0)}$, $R_{mf-mf(0)}$, $R_{mf-mf(1)}$ and $R_{mf-wax(0)}$

$$R_{waxy(0)(0)} = \frac{b_{wax}/2}{k_{wax}t_{wax}L_{z(0)(0)}} \quad (3.19)$$

$$R_{mf-mf(0)} = \frac{t_{wax}/2}{k_{Al}L_z t_{mfe}} \quad (3.20)$$

$$R_{mf-mf(1)} = \frac{t_{if}/2}{k_{Al}L_z t_{mfe}} \quad (3.21)$$

$$R_{mf-wax(0)} = \frac{t_{mfe}/2}{k_{fin}t_{wax}L_{z(0)}} \quad (3.22)$$

3.8 The numerical modelling of the inner fin in the PCS system calculation

The inner fin calculations are conducted in a similar fashion to those of the main fins, but with the difference that heat is transferred across all four of the sides as seen from the top. This is true except for the final row of control volumes that also have a thermal symmetry boundary condition.

$$T_{if(0)(0)}^{t+\Delta t} = T_{if(0)(0)}^t + \frac{\Delta t}{m_{if}c_{p(al)}} (\dot{Q}_{if(0)(0)netto}) \quad (3.23)$$

where the netto power entering into the first inner fin control volume is calculated by:

$$\begin{aligned}
 \dot{Q}_{if(0)(0)nett} &= \frac{T_{if(0)(1)}^t - T_{if(0)(0)}^t}{2R_{ify}} + \frac{T_{mf(1)}^{t+\Delta t} - T_{if(0)(0)}^t}{R_{mf-if} + R_{ify}} \\
 &+ \frac{T_{wax(0)(0)}^t - T_{if(0)(0)}^t}{R_{if-wax(0)(0)} + R_{waxx(0)(0)}} \\
 &+ \frac{T_{wax(1)(0)}^t - T_{if(0)(0)}^t}{R_{if-wax(0)(1)} + R_{waxx(1)(0)}} \quad (3.24)
 \end{aligned}$$

Where the resistances $R_{ify}, R_{mf-if}, R_{if-wax(0)(0)}, R_{if-wax(1)(0)}, R_{waxx(1)(0)}$ and $R_{waxx(2)(0)}$

$$R_{ify} = \frac{b_{if}/2}{k_{Al}t_{if}L_z} \quad (3.25)$$

$$R_{mf-if} = \frac{b_{mfe}/2}{k_{Al}L_z t_{mfe}} \quad (3.26)$$

$$R_{if-wax(0)(0)} = \frac{t_{if}/2}{k_{Al}b_{if}L_{z(0)(0)}} \quad (3.27)$$

$$R_{if-wax(1)(0)} = \frac{t_{if}/2}{k_{Al}b_{if}L_{z(1)(0)}} \quad (3.28)$$

$$R_{waxx(1)(0)} = \frac{t_{wax}/2}{k_{wax}b_{wax}L_{z(0)(0)}} \quad (3.29)$$

$$R_{waxx(2)(0)} = \frac{t_{wax}/2}{k_{wax}b_{wax}L_{z(1)(0)}} \quad (3.30)$$

The heights of $L_{z(0)(0)}$ and $L_{z(1)(0)}$ and each control volume in the x, y array are calculated from the following correlation:

$$L_{z(j)(k)} = \frac{V_{(j)(k)}}{t_{wax}b_{wax}} \quad (3.31)$$

Where the values of the volume control volumes V are calculated from:

$$V_{mix(j)(k)} = \frac{m_{mix(j)(k)}}{\rho_{mix(j)(k)}} \quad (3.32)$$

The density $\rho_{mix(j)(k)}$ is calculated from the mass fractions X_s and X_l and the densities ρ_s and ρ_l of the wax control volumes which are next to the fin control volumes.

$$\rho_{mix} = \left(\frac{X_{s(j)(k)}}{\rho_s} + \frac{X_{l(j)(k)}}{\rho_l} \right)^{-1} \quad (3.33)$$

The mass fractions of X_s and X_l are calculated every time step by the following correlation:

$$X_{s(j)(k)} = \frac{m_{s(j)(k)}}{m_T} \quad (3.34)$$

$$X_{l(j)(k)} = \frac{m_{l(j)(k)}}{m_T} \quad (3.35)$$

3.9 The numerical modelling of the wax control volumes in the PCS system

In the calculation of the wax control volumes the melting or solidification phases are taken into account. During this phase the netto energy into or out of the wax control volume determines how much wax has melted, or alternatively how much has solidified. During each time step of the sensible solid or liquid phases the calculation is very similar to that of the main fin and inner fins. The difference comes in when the paraffin wax changes phase. In Figure 3.6 the temperature of a wax control volume is plotted during a heat up and cool down cycle. The time steps during the numerical analysis are drawn roughly to explain the analysis procedure. During this cycle the wax first absorbs heat from another control volume which is set first to a temperature of T_h and afterwards it heated up. It is then cooled by changing the temperature of the control volume to T_{cold} . When the wax starts to heat up when it is placed next to a control volume with a temperature T_h , the wax heats up sensibly and its temperature rises just like a normal mass control volume would do. This is indicated discreetly during numerical transient analysis by t_0 up till t_{4a} .

At this time step some of the wax has already started to melt and the correct position is t_{4b} . This point is determined by taking the energy used to overheat the wax past the melting temperature and equating it to an effective mass of wax that has melted during the fourth time step. From time steps t_{4b} - t_{7a} the wax control volume continues to absorb heat at a constant temperature, but during each time step more and more wax becomes liquid until at point t_{7a} more wax has melted than there is wax present in the wax control volume. So the amount of wax that has melted past the total physical amount is equated to the sensible heating that has occurred in the liquid wax. In this manner point t_{7b} is determined. The wax is now sensibly heated while it is totally in the liquid phase. The wax is then cooled and it starts to solidify when it drops below the melting temperature T_m . The solidification phase occurs during time step t_{11a} and it is equated to the mass that has already solidified. The wax

control volume then continues to solidify at melting temperature until all the wax is solidified. This happens during time step t_{14a} . After the mass that has solidified is equated to the sensible cooling that has been experienced in this time step, the analysis continues from point t_{14b} . The wax now cools down sensibly until time step t_{17} by conducting heat to the cold temperature T_{cold} .

$$T_{wax(0)(0)}^{t+\Delta t} = T_{wax(0)(0)}^t + \frac{\Delta t}{m_{wax} C_p(wax)} (\dot{Q}_{wax(0)(0)net}) \quad (3.36)$$

where the netto power entering into the first wax control volume is calculated by:

$$\begin{aligned} \dot{Q}_{wax(0)(0)net} = & \frac{T_{hp1ei}^{t+\Delta t} - T_{wax(0)(0)}^t}{R_{hp1ei} + 2R_{ew(0)} + R_{waxx(0)(0)}} \\ & + \frac{T_{mf(0)}^{t+\Delta t} - T_{wax(0)(0)}^t}{R_{mf-wax(0)} + R_{wax(0)(0)}} \\ & + \frac{T_{if(0)(0)}^t - T_{wax(0)(0)}^t}{R_{waxx(0)(0)} + R_{if-wax(0)(0)}} \\ & + \frac{T_{wax(0)(1)}^t - T_{wax(0)(0)}^t}{R_{wax(0)(1)} + R_{wax(0)(2)}} + \end{aligned} \quad (3.37)$$

where the resistances R_{mf-wax} , $R_{waxy(0)(0)}$, $R_{waxy(1)(0)}$ and $R_{waxy(2)(0)}$

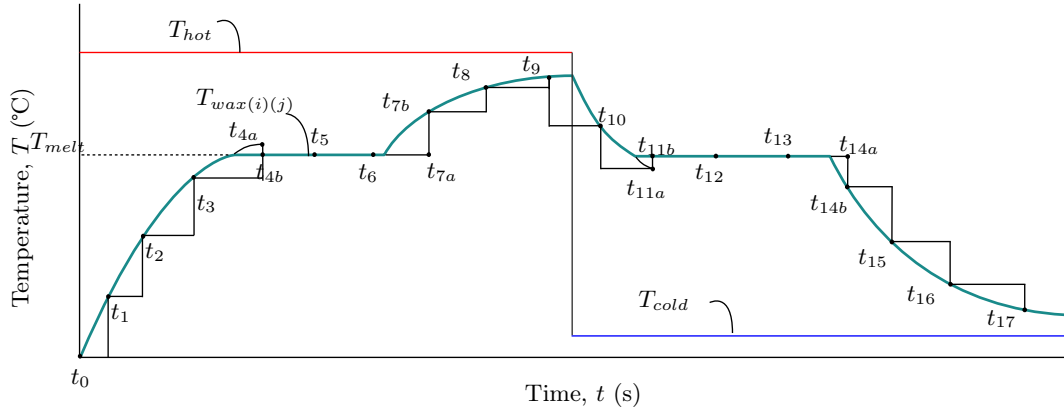


Figure 3.6. The numerical analysis of a wax control volume during heating and melting and cooling and solidifying.

$$R_{mf-wax(1)(0)} = \frac{t_{mfe}/2}{k_{Al}t_{wax}L_{z(0)(0)}} \quad (3.38)$$

$$R_{waxy(0)(0)} = \frac{b_{wax}/2}{k_{wax}t_{wax}L_{z(0)(0)}} \quad (3.39)$$

$$R_{waxy(0)(1)} = \frac{b_{wax}/2}{k_{wax}b_{wax}L_{z(0)(0)}} \quad (3.40)$$

$$R_{waxy(0)(2)} = \frac{b_{wax}/2}{k_{wax}t_{wax}L_{z(0)(1)}} \quad (3.41)$$

The calculation of the wax control volumes are subjected to phase condition statements such as whether the wax control volume has started to melt $T_{wax(0)(0)}^{t+\Delta t} > T_m$ and $T_{wax(0)(0)}^t < T_m$. Now a small amount of wax has started to melt and the liquid mass fraction $X_l > 0$ and the solid mass fraction $X_s < 1$.

$$m_{melted} = \frac{m_T C_{p(wax)} (T_{wax(0)(0)}^{t+\Delta t} - T_m)}{h_{sl}} \quad (3.42)$$

When the wax is in the melting or solidification phase the melted wax becomes more or less depending whether heat is absorbed or released to the colder environment. The melted mass can then be calculated from the following relation:

$$m_{melted} = m_{melted} + \frac{\dot{Q}_{wax(0)(0)nett}}{h_{sl}} \quad (3.43)$$

The mass fraction in the liquid or solid state is then calculated and used in the condition statements to determine whether the wax in the control volume is still melting or solidifying or whether it has completely melted or solidified.

$$X_l = \frac{m_{melted}}{m_T} \quad (3.44)$$

$$X_s = \frac{m_T - m_{melted}}{m_T} \quad (3.45)$$

In the phase change zone it is determined whether the control volume is still in the melting zone and whether all the wax has melted or solidified in the control volume. If for example all the wax has melted then $T_{wax} > T_m$ and $X_{M(l)} = 1$. The logic of the computer program is also depicted in Figure 3.5.

3.10 The numerical modelling of the PCS-SWH system

A novel solar water heater that has an intermediate PCS system is under development. In the current analysis the ideal geometry of such a system for a given load case and geographic position is determined. To achieve a reasonable comparison between different geometries a thermal analysis is conducted that quantifies the incident solar energy on the solar collector and the backup electric energy in order to keep the geyser hot enough, as well as the thermal response of the system under normal environmental conditions. The heat transfer model takes the phase change phenomenon into account as well as convection and radiation losses to the environment. An energy analysis is also conducted to determine where improvements might be made in material selection. The overall system operation can be readily determined and the total hot water that a solar collector system can deliver to the customer is determined under certain usage profiles. The size of the collector, PCS system and geyser is varied while keeping the environmental conditions and the usage profiles similar.

The PCS SWH system that was analysed has the following parameters: The solar collector had a total area of 3.59 m^2 and consisted of 8 heat absorption heat pipes that are each connected to two 75 mm wide 1 mm thick fins inside the solar collector on the lower end. On the higher end it is connected to the PCS system. The solar collector was positioned in a North facing orientation and it was tilted 45° from the horizontal to capture more heat energy in the winter and less in the summer in order to produce a high average throughout the year for the current latitude angle at Stellenbosch of $\sigma = -33.9301^\circ$ and a longitude angle of $\lambda = 18.8647^\circ$. The PCS system consists of 150 kg of PCM with an aluminium volume fraction of $X_{V(al)} = 9.5\%$ which equates to a mass fraction of $X_{M(al)} = 28\%$. The masses of the two components equate to roughly 107 kg of wax and 43 kg of aluminium. The geyser consists of a 150 L tank of water. Both the storage tanks were well insulated with 75 mm of polyurethane insulation with a thermal conductivity of 0.026 W/m K . The storage tanks were covered with a galvanized steel sheet that has a solar absorptivity $\alpha_S = 0.7$ and an emissivity of $\epsilon_S = 0.2$. This resulted in a much lower loss to the environment because of some solar gains during the day and low losses through radiation to the cold night sky.

The user load profile was determined by allowing the user to extract all the available hot water above 41°C at a rate of 10 L/min which is a reasonable rate of hot water draw off for a low flow shower head fully open (Saving Energy, s.a.). The draw off times were selected to be at 07:00 and at 19:00. If the geyser was not heated above the minimum temperature by 06:00 or 18:00 then the geyser was switched on.

The system holds the potential to reduce the annual electric energy peak demand of the residential sector during sunny conditions. This is done by effectively decoupling the electric control volume at the time at which electric energy is used to heat the geyser only during times when there is low demand for electric energy. The main advantage of this system is that this is done without compromising the hot water utility of the solar geyser. The analysis gives further insight into transient analysis of solar thermal PCS systems which incorporate phase change material to store heat at a lower temperature than would be required with a sensible storage material, which results in lower environmental losses as well as a more reliable high temperature heat source for any solar thermal energy application.

The system analysis is divided into the following sections: The solar collector,

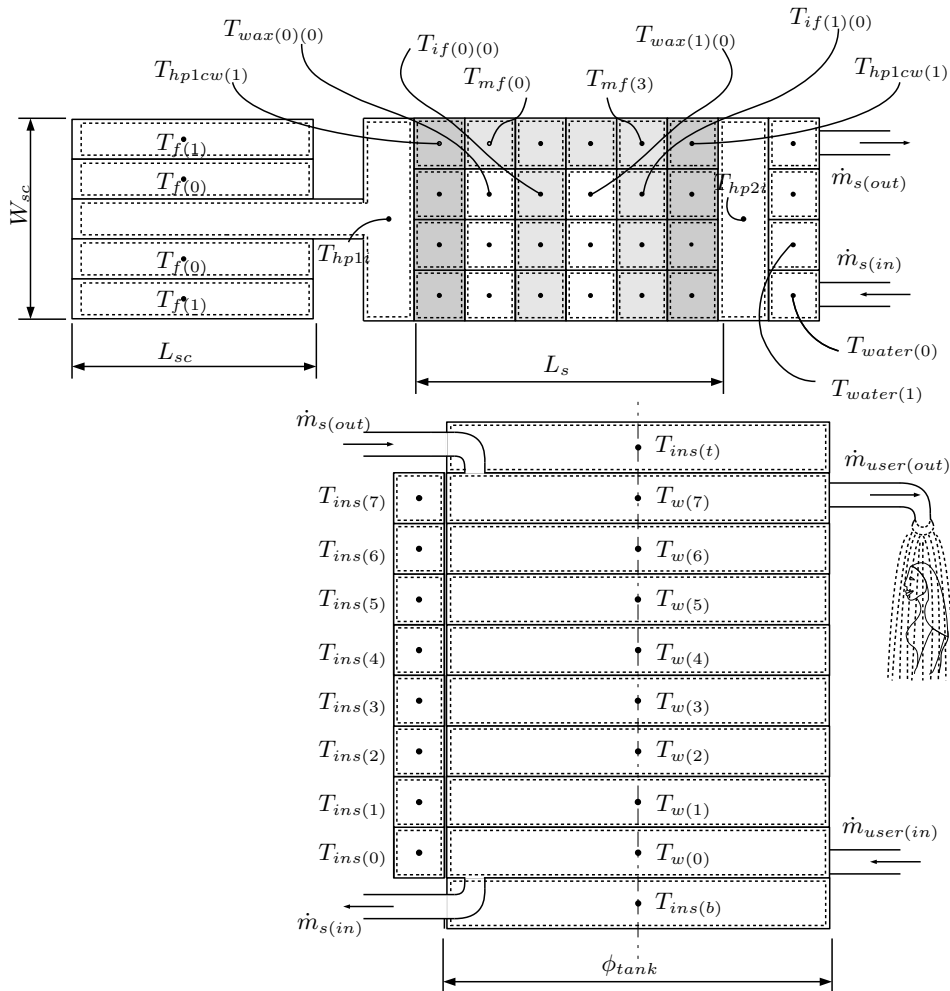


Figure 3.7. The control volumes of the PCM SWH used in the system simulation.

the PCS system, the heat exchanger and the geyser. The solar collector is thermally connected to the PCS system with the aid of the heat absorption heat pipe. The PCS system is also thermally connected to the heat exchanger with the aid of the heat removal HP2. The whole system is modelled to be exposed to the surroundings, this entails that all the components experience heat gain or heat loss due to environmental conditions such as solar radiation, convection to the ambient air and radiation to the sky temperature.

In the thermal simulation model the incident solar energy $Q_{incident}$ as well as the losses to the environment at the collector side $Q_{g(cv)}$ and $Q_{g(rad)}$ are taken into account. The losses from the fins $Q_{fg(cv)}$ and $Q_{fg(rad)}$ will give an indication of how much more energy can be absorbed if the collector is evacuated or if the radiation loss is lowered by decreasing the emissivity of the fin control volumes. The total energy absorbed by the heat pipes that heat up the PCS system needs to be determined. There are 8 heat pipe risers so that means $Q_{hp1(abs)}$ needs to be multiplied by a factor of 8. These risers each go into the PCS system and are each exposed to a number of fin and PCM parts through the heat pipes condenser wall. The energy absorbed in the PCS needs to be calculated by multiplying each PCS control volume with the number of parts, as well as the number of risers. This gives the total energy absorbed by the PCS system. The PCS gives its heat to the heat exchanger through the heat removal HP2. The evaporator is exposed to the PCS control volumes, and the condenser is exposed to the heat exchanger that contains a number of tubes. Water is pumped from the geyser through the tubes which receive heat through the heat removal HP2.

The solar radiation incident on the solar collector is of prime importance, because this is where the main heat absorption from the sun takes place. The position of the solar collector and its tilt angle have a large effect on how much incident radiation will be experienced by the solar collector. The solar radiation is calculated according to the time of year, time of day and geographic position to accurately model the solar radiation that will be received by the solar collector if it is placed in the sun.

The heat pipe acts as a thermal diode in the sense that heat transfer occurs at a high rate when heated from below and heat is extracted from the condenser side. When the bottom is cooled and the top condenser side becomes hotter than the lower evaporator side, then the only heat transfer that takes place is conduction along the thin-walled heat pipe. The difference in heat transfer rates is immense and the heat pipe effectively transfers heat only in one direction.

The PCS system consists of a series of heat pipes that are connected to the solar collector that heats the PCS section. On the other end of the PCS system

the evaporator of the heat removal HP2 extracts heat when the heat exchanger receives cool water from the geyser. The PCS system itself consists of fins that span from the heat absorption side to the heat removal side and are called the main fins. Thin inner fins that are connected to the main fins further distribute heat throughout the PCS system and also act as convection suppressors and form heat paths into the phase change material. Both the heat pipes and the fins act as heat transfer enhancers that increase the rate at which heat can be stored or extracted from the phase change material.

The heat absorption heat pipe and the fins heat up the PCM which stores heat in sensible and latent form during solar irradiation periods and release this absorbed heat during the heat removal phase to the heat exchanger. This heat exchanger delivers heated water to the geyser. The PCS system thus acts as an additional intermediate PCS system that is able to heat up the geyser especially when no solar radiation is available. If this system is to be implemented it is suggested that a thermocouple be placed at the heat removal side of the PCS system and if it measures a temperature sufficiently higher than that in the geyser, then the pump that circulates water through the heat exchanger to the geyser, must be switched on. The geyser backup element must also be linked to the control system and only be switched on if there is not enough heat stored to heat the geyser at a sufficient rate.

The geyser is modelled as an upright cylindrical tank with its diameter equal to its height to reduce heat loss rates to the environment. The geyser is insulated with 50 mm of rock wool. The water control volumes $T_{w(0-row_x)}$ are modelled as horizontal disks that loses heat to the environment to the sides, top and bottom of the geyser. The inside water control volumes lose heat through natural convection to the sides, top, and bottom. The heat is then conducted through the insulation to the outside where heat is transferred to the ambient air through either natural, mixed or forced convection depending on the wind speed around the geyser.

Heat is also transferred to the cold sky temperature through radiation. The geyser element is located in the bottom of the geyser and heats up the bottom control volume if there is insufficient heat energy available in the system. For example, after the PCS system has had the whole night to heat up the geyser and it is still not hot enough, than the geyser switches on in time before the residents wake up to use hot water. After the geyser has switched on the bottom control volume may become hotter than the one above it. If the bottom control volume is hotter than the control volume above it, then the switch places with each other. In this way the whole tank may be heated with the geyser element. In the simulation the consumer uses warm water from the geyser in the morning and in the evening until the water temperature falls below 41 °C at a rate of 10 L/min, which is the rate at which a normal shower

head discharges water during use.

The system analysis consisted of a solar collector, PCS tank, heat exchanger and solar geyser. Each component is dynamically linked to the other components. If the solar collector geometry is altered this will have an effect on both the temperatures that the PCS system and the solar geyser will achieve. The sizes chosen for the present analysis are a 2.4 m² solar collector, a tank of 150 kg of PCM with a 5% volume fraction of fins. The geyser selected is a 150 L geyser. The solar collector is tilted 45° from the horizontal and is aimed north because of its location is in the southern hemisphere. Both the PCS system and the geyser are modelled as cylindrical containers that have lengths equal to their diameters to minimise losses to the environment through convection and radiation.

The system is modelled for four consecutive clear sky days during the time period of the summer solstice that occurs during December 21. The simulation runs from December 20-23 to eliminate the effect of start-up conditions. It is noted that the first day acts as a start-up period. For example the start-up conditions are set to 21 °C but after the first day of simulation all temperatures of the PCS are above 30 °C. Also the maximum temperatures reached are lower in the first day compared to the simulation days after it. Because the next three days closely resemble each other it was deemed sufficient to test only for four days to determine the specific case's performance. It is noted that the system acts as a system in series. The whole system heats up throughout the day, both the solar collector, PCS and the geyser. During such a sunny day both the phase change material and the water in the geyser heat up above melting temperature as well as above the minimum water temperature of 40 °C. This enables the system to deliver hot water for nighttime use. The extra energy acquired in the PCS medium is also sufficient to heat up the water for early morning use, although there is slightly less hot water available in the morning because of the lower temperatures of the water control volumes in the geyser. It is however still hot enough to be usable without the need for the electric backup element to be switched on. The backup element will therefore only be used during long periods of overcast or rainy weather or during periods when an excessive amount of hot water is utilised.

3.11 Conclusion of numerical model

In the thermal numerical model the experimental module described in Section 4.4 which comprises of wax melting at a constant temperature of 59 °C and which expand from a density of 910 kg/m³ to 790 kg/m³ and the wax control volumes expand in the height while the wax absorbs its latent heat of fusion

of 200 kJ/kg during melting. Only a small section of the module is modelled by discretising the section into control volumes. The storage section control volumes are divided into long single control volumes in the height as shown in Figure 3.3. The different control volumes that are found in the model are described, and the phase change of the wax is described by the discrete approximation Figure 3.6 where it is depicted how the wax heats up or changes phase or cools down and how the numerical model uses the different equations to keep track of both the temperature, density and melt fraction of each wax control volume.

The numerical model of the storage module is then linked thermally by connecting the heat absorption side of the PCS system to a solar collector as well as linking the heat removal side of the PCS system to a geyser. The whole system is modelled using solar irradiation values that may be experienced when a clear day is experienced, as well as calculating convection and radiation losses from the solar energy system.

Chapter 4

The experimental set-ups, testing and analysis of the designed thermal storage module

In Chapter 3 the numerical model that is used to calculate theoretically how fast the storage module absorbs heat during heat up or how fast heat is removed during cool down. This chapter describes the experimental set-ups used and the rationale for choosing the finned PCS module with heat pipes set-up is described in Section 4.1. The experimental set-ups include the initial tests, such as the heat pipe characteristic test and the kettle cool down test, as well as the full heat absorption and heat removal cycle of the PCS modules. The experiments include the analysis of the temperature change that occurs during the heat absorption and heat removal cycles of the PCS module and the calculation of the heat transfer to and from the PCS module. Using the experimental tests as a point of reference, the numerical model of the PCS module will be compared and finally calculate how well a SWH system that has an additional PCS system connected to it will perform.

4.1 The modular set up rationale for using rectangular test section, paraffin wax, heat pipes and an aluminium fin matrix

The experimental PCS unit needs to consist of a module that could be replicated easily to build up a passive PCS system. It is decided that an organic paraffin wax should be used as PCM because it has highly uniform cyclic ability with low thermal degradation, is non toxic and has a reasonably high energy density. The basic HTE building blocks that the author chose are rectangular micro heat pipes and aluminium fins. The shape of the rectangular heat pipes are ideal for distributing heat all across its exposed heat transfer surfaces in a uniform manner. A kettle is chosen as a heat source because the temperature range that the water can be heated to is between ambient and boiling temperature. This high temperature is sufficient to melt the wax within a reasonable period of time, and in a solar collector, where such storage

systems will be incorporated in future, similar temperatures could be reached in the solar collector. When the evaporator section of the heat pipe is placed in the heated kettle water it will transfer heat uniformly to the condenser section because of saturation conditions that exist within the heat pipe. The fins effectively enlarges the effective surface between hot fins and the cooler wax and reduces the distance that the heat needs to be transferred through the wax and shortens the melting and solidification period.

The main work are the PCS modules' heat absorption and heat removal tests. During heat absorption the PCS modules are heated up to 80 °C and during heat removal they are cooled to below 35 °C. A suitable PCM for this test set-up was chosen, namely paraffin wax, with a melting point of 59 °C. The selection is based on the temperatures that can be achieved in the experimental tests, see Figure 4.2. The hot temperature can't reach temperatures far above 90 °C before the water in the kettle boils. The cold side of the experiment is at about 16 °C, so 59 °C seems like a good intermediate temperature for the test. In real solar water heating applications using the concept design in Figure 1.5, a wax melting temperature of at least 59 °C and possibly up to 80 °C is suggested, since this hotter intermediate PCM will result in heating the water faster and to a higher temperature.

The storage section is chosen to be long and rectangular in shape with the heat pipes placed flush on either side. The reason being that the heat pipes will either introduce or remove heat all along its exposed surface and the heat front will effectively progress horizontally all along the height of the storage module. Furthermore by choosing a narrow width of 72 mm the heat absorption and heat removal period is reduced because the absorbed heat only needs to be transferred a maximum of 72 mm through the fin material. This width is sufficient to measure the heat front progression during the test.

Also the fins were baked together such that when the wax is poured in between the fins the wax will form long narrow components. These wax control volumes will be able to expand or contract in the vertical direction. Heat will be transferred by conduction because the long narrow wax compartments will not experience strong convection currents because of the long very narrow shape of the compartment. The heat removal rate will be increased because of the many finned heat conduit passages, which will result in fast solidification periods.

4.2 Indoor test set-up of the heat pipe

The heat pipe was tested separately by placing the bottom part known as the evaporator inside the kettle water. The top section is connected to a heat exchanger as indicated in Figure 4.1. The tests conducted included slowly

heating the kettle while also passing water through the heat exchanger. From this continuous operation during both heat up and cool down of the kettle the heat transfer characteristics of the heat pipe were determined. The results are summarised in Section B.1.1.

4.3 Indoor testing of the wax only PCS module

The experimental modules shape were specifically selected to be long and rectangular. This rectangular PCS system was heated from the heat absorption side until completely heated, and then heat was extracted from the heat removal side. This specific geometry, heat source and heat sink enable virtually uniform heating from the side, as well as cooling from the other side. By using the rectangular heat pipes which use a working fluid that exist at a given saturation temperature all along its length during operation heat is uniformly supplied or extracted along the length of the PCS system. Heat is also transferred uniformly along the depth of the rectangular heat pipe which will result in two dimensional flow as seen from the side. A few similar heat

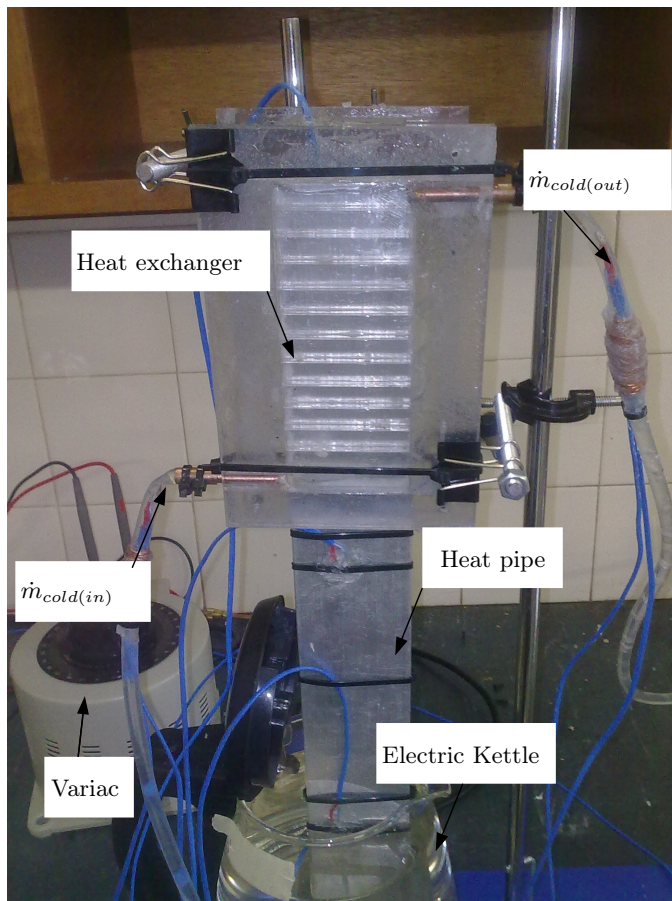


Figure 4.1. The test set-up for the indoor heat pipe characteristic tests.

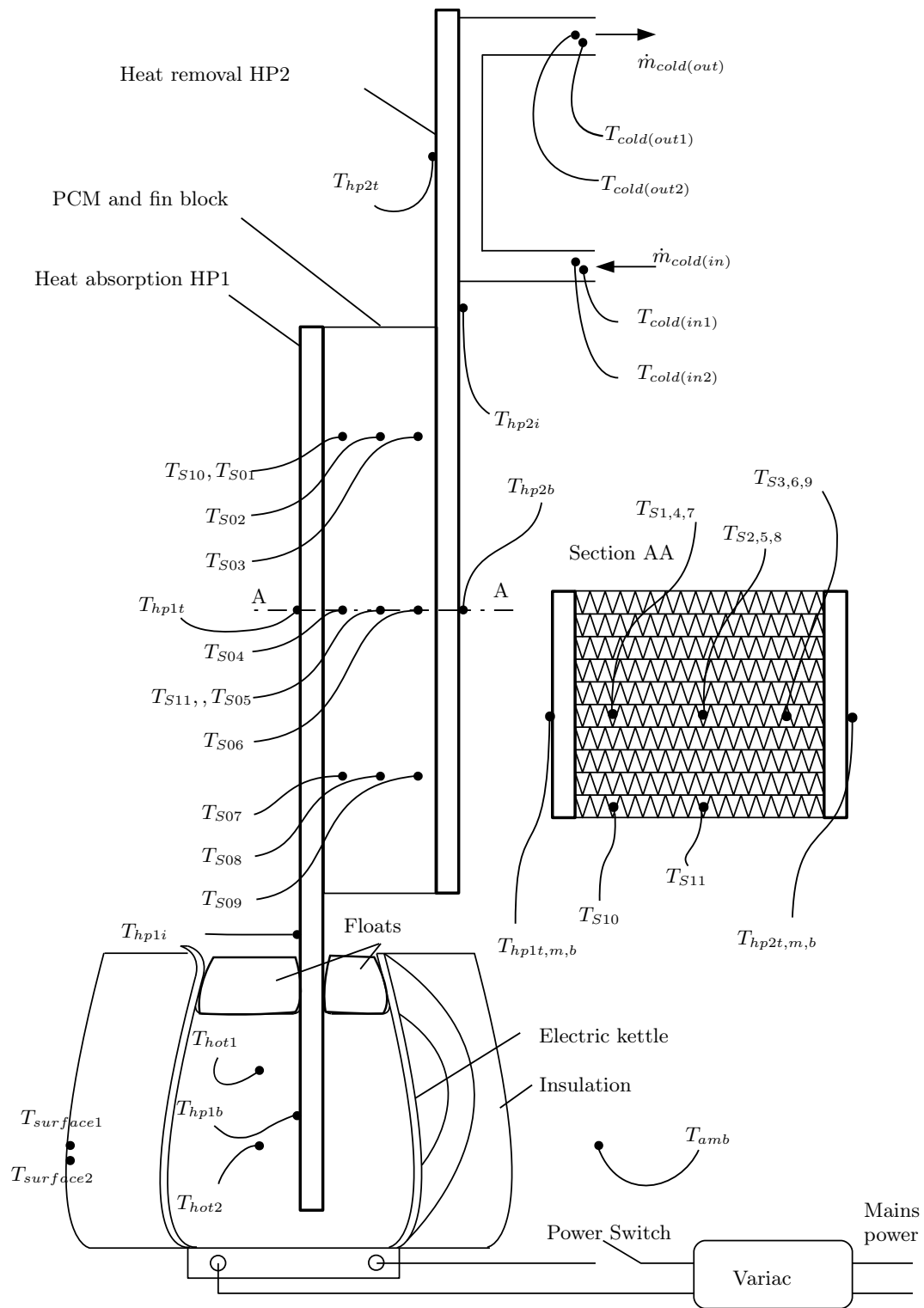


Figure 4.2. The diagram of the test set-up of the indoor experiment depicting the thermocouple names.

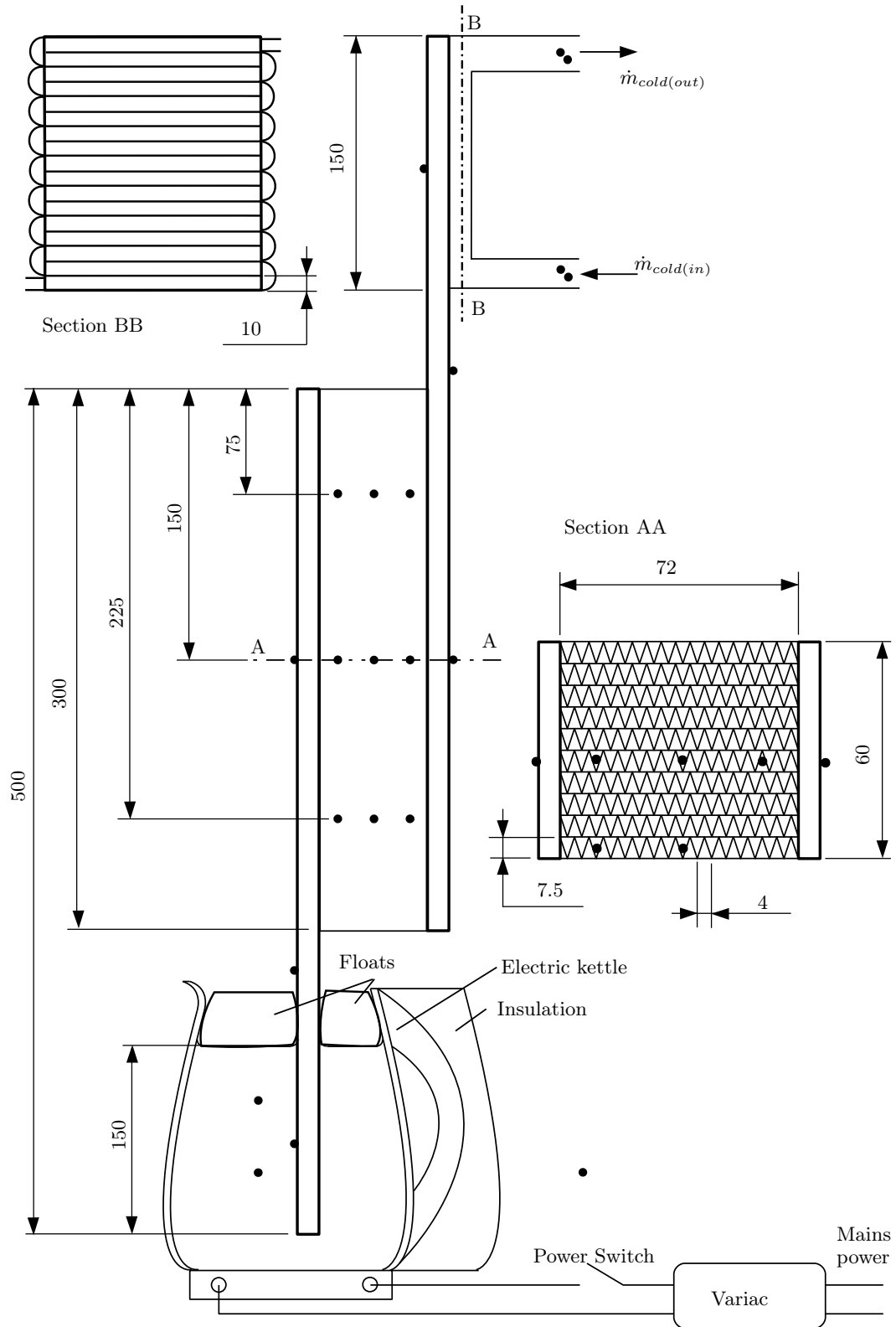


Figure 4.3. The diagram of the test set-up of the indoor experiment depicting the important dimensions in mm.

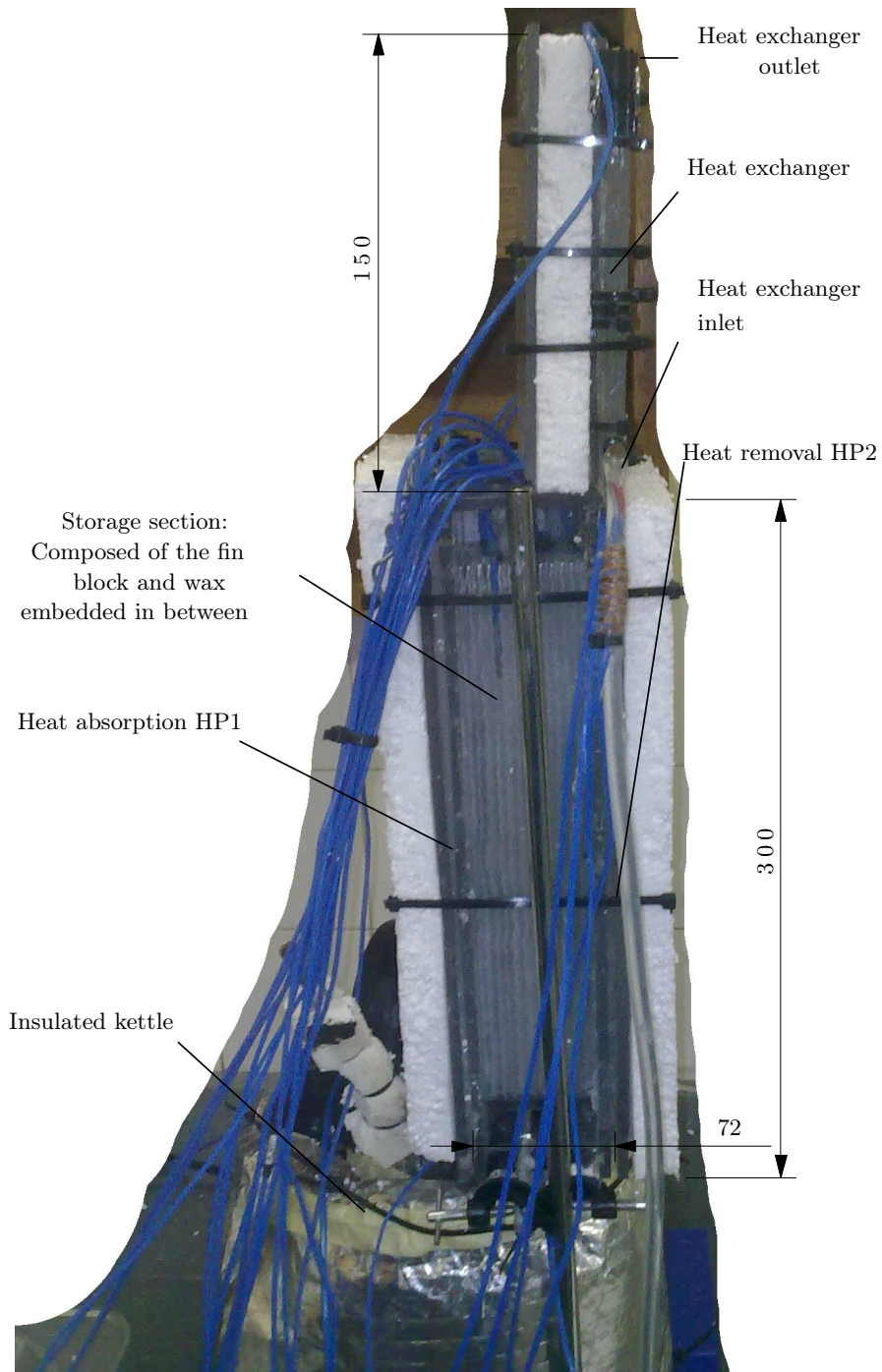


Figure 4.4. The photograph of the test set-up of the indoor experiment. Dimensions in mm.

absorption and heat removal cycles of the experimental tests were conducted on both the experimental modules to detect the sensitivity of the system under certain conditions and to establish that there is reliability in the system during operation. Three tests were conducted on the heat pipe that was placed one end in the kettle and the other end connected to the heat exchanger. A total of three heat up and cool down tests were conducted on the wax only test module, and a total of six heat up and cool down tests of the finned PCS module was conducted.

The test set-up comprised a variable heat input electric kettle and one thermal storage unit that comprised two heat pipes, one at the heat absorption side, and one at the heat removal side. It also contained the thermal PCS system containing either wax as heat storage material or wax with fins in between, as shown in Figures 4.2 and 4.4. The temperature measuring points of the experimental set-up were placed at certain positions to measure the heating up and cooling down of the wax during the heat absorption and heat removal cycles. The thermocouple measuring points were placed along the width and along the height. This was done to capture the heat absorbed in the horizontal and in the vertical directions.

The one test consisted of the storage module filled only with wax. The heat absorption HP1 was immersed in the hot kettle water at the lower evaporator side. The wax only tests consist of the heat absorption test and the heat removal test. First the wax was heated through the heat absorption HP1 until it was completely molten. The heat removal side was insulated during this test. Then the heat removal test was conducted by first extracting the hot water from the kettle and then the cool down test was conducted by letting cold water from the constant head tank flow through the heat exchanger that was connected to the heat removal HP2 T_{hp2} .

4.4 Indoor testing of the PCS module with fins as HTE

Metallic fins are a cheap and widely available option to consider to enhance heat transfer. Their application in car radiators make them available at mass production prices. The aim was to manufacture fins that enables sufficient heat transfer during solidification when the PCM solidifies onto the fin surfaces and forms an insulative layer which reduces heat extracted from the PCM. The final fin geometry is measured and incorporated into the thermal simulation. The enhancement can readily be altered by using thicker or alternately thinner fins to enhance heat transfer and contain the wax in long vertical convection suppressed containers. The fins used in the experimental module were baked together in a factory in an oven at 590 °C with aluminium paste and cut to

size for the experimental module. Thermocouples were placed inside the finned PCS system. The fins were then heated above melting point before pouring liquid paraffin wax in between the fins. Tests were done by heating up the PCS module to above the melting temperature or alternatively cooling it to below the melting temperature to capture the whole heat absorption and heat removal cycle characteristics of the PCS system.

To quantify the inner parts of the PCS system, comprising the heat pipes and the PCS system (the wax and HTE mix), it is suggested by Rausch *et al.* (2011) that each major component be tested separately and then grouped together in the final analysis of the system. This will aid in fault detection of the heat pipe and component characteristic tests, for example it will help to test the components separately to make sure the heat pipe is working optimally and that the simulation of the particular component is correct, and a better overall understanding of the interactions between components will be realized. This relates experimentally to testing and simulating the heat pipe with a hot source at the bottom evaporator side, and a cold water draw off at the condenser side. The inner heat transfer coefficients of the heat pipe are obtained in the initial test set-up shown in Figure 4.1 . The coefficients are determined by solving the resistance diagram in Figure 3.2 after including the temperature measurements. Temperature readings are taken on the wall of the heat pipe at the evaporator, adiabatic and the condenser section. The temperatures of the hot side and the inlet and outlet temperatures of the heat pipe are also measured. The resulting distribution is calculated, and then the heat pipe and the wax section is tested together. The initial set-up comprises one heat pipe with its lower end immersed in hot water, which receives a constant flux of energy at the evaporator side, and a constant water flow rate across the top heat exchanger in the condenser.

4.5 Methodology of analysing the absorbed heat in the the storage section of the numerical and experimental modules

The heat transferred to the wax is calculated numerically by calculating the net heat transfer to each control volume and adding all the control volumes that exist in the PCS module. The heat transferred to the experimental section is calculated from the temperature measurements. The sensible heat absorbed as well as the latent heat absorbed by making use of the effective heat capacity method. This method entails assigning a melt fraction to each temperature measurement ranging between 40 °C with a melt fraction $X_{M(l)} = 0$ and 59 °C with a melt fraction of $X_{M(l)} = 1$. It is assumed that the melt fraction varies linearly with temperature for this approximation. The wax and fin container

was divided into 5 vertical sections and each section was approximated as having the same temperature as if it is one control volume each.

4.6 Observations of flow phenomena during the experiments conducted

During the testing of the PCS module, it was observed that all the wax does not stay within its column, but because of expansion during melting and contraction during solidification the wax migrates between vertical segments, especially during solidification. During this phase the wax is effectively sucked to the extractor side and large and small voids form at the heat absorption side. This phenomenon is not accounted for in the mathematical modelling, but rather each container of wax is modelled to stay static inside its respective compartment.

4.7 Sensors and instrumentation

The instrumentation for experimental analysis consisted of two data acquiring modules connected to a data acquiring system. The data acquiring system connects through a USB connection to a laptop containing National Instruments software. The sensors consisted of T-type thermocouples, a stopwatch and a 600 ml measuring container. The thermocouples were calibrated with the aid of a variable temperature machine and a resistance thermometer. In Appendix A the results are given with an in depth description of the calibration procedure. The flow rates were very slow and the total error in measuring the time was negligible. Several measurements were taken of each flow rate to establish that constant flow at a certain rate was achieved. This was done to reduce the measuring error even further.

The sensors and instrumentation used were composed of the following components: A DAQ system: National instruments p/N 190415B-01 that has four slots and in which two National Instruments 16 sensor points data acquisition drives were placed. Their model number and serial numbers are: DAQ01 model number 198854B-01L serial number 1537000, and DAQ02 model number 199272A-01L serial number 148DA46. The calibrating equipment which was used was a calibrator, which is described as a Field metrology well with process readout: model 9142 serial number B29291. The reference thermometer that was used was a platinum resistance thermometer with model number 9351472 and serial number 191069. The thermocouple was calibrated Feb 2013 by SANAS calibration laboratories certificate number RAP 15738



Figure 4.5. The solidification of the wax during the heat removal cycle.

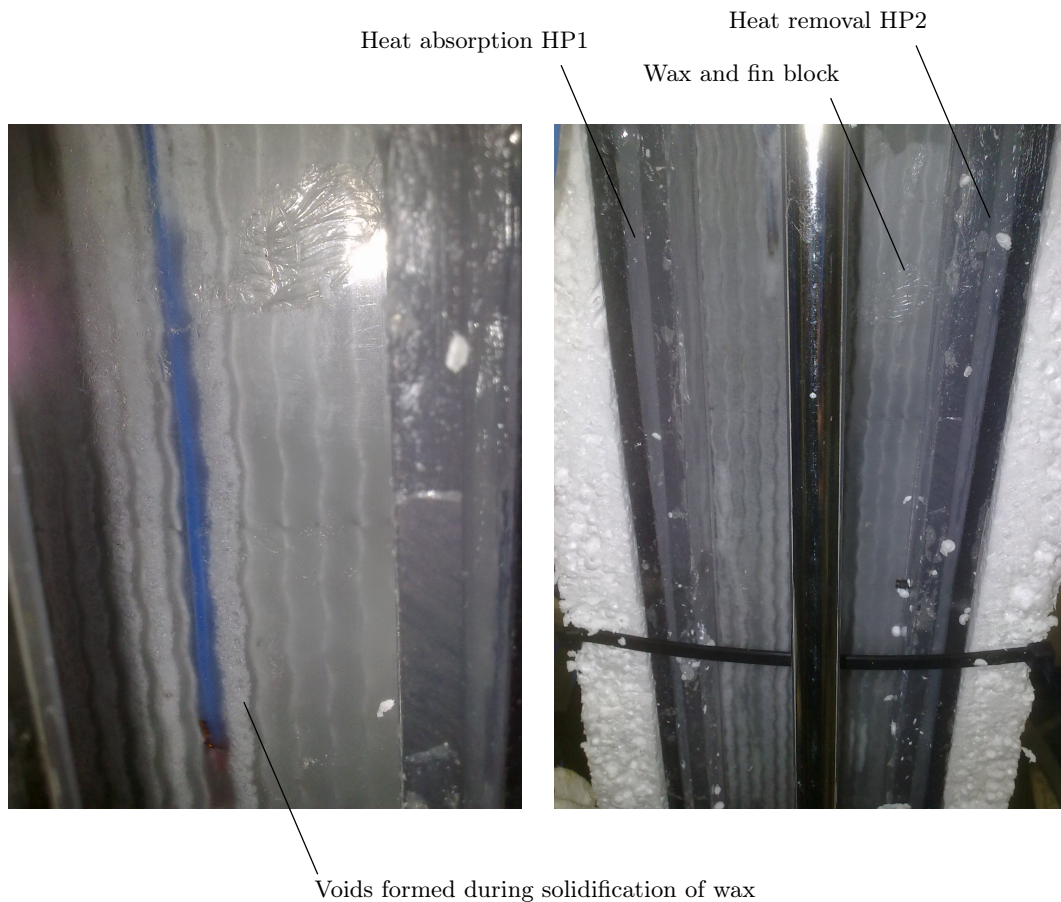


Figure 4.6. The final state of the wax after a complete heat removal cycle.

4.8 Health and safety

Safety is of prime concern. The manufacturing and testing procedures were developed with the possible risks and hazards in mind. For example the heat pipes contain acetone which looks similar to water but which is poisonous if drunk and if it gets in your eyes it may cause serious damage. The acetone was handled with care and kept only in clearly marked containers and it was stored away safely after use. The heat pipes were also developed to handle the internal pressures that the vapour in the pipe exerts on the pipe walls when overheated, and the heat pipes performed well under normal operating conditions. The wax used in the tests was ordinary candle wax with a melting temperature of 59 °C. This is the legal melting limit for candle wax to prevent scalding when a drop of liquid falls onto your skin. The containers were well sealed to prevent leakage and decrease the risk of scalding in the extreme case where a large amount of wax splatters onto your skin. Wax was melted with a resistance heater and with boiling water that both have the inherent risk of causing burning or scalding a person who is unaware of the risks involved. Clear caution signs were put in place during PCS module creation and during test

operations and no burns were experienced during the testing of the systems. The design can be made even safer by either embedding the wax into a clay mixture or fusing it with plastic. Afterwards there would be no risk of leakage even when the wax is melted. This added safety measure is an important factor to consider when choosing designs.

4.9 Conclusion of experimental set-ups

In this chapter the different experimental set-ups are described. Starting with a short introduction, which is followed by a description of why this particular set-up was chosen in Section 4.1. It was described how the current experimental setup was chosen not only for easy analysis by making use of a thermally symmetric geometry, but also because the set-up is modular and can easily be scaled to form a storage system that is able to store heat at a low temperature that will reduce losses to the environment. A description of how the heat pipe was set up and analysed is given in Section 4.2. The set-up of the wax only experimental module is described in Section 4.3 and the finned module is described in Section 4.4. Then the Methodology is described and the visual observations are recounted. The sensors and instrumentation is described as well as the health and safety aspects inherent in the design and set-ups. The set-ups were chosen to shed light on the operation modes of the heat pipes and the modules were designed to have transparent container materials in order to easily observe the melt front and the expansion and contraction during the phase change processes.

Chapter 5

The numerical and experimental results

The experiments were conducted with the aim of characterising the thermal storage unit. The tests conducted give in depth information about the characteristic response of the heat absorption and heat removal heat pipes, the electric kettle and the wax and aluminium fin PCS system. During the analysis of the PCS system energy balances of the different components were calculated from the experimental measurements. From these calculations the heat loss of the kettle to the environment, the heat loss from the PCS system to the environment and the energy flows from the kettle into the PCS module was calculated during the heat absorption cycle. Also during the heat removal cycle the heat flow from the PCS module to the water passing through the heat exchanger was calculated. The total energy transferred into and from the PCS system was calculated as well. The characteristic response of the heat absorption and heat removal of the heat pipe was also determined and compared to the initial characteristic response of the multichannel rectangular heat pipe.

5.1 The results of the tests done with the experimental wax only PCS module

The control test that only contains wax in the PCS PCS system develops a clearly defined melt front during melting. The shape resembles the letter 'P' as shown in Figure 5.1. The heated heat pipe melts a vertical layer of wax. This layer contains hotter liquid which is less dense at the top than at the bottom, this hot wax cools down when it interacts with the solid wax surface. More wax is melted at the top by the hotter liquid wax than at the bottom. This results in a hotter liquid wax region at the top and a colder solid region in the right bottom corner that takes a very long time to melt completely.

When the wax is cooled down there is no visibly clear solidification front. There is however a clear heat front which is captured by the thermocouples inside of the PCS system. The sensible liquid heat is first extracted during the initial heat removal period and then a solid layer forms on the heat removal

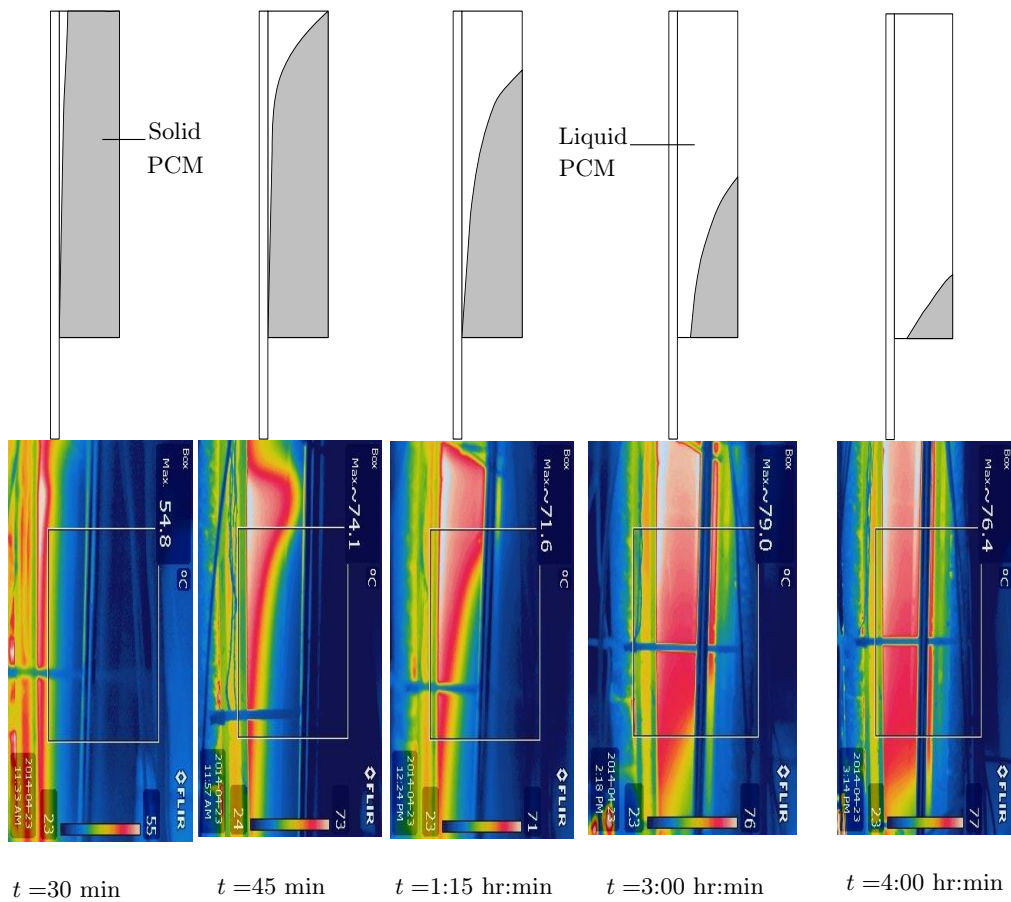


Figure 5.1. The melt front development during a heat absorption cycle of the control PCS module.

HP2. Heat removal rates into the heat exchanger decrease quickly to very low values. The solid wax therefore forms an insulative layer which decreases heat transfer to the heat removal HP2. The rest of the wax clouds over and small solid pieces form. Finally as it completely solidifies a large void forms in the centre of the wax structure almost all the way to the bottom as it solidifies and contracts.

The PCS module without fins takes a very long time to cool down (more than 6.5 hours), and after an hour and a half the temperature difference across the heat exchanger becomes very small even at very low flow rates and it becomes difficult to measure the heat removal rate accurately, as almost no heat is extracted from the PCS system through the heat exchanger. During such a long heat removal period the total energy loss to the environment through the polystyrene insulation also becomes significant. It is noted that the wax in the control test is initially much hotter than in the wax and fin test set-up. The control set-up acts as a minimum baseline test. These test results are now

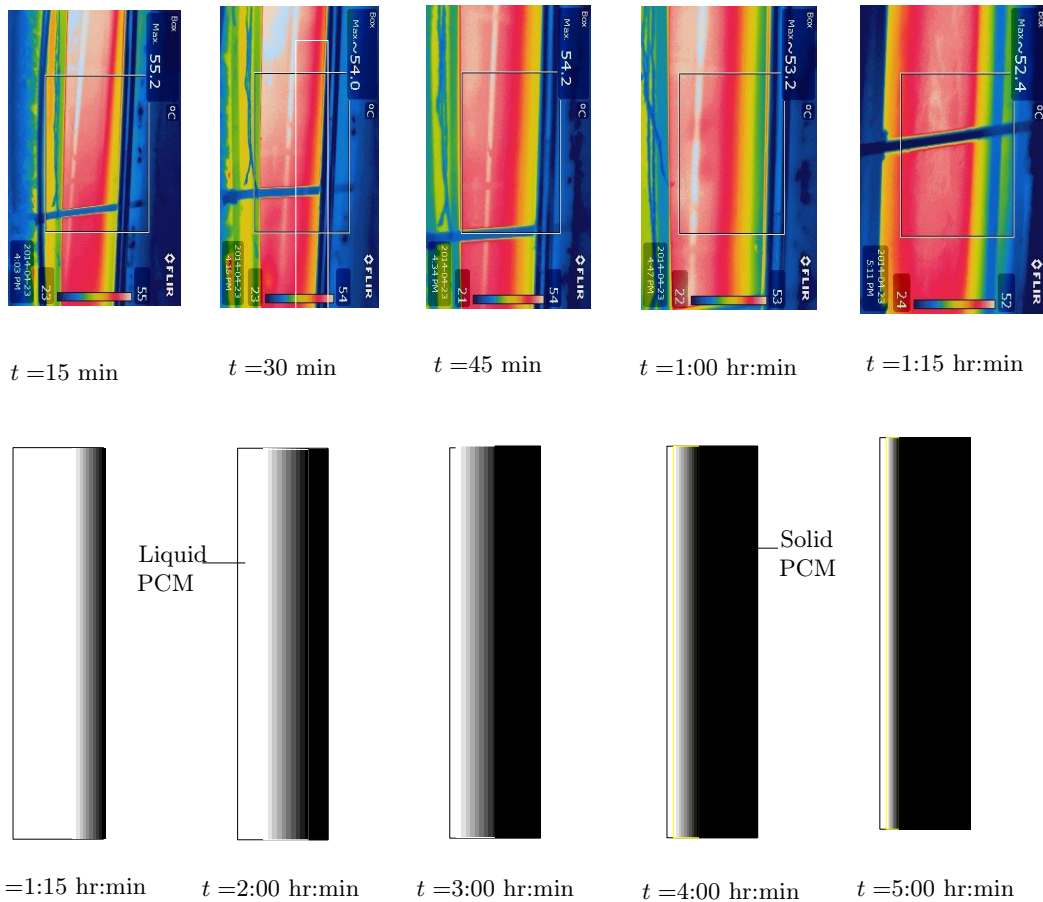


Figure 5.2. The heat front development during a heat removal cycle of the control PCS module.

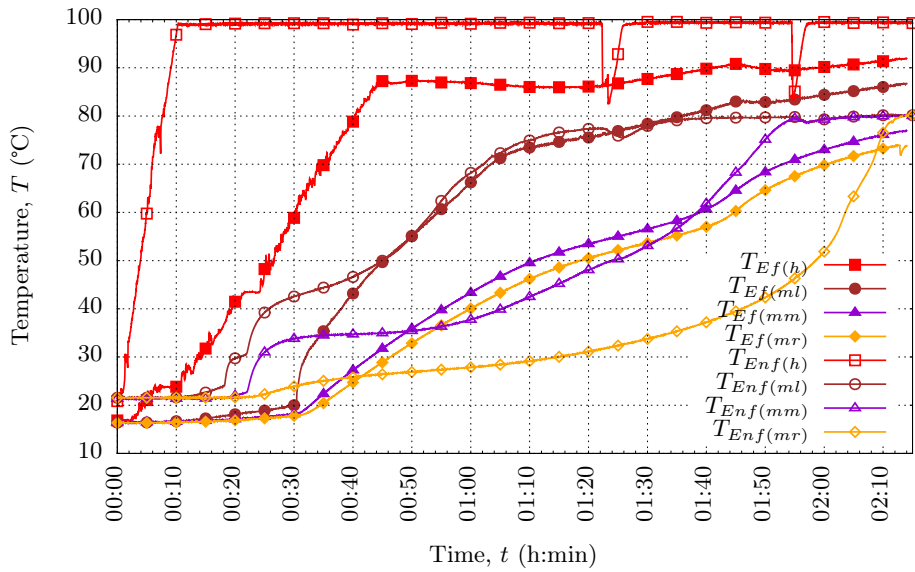


Figure 5.3. Temperature comparison between the PCS module with and without fins during a typical heat absorption cycle.

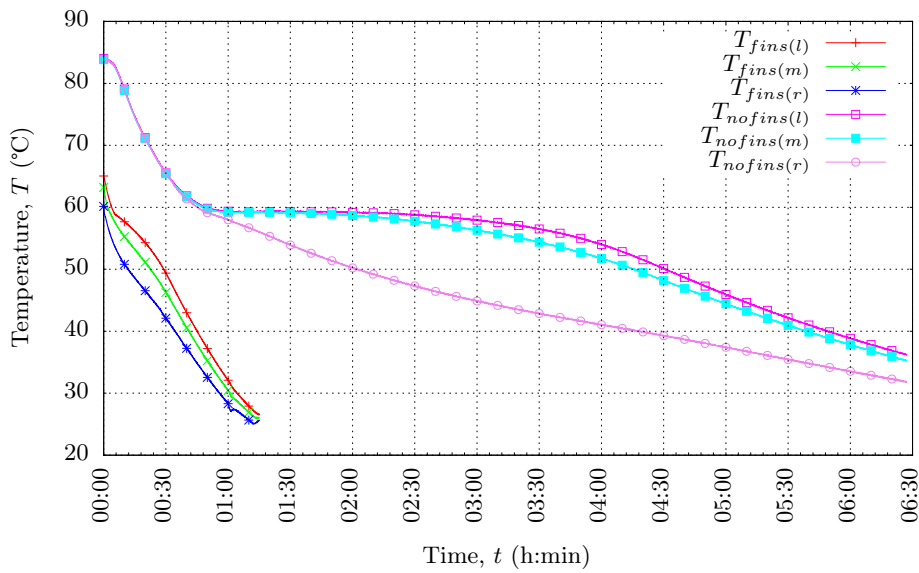


Figure 5.4. Temperature comparison between the PCS module with and without fins during a typical heat removal cycle.

compared to the results of the test of the module with fins and it can be seen in Figure 5.4 that the fins significantly improves the heat removal rate to the heat exchanger.

The power and total energy extracted from the PCS system for the control test and the test with fins is given in Figure 5.5. The difference between the tests was that the initial temperatures of the control test were higher because of the long heat absorption test that was done to melt all the wax in the PCS system. Even though the control test was hotter initially and the PCS system contained 20% more wax than the fin test the wax only control test was unable to transfer all its heat to the heat exchanger to heat up the water in it. During the heat removal cycle only 130 kJ was extracted in the test period of one hour fifteen minutes. During the fin test on the other hand, 260 kJ was extracted which is twice as much energy during the same time period even though the finned PCS module was colder initially than the control test. This shows that the fins have a dramatic effect on the heat removal rate as well as the total energy that will be delivered to the water that is circulated to the geyser.

5.2 The results of the tests done with the experimental and numerical PCS module with HTE

The temperatures inside the wax and fin PCS system increase quickly when heated from the heat absorption side until the wax starts to melt as indicated in Figure 5.6. The rate of temperature change then decreases and this rate is then maintained until all the wax has melted. The temperature then rapidly increases again but it flattens out quickly before reaching thermal equilibrium. The reverse is also true for the heat removal cycle as indicated in Figure 5.7. The temperature quickly decreases until the first control volume starts to solidify. The rate of temperature change then decreases until all the wax is solidified. The rate then quickly picks up again before finally flattening out at the thermal equilibrium. The general temperature variation trend is similar to the experimental results, but with clearer cut zones which signify the initiation or the total change in phase. This may be because the thermocouples measure a discreet point, while the discretised control volumes calculate a small section of wax.

The temperature profile shown in Figure 5.6 gives an indication how much heat has been absorbed in the PCS system. The experimental and numerical responses differ. The differences are that the change in the gradient during a heat absorption cycle occurs at a lower temperature. This occurs at about 40 °C, and it increases again when all the wax is completely melted at 59 °C.

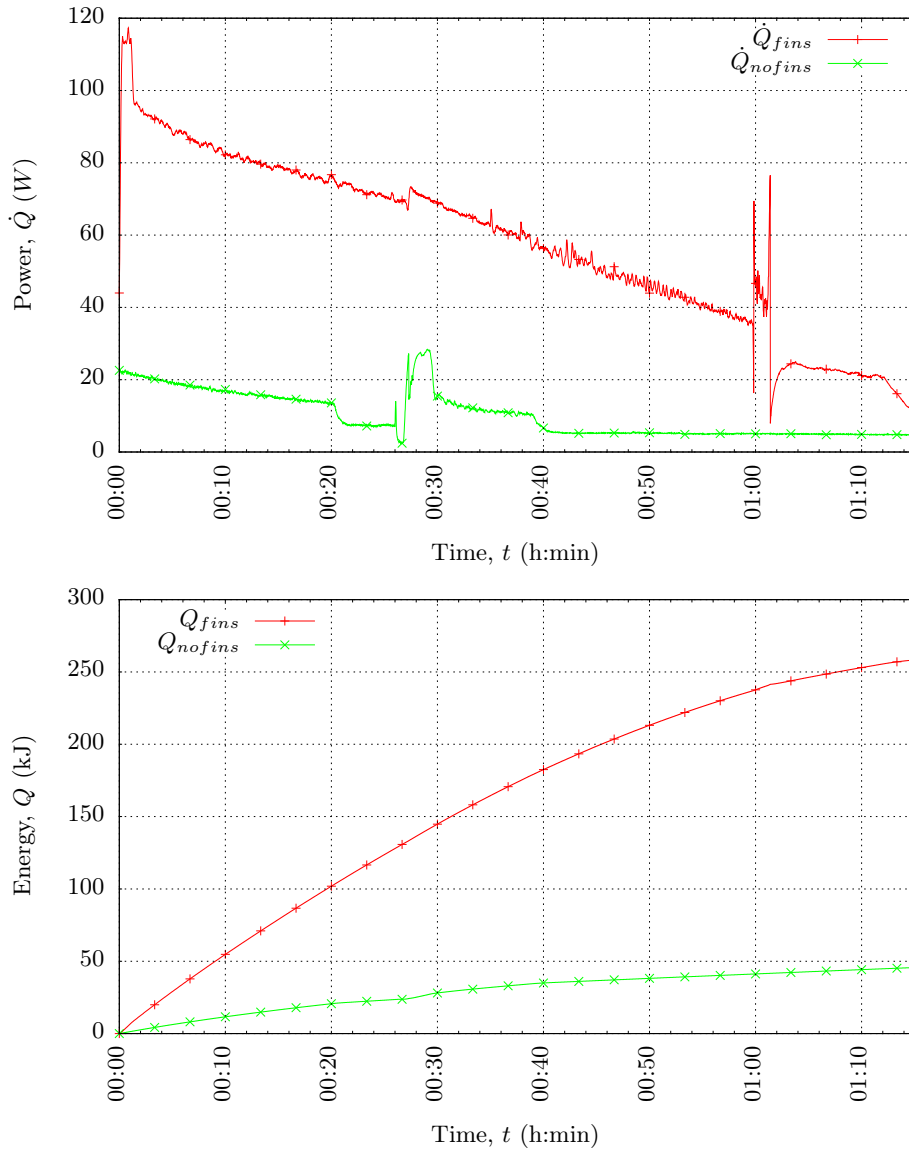


Figure 5.5. Power and energy comparison between the PCS module with and without fins during a typical heat removal cycle.

The probeless thermocouples indirectly indicate the onset of melting in the finned PCS system by the decrease in temperature gradient when the wax starts to absorb heat in latent form and melting is initiated. It is assumed in the calculation of the absorbed energy in the wax storage that the wax absorbs sensible heat as it heats up, as well as latent heat in the temperature range between 40 °C and 59 °C. The energy absorbed in a wax section is given by the following correlations. First the sensible energy is taken into account:

$$Q_{wax\,sensible} = m_{wax}c_pT_{wax} \quad (5.1)$$

extra

During the heat up experiments there is time lag between the onset of heating by the hot water in the kettle and the thermal response to heat up. This is mainly caused because the micro heat pipe only starts to transfer heat effectively when the temperature difference between the hot kettle water T_h and the condenser wall temperature is large enough. In this case it was about 20 °C. The time period for complete heat absorption of the PCS system was about the same if the 30 minutes lag period is taken into account.

As indicated in Figure 5.7 there is no lag period during heat removal because initially the temperature difference between the PCS system and the water coming from the heat exchanger is quite large. This causes immediate start-up of the heat removal HP2. The main differences between the experimental and numerical modules are that the numerical module cools down to water inlet conditions, but the experimental module cools down more slowly and decreases more slowly than the numerical module. This may be because of the contact resistance between the heat pipe and the fins, as well as the insulating effect of the solidified layer of wax that forms on the fins and the heat pipe and again the thermocouples measure at a location close to the centre of the wax compartment, which results in a slightly higher measurement than the wax interfacing with the fins. Overall the temperatures indicate close correlation between the experimental and numerical module test findings and the numerical module is validated.

In Figures 5.8 and 5.9 the temperature variation and melt fraction is indicated during a typical heat absorption and heat removal cycle. The sensible heating takes place first, but almost comes to a standstill when the heat front progresses by means of melting the wax control volumes. This is noted by taking a good look at the progression of the melt front in the wax control volumes. Then when all the wax is melted the wax heats up sensibly to thermal equilibrium. During the heat removal cycle the reverse happens and the freeze front progresses from the right to the left. This finite control volume visualisation aids in understanding the operation during heat absorption and heat removal of the PCS system and is used as a means of numerical model verification.

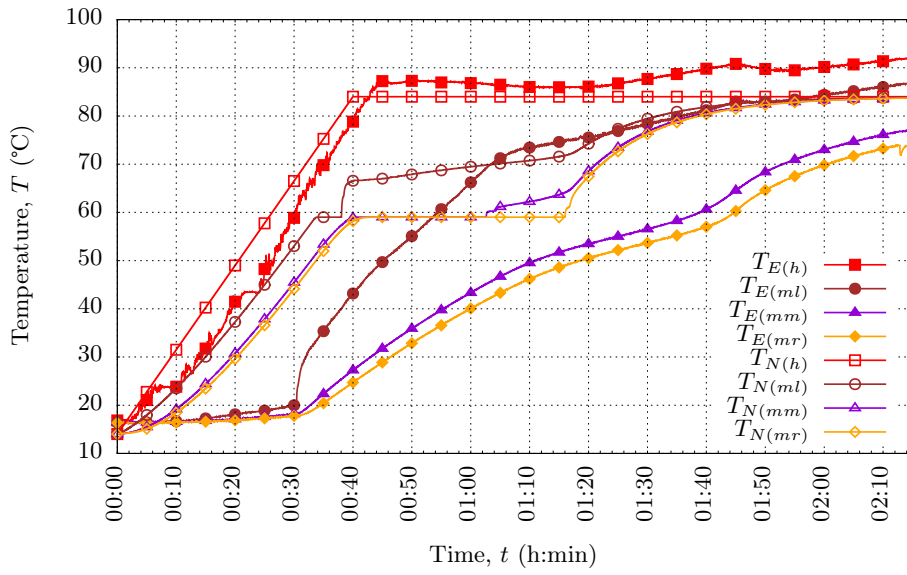


Figure 5.6. Temperature response during a heat absorption cycle of the experimental and numerical module.

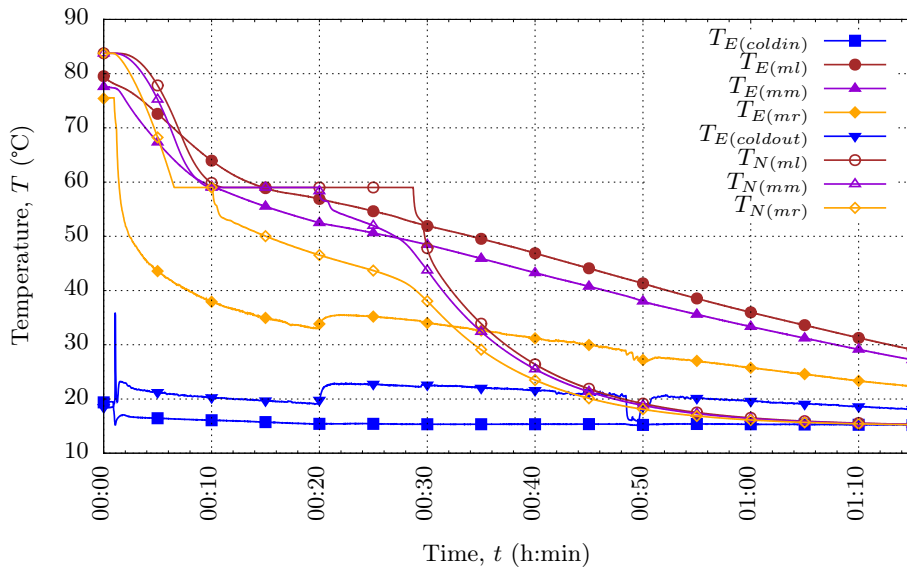


Figure 5.7. Temperature response during the heat removal of the experimental and numerical module.

The heat transfer rates that result during the heat absorption of the PCS system follow the characteristic sequence as depicted in Figure 5.10. The power absorbed increases as the temperature difference between the kettle and the wax control volumes increases, but then when the melting initiation point is reached the power absorbed starts decreasing. The rate then decreases very slightly until the melting is completed. The rate of heat absorption then decreases to zero as thermal equilibrium is reached.

During the heat removal mode there is a difference between the experimental and numerical responses. This is mainly due to the slower flow rate in the experimental heat removal test which was kept so in order to ensure that the temperature difference stays large enough to minimise the error readings when calculating the heat absorption in the heat exchanger. The rate of heat removal is initially large in the first 10 minutes, but then it drops down to round about 100 W and it stays close to constant for about 30 minutes. The rate then decreases until no significant heat is removed from the PCS module. It is noted that the rate of net energy uptake of the aluminium fins drops to almost zero during the melting and the solidification modes and that they act as pure isothermal heat conductors to the melting wax control volumes. It is also noted that the shape of heat uptake and heat removal rates closely correlate with the measured experimental rates.

It is also noted that the numerical model extracts heat faster than the experimental test. The shape of cool down is however very similar to the physical experiment. The difference may be due to the wax storing some latent energy across a temperature range between 40 °C and 59 °C and does not deliver all its latent heat at the higher assumed temperature of 59 °C used in the numerical analysis. It is suggested that a micro-crystalline wax melting at above 59 °C be used in SWH applications to increase heat transfer to the geyser.

During the analysis the energy absorbed in the PCS module is kept account of by equating the energy absorbed to the amount that the PCS system heats up and by the amount of wax that has melted in each control volume. In Figure 5.8 the heat absorption cycle of the PCS module is graphically represented. The temperatures in the PCS system initially heats up quickly because of the large temperature difference between the hot water and the wax and fin control volumes. The wax temperature variation then dramatically changes when it starts to melt. The fins now act as heat conduits that transfer heat to the melting wax, and the melt fraction progression can be clearly seen in Figure 5.8.

The cool down phase is graphically represented in Figure 5.7. The cool down occurs at a much faster rate because of the high heat transfer rate caused by the forced convection in the heat exchanger. During the heat removal cycle

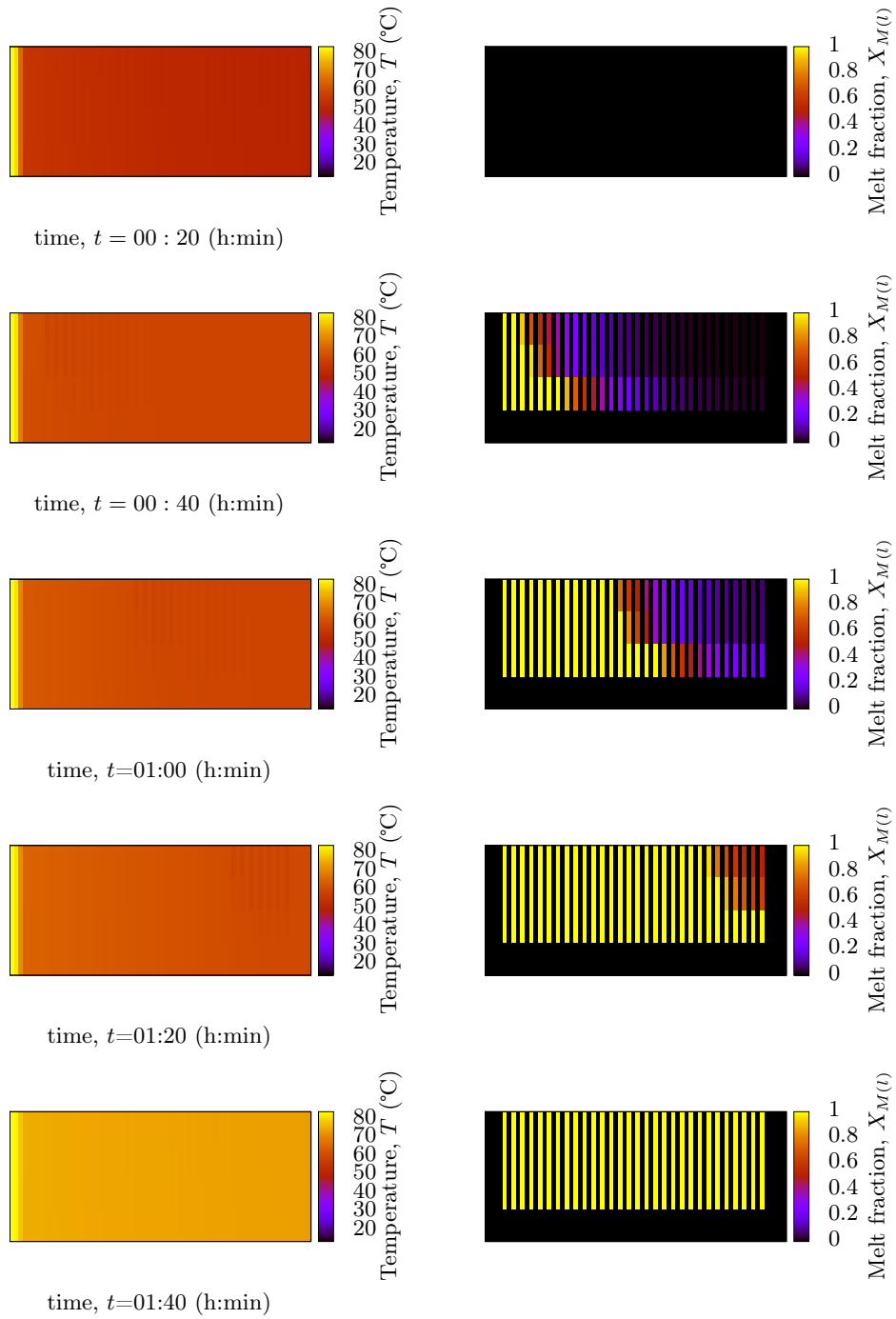


Figure 5.8. The numerically determined temperature variations and the melt fraction of the PCS module as viewed from the top during heat absorption only from the heat absorption side.

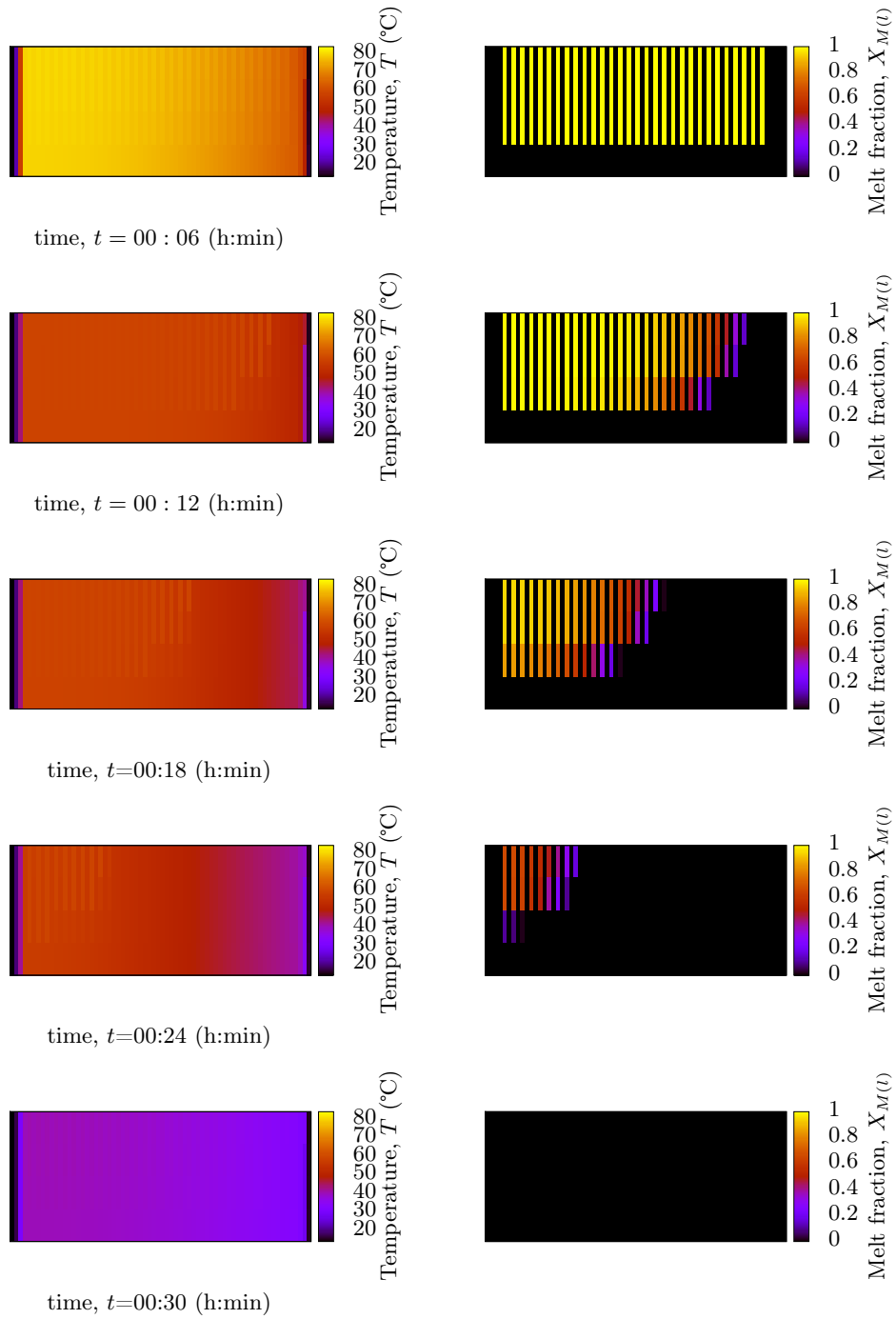


Figure 5.9. The numerically determined temperature variations and the melt fraction of the PCS module as viewed from the top during cool down only from the heat removal side.

the whole PCS system cools down until all the sensible energy in liquid form is extracted. Then the melt fraction decreases in the rightmost control volumes first because it is cooled from the heat removal side of the PCS module. The molten wax becomes less and less until it is totally solidified in all the wax control volumes.

The fins are heat transfer enhancers that aid the absorption of heat as well as the heat removal from the storage module. The fins form vein-like heat conduits that reach deep into the PCS system and delivers heat at a close to constant temperature during heat removal. It is noted that the heat transfer coefficient acting upon the PCS system has a large effect on the heat absorption or alternatively the heat removal rate of heat to and from the PCS system. These heat transfer coefficients are therefore determined experimentally and checked against theoretical calculations so that the numerical system is well matched with the experimental module. These comparisons make it possible to validate the numerical model.

The heat absorption heat transfer rates can be seen in Figure 5.10. The numerical analysis indicates that the heat transfer rate forms a ‘dome’ shape, first the heat rate increases strongly and as the module heats up the temperature difference between the hot kettle water and the wax storage decreases. This results in the heat transfer rate decreasing until thermal equilibrium is finally reached. The assumption to divide the test module into five sections resulted in a jagged heat transfer result, but overall the numerical simulation is approximated by the five control volumes.

During heat removal the numerical heat removal heat transfer rates are considerably higher than those of the experimental module, as can be seen in Figure 5.11, and as already mentioned the reasons for this could be thermal contact resistance between the heat pipe and fin or the insulating effect of the wax as it solidifies onto the heat transfer surfaces. The flow rate was also not precisely the same as in the numerical simulation, therefore the heat removal was slower in the experiments to keep the temperature difference high enough to keep the measurement error small. Finally void formation could also play a role to decrease the heat transfer rate.

The total energy absorbed in the PCS system is the highest line in Figure 5.12. When melting starts the aluminium main fin suddenly greatly slows down in energy uptake. The aluminium almost stops heating up and transfers almost all its absorbed heat to the melting wax. The wax absorbs heat at a constant rate because of the constant temperature condition of the melting wax at $T_m = 59^\circ\text{C}$. The aluminium absorbs more energy only when all the wax has melted before it comes to a quasi steady state at thermal equilibrium. The heat extracted from the PCS system is at first very fast, then it slows

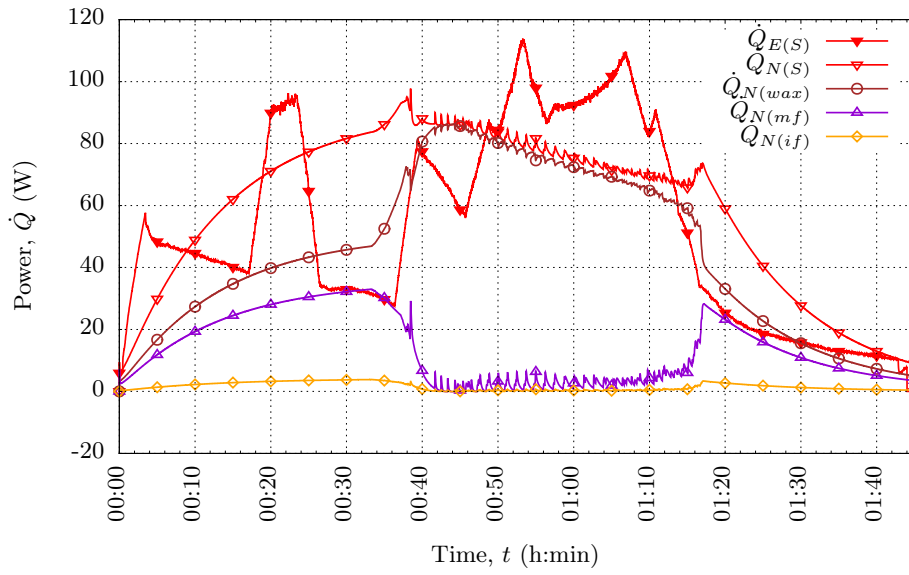


Figure 5.10. Heat transfer rates during a heat absorption cycle of the experimental and numerical module.

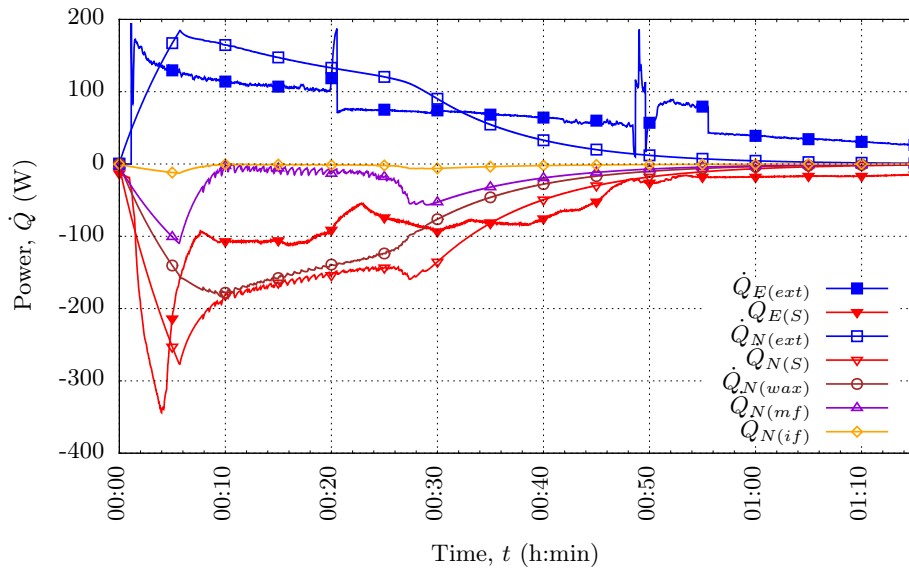


Figure 5.11. The heat transfer rates during heat removal of the experimental and numerical module.

down before coming to a complete stop at thermal equilibrium when the PCS system is completely heated.

Figure 5.12 shows how much energy is absorbed during the heat absorption test of a 0.87 kg wax storage unit. Most of the energy is absorbed in latent form and this is indicated by the close to constant rise in absorbed energy during the heat absorption test. The experimental and numerical tests correlate very well with each other, and taking the 30 minute lag time into account the results are very similar both in magnitude and in time needed to heat the unit.

The extracted energy indicates that the time it takes to physically remove the heat from the PCS unit is in fact longer than the numerical model predicts. This is partly due to differences in the heat removal rate of water through the heat exchanger and the numerical model as well as contact resistance and the insulating effect of the solidifying wax layer. The energy was however extracted much faster with the fins than without them and the model shows a similar shape during energy removal. This verifies the numerical model for the current shape and fin geometry and it can therefore be used with confidence to model PCS systems in solar applications.

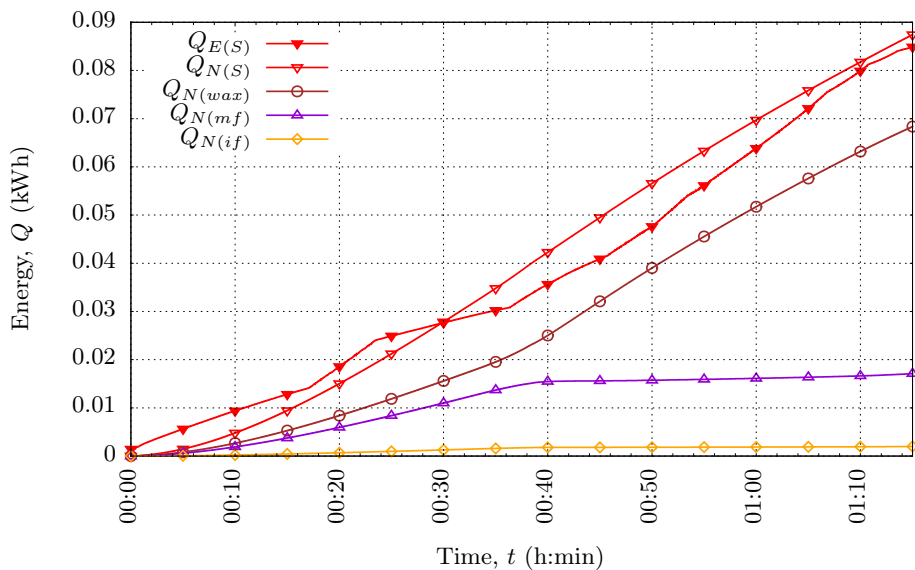


Figure 5.12. The energy absorbed during heat absorption of the experimental and numerical module.

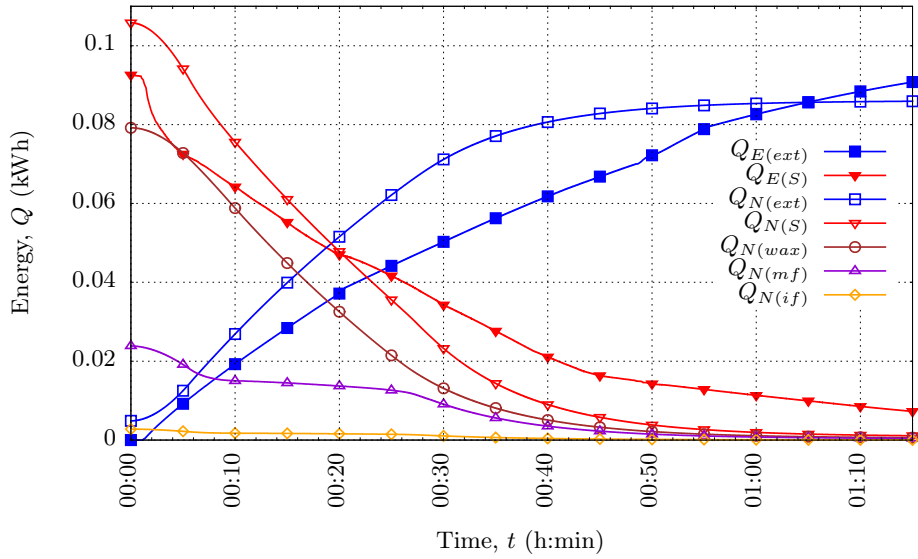


Figure 5.13. The energy extracted during heat removal of the experimental and numerical module.

5.3 The results of tests on the numerical PCS SWH system with HTE

For the final analysis the geyser was never required to be switched on, because the PCS system was capable of heating the geyser to the required temperature during the nighttime after the hot water had been extracted from the geyser.

The simulation was run for four consecutive days during the summer solstice period from 20-24 December in the southern hemisphere location of Stellenbosch. The resulting temperatures during this transient analysis were plotted in Figure 5.14. The plot indicates the last two days of testing to indicate the pattern that was followed during the analysis. The temperatures indicate that all the wax melts during the day, and that during the nighttime it completely solidifies as it transfers its absorbed heat to the geyser water. This results in a whole tank full of hot water for early morning use.

The total incident energy that the collector experiences is given in Equation 5.2 and it is plotted in kWh in Figure 5.15.

$$Q_{inc} = \sum_{t=0}^{t_{end}} \dot{G}_{sc} A_{sc} \Delta t \quad (5.2)$$

The total energy absorbed by the solar collector is also given, as well as the energy finally absorbed from the PCS system into the geyser. The total

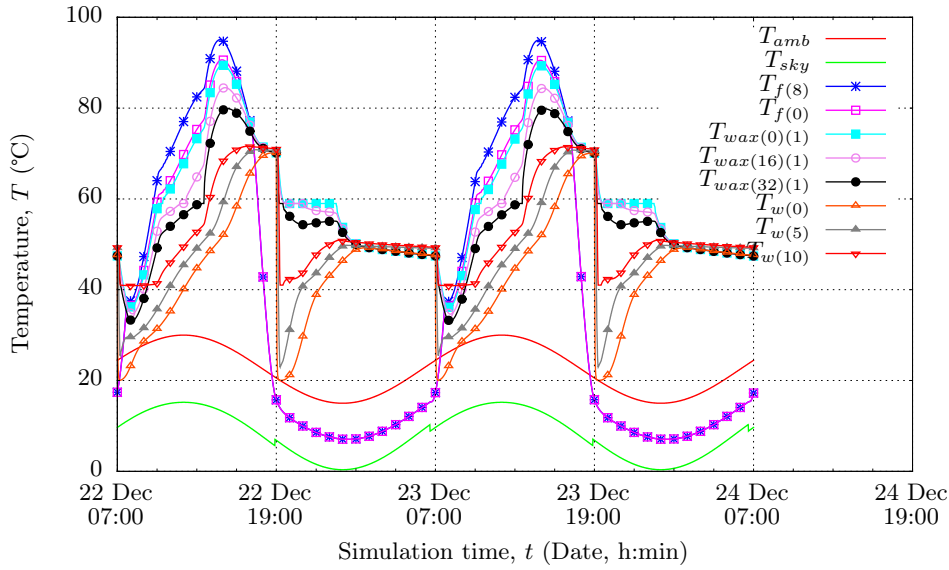


Figure 5.14. The temperatures that the solar collector, PCS system and geyser reach during two typical sunny days during the summer solstice.

energy extracted from the solar collector during the four consecutive days of testing is also given. The solar collector was treated with a selective coating that has an absorptivity $\alpha_{sc} = 0.87$ and an emissivity of $\epsilon_{sc} = 0.1$. The total absorbed energy during the four days amounted to 19 kWh which is less than half of the incident solar irradiation on the solar collector. It is noted that the losses to the environment of the two storage tanks were offset by the solar irradiance incident on the storage tanks. Also quite a lot of the incident energy upon the solar collector is either lost through convection or it is radiated out of the solar collector. This high value is partly because of the relatively high operating temperatures of the solar collector which is required to melt the paraffin wax and heat it sufficiently to increase the temperature of both the geyser and the PCS tanks to above 60 °C during the day.

The energy contained within the PCS and the geyser is plotted in Figure 5.16. This gives an indication of how much energy is absorbed and where it is stored before it is used by the consumer. During the day both the PCS and the geyser are heated up in series, first the PCS heats up and then the geyser follows suit. During hot water use by the consumer the energy level in the geyser is dramatically lowered, after which it is increased again by the heat transfer from the PCS system to the geyser.

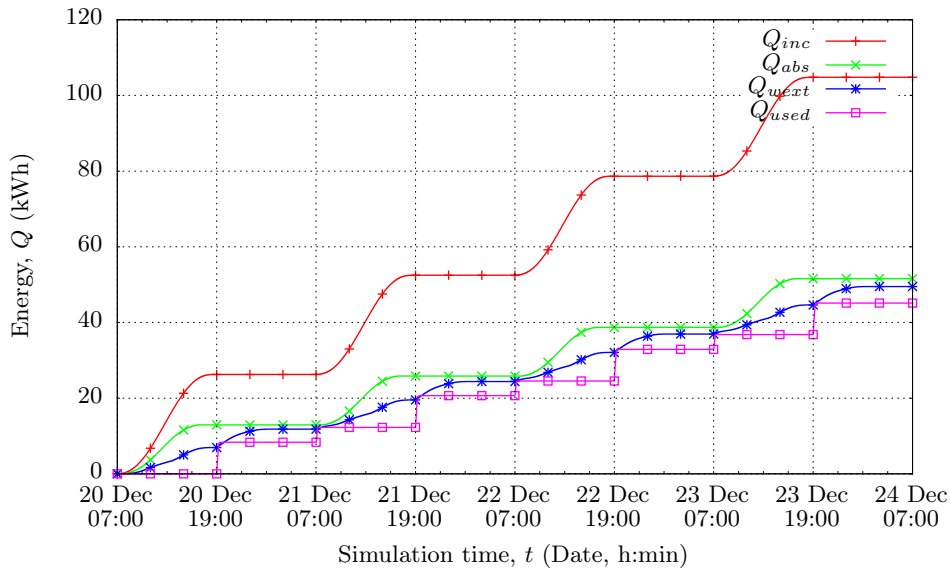


Figure 5.15. The total energy incident on the solar collector, as well as the total energy absorbed by the solar collector and extracted from the PCS system to the solar geyser as well as the total energy used by the consumer.

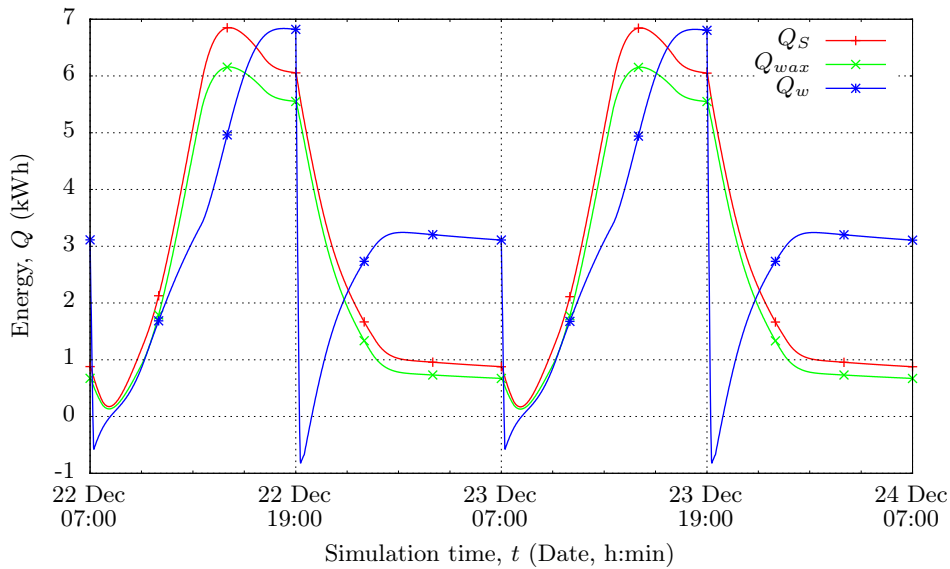


Figure 5.16. The absorbed energy in the PCS system and specifically the wax as well as the energy in the geyser during two consecutive days of operation.

5.4 Discussion of the results

The experimental and numerical test results are given in this chapter and in Appendix B. This included heat transfer tests that was conducted on the heat pipe. The heat pipe was tested by submerging the lower condenser part in an electrically heated kettle and connecting a heat exchanger to the top evaporator part. The steady operation of the heat pipe gave an indication of how fast heat could be transferred through the heat pipe. The heat pipe was found to exhibit three stages of heat transfer as indicated in Figure B.1. The first of these is a proportional initial heat transfer stage, when the temperature difference between the hot source and the cold sink is small. When the temperature difference increases the heat pipe reaches a transition stage where heat transfer rates decrease. Finally when the temperature difference is very large the heat transfer rate drops to a plateau or to a limit phase of heat transfer.

A cool down test of the electric kettle was also conducted. The tests gave an indication of how fast heat would be transferred to the environment at any given kettle temperature. It was found that the hotter the temperature of the insulated kettle becomes, the higher the losses to the environment will be as shown in Figure B.4. The heat loss relation was however only found to be accurate when the kettle wasn't boiling the water as this resulted in high losses of the kettle water by evaporation. Tests were therefore conducted without the kettle boiling to keep better track of the energy transferred into the system from the electric kettle element, to the kettle water, which in turn heats the PCS module through the aid of the heat absorption HP1 during the charge cycle, and from the PCS module to the water that is passed through the heat exchanger.

The experimental test module without fins was characterised by very slow heat removal rates, the heat absorption rate however was enhanced by increasing the kettle temperature to very close to boiling, and convection currents in the liquid wax played a significant role in melting the solid wax, as can be deduced from the melt profile in Figure 5.1. The finned PCS module heated up slightly faster and more uniformly than the wax only PCS module, even though the kettle temperature was kept below 90 °C in the finned test. During heat removal of the finned PCS module, heat was extracted at a much higher rate than in the wax only PCS module, as can be seen in Figure 5.4, even though the temperature in the finned PCS module was lower at the beginning of the heat removal cycle.

The thermocouples in the finned wax PCS system measured the temperature variations that occur during heat absorption and heat removal cycles. It was found that the temperature variation along the height is small during normal operation when heat is uniformly applied from the side as shown in Figure

B.7, or uniformly extracted from the side as shown in Figure B.8. It was also found that the whole PCS system increases in temperature as it is heated from the side and the heat is therefore transferred very effectively in the horizontal direction as indicated in Figure B.5 during heat up, and during cool down in Figure B.6. The thermocouples' temperature readings were used to model the heat absorption or heat removal rate and energy absorbed or extracted from the wax module. It was found that by representing the thermocouple reading as a representative energy level of the control volume, good correlation could be found between the energy removed from the wax and the energy absorbed in the water passing through the heat exchanger.

The heat transfer coefficients of the heat pipe during heat absorption and heat removal cycles were calculated from the experiments. An average value was then used in the numerical analysis. With these values included in the numerical model, the experimental and numerical test results compared very well. The numerical model of the test module is validated from these tests.

This numerical model was set up to model the experimental tests of the module containing fins. The correlations found experimentally of the heat transfer coefficients from the water to the heat pipes, the heat transfer coefficients experienced inside the heat pipes, the thermal material properties and geometry of the wax and fins, as well as the test conditions that were applied to the experimental test were incorporated in the numerical model. The results indicated in Figure B.13 showed that there is a very good correlation between the experimental and numerical models. The numerical model was able to calculate the time period that it would take to transfer heat to the heat exchanger, and the amount of energy that would be transferred from the wax to the water. The numerical model successfully calculated the thermal response during heat absorption and heat removal cycles of the PCS system. It is concluded that the numerical model of the PCS can be used as a building block in solar thermal system analysis.

The PCS module without fins is comparable to the 5 cylindrical heat pipe and PCM storage section designed and tested by Robak *et al.* (2011b) and given in Figure 2.3. It also took 4 hours (when comparing Figure 2.4 with Figure 5.4) to solidify completely during the heat extraction mode. Take into consideration that this is a very rough comparison which does not take into consideration the mass flow rate of the cooling water or the possible temperature that the storage can heat water to. The finned PCS however was able to extract all the heat that was previously absorbed in latent form in the wax as well as most of the sensible heat within only one hour. This is a vast improvement and opens up possibilities of using finned systems even without heat pipes to transfer the heat throughout the PCM.

When comparing the natural convection currents that exist in the molten wax during melting of the wax only PCS module the natural convection currents were significant in increasing the melt front propagation just like in the tests conducted by Robak *et al.* (2011a), but it was much easier to distinguish it because of the two dimensional melt front as shown in Figure 5.1. The very long solidification time period underlined the possible improvements that can be obtained with fins. In the work conducted by Laing *et al.* (2009) aluminium fins are suggested because of their high thermal conductivity and low density that results in low cost per volume of fins. They do however suggest that the fin configuration be optimised, and for a PCS-SWH this could result in a good mass production solution. Laing *et al.* (2009) tested a 8.51 kWh PCS model that has NaNO_3 as PCM that melts at 306°C . Rectangular horizontally placed fins were used and pipes were passed through these fins. The finned configuration was then placed in the storage container before liquid PCM was poured into the container. It was found that the system could deliver an average of 4.3 kW for 1 h 40 min to deliver a total of 7.2 kWh during the heat removal phase.

The possible improvement noted by Laing *et al.* (2009) is that the fin material could still be optimised to use less material and still yield good thermal results. Such a system was developed by Laing *et al.* (2013) which is composed of a 700 kWh finned PCS system. This system is depicted in Figure 5.17 and shows the snowflake like fins that extend from the circular pipes. In a similar way the rectangular system can be optimised to use less material and still deliver sufficient heat during the heat removal phase.

When comparing the proposed PCS-SWH to the system studied by Metawee and Assassa (2006) that which is described in Section 1.5 the new concept is able to extract heat much more uniformly and quicker because of the heat pipes and fins that extracts the heat from the PCM. When compared to the system also described in Section 1.5 of citeCanbazoglu2005 the new PCS-SWH was able to be stored at temperatures far higher than the melting temperature, thereby increasing the possible energy capacity per volume of PCM. When looking at the wax movement during expansion and contraction during the phase change the new PCS-SWH is more predictable when compared to the system of Liu *et al.* (2006a), because the wax compartments are allowed to expand in the vertical direction and stays within its respective compartments.

The numerical model of the PCS module was validated by comparing it to an experimental module exposed to similar operating conditions. The numerical model was then used in a solar water heating simulation. It was found that by using many modules, that each use a smaller amount of fin material, that amounts to 150 kg of wax and 34 kg of fin material, the PCS system was able to heat up a cold geyser during the night for morning use, as indicated in Figure

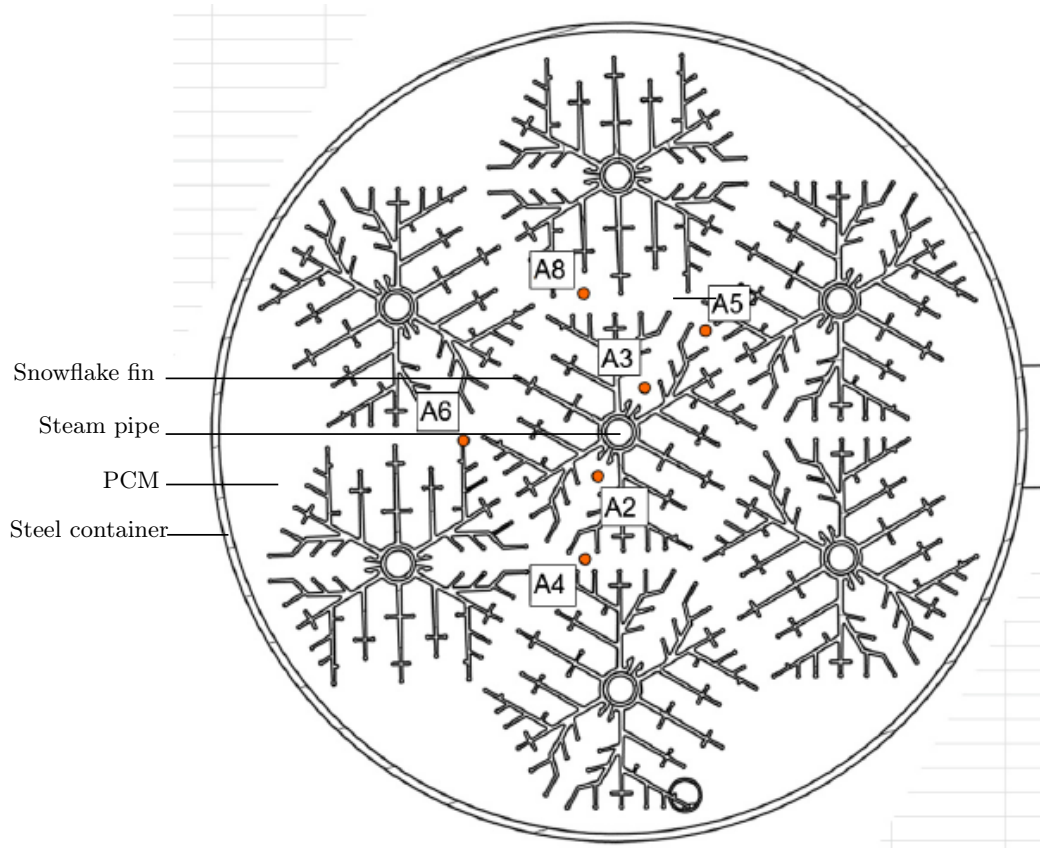


Figure 5.17. The finned PCS system cross section as seen from the top which was developed by Laing *et al.* (2013).

5.16. It was found that a large amount of latent heat was stored inside the wax during sunshine periods and that the PCS could store and finally deliver heat at a constant temperature. It was successful in heating a solar geyser to above 50 °C. It is suggested that further tests be conducted with an evacuated tube and a higher melting synthetic wax melting at least at 80 °C. This could result in faster heat absorption times because of the larger temperature difference between the hot wax and the cold water that enters the geyser during use.

Chapter 6

Discussion and conclusions

The purpose of the project was to analyse an alternative means of storing thermal energy, and in particular storing heat for a solar water heating application. The motivation for this is to increase the hot water available from a given solar collector system consisting of a solar collector and geyser. This must be done by decreasing the amount of time the backup element is switched on. By adding an additional PCS tank, which is able to store more heat at a lower temperature, more energy may be available from the same solar energy system for evening and morning use. This would result in an overall increase in hot water available throughout the year. In the experimental set-up such a latent heat PCS system was analysed. This system comprised rectangular extruded heat pipes, rectangular vertical fins forming extended heat transfer surfaces, and paraffin wax as PCS material. These components were tested together experimentally and the thermal response was calculated numerically. To analyse the system two experimental modules were designed, built and analysed thermally during heat absorption and heat removal cycles. One of the test modules contained only two rectangular heat pipes placed parallel to each other with a long vertical rectangular wax section in between the heat pipes. One side is used to heat the test section, and the other heat pipe removes heat from the PCS system. The other test section also contained aluminium fins with wax embedded in between the fins. In this concluding chapter the contribution that each part of the analysis made is described: Firstly the contribution of the component analyses, both of the heat pipes and the wax in the PCS module with fins are discussed in Section 6.1. A discussion follows in Section 6.2 which describes the contribution of comparing a PCS module with and without fins. The advantages of using heat pipes with fins are noted and the contribution of such a PCS system numerical model is described in 6.3. The contribution of comparing this numerical model to its experimental equivalent and thereby validating the numerical model is discussed in Section 6.4. The potential improvement that could be made to a given solar water heater by adding a PCS system is discussed in Section 6.5.

6.1 The contribution of the heat pipes and wax experiments to the experimental analysis

During the analysis of the heat pipe three characteristic tests were plotted together on Figure B.1a and different modes of operation were observed. These modes are dependent on the temperature difference between the evaporator and the condenser of the heat pipe. Three modes of heat transfer exist in the heat pipe: Firstly for low temperature differences a linear fit was found to reasonably fit the data, as indicated in Figure B.1b, then a transition zone was entered upon, and the point of this occurring was found to occur between 120 W and 140 W and finally a constant rate of heat transfer is realized at very high temperature differences, which occurred between 100 W and 75 W. This shows that the heat pipe has an inherent limitation in its heat transfer characteristics and that it has different modes of operation which are dependent on the size of the evaporator and condenser surfaces, as well as the temperature differences.

The mode of heat transfer in the heat pipe was determined as depicted in Figures B.9 and B.10 on Pages 111 and 111. It was found that there are two modes of heat transfer during the heat absorption cycle, and only one during heat removal. A linear and quadratic regression fit were imposed on the data set and the quadratic fit suited the data set very well during heat removal of the PCS module.

The energy analysis during the heat absorption cycle of the PCS system exhibited close correlation between the energy transported to the kettle, the energy absorbed in the wax and the kettle, and the energy lost to the environment. The energy absorbed in the wax was lower than the value calculated and this is ascribed to the evaporation from the kettle during heat up mode. Two ways of analysing the wax control volumes were used. One used instantaneous melting at the melting temperature, which inaccurately calculated that the energy uptake occurs suddenly. The preferred method was to look at the gradients in the temperature variation and to use the change in gradient to gain a point of melting initialisation and complete melting and to use latent heat absorption in a range of temperatures as described in Equation ???. It was found that the melting initialisation point starts at about 40 °C. This is a point at which the gradient starts to change and if the PCS system is compared on an energy basis the rate of absorption of the PCS module correlates closely to the energy input from the kettle water. Similarly during heat removal from the PCS system the decrease in energy in the PCS closely correlates to the energy uptake by the water in the heat exchanger. In Figure B.13 on page 115 this correlation is plotted next to the measured energy absorbed in the water of the heat exchanger. The total energy extracted from the wax is given in gray under the heading $Q_{waxtotal}$ and it closely resembles the energy extracted in the heat exchanger both in shape and magnitude.

6.2 The contribution of the PCS system comparison with and without fins to the experimental analysis

In the current experimental research aluminium fins and rectangular heat pipes were utilised to enhance heat transfer into and out of a paraffin wax PCM. The reasons for this were that the heat transfer rate into and out of the phase change material was much slower when no fins were used than when fins were used during heat absorption and heat removal cycles. For example, during the heat absorption cycle of the PCS module which only contains wax and no fins, the wax only module took two times as long to melt (4h) compared to the PCS system with fins (2h) as indicated in Figures 5.1 and 5.6. During the heat removal cycle over a period of 1 hour 15 minutes, 2 times more energy was extracted from the finned configuration (260 kJ) than from the wax only configuration (130 kJ) as indicated in Figure 5.5. This was in spite of the wax only PCS module containing 20% more wax. The wax only module was thus unable to extract the absorbed latent energy trapped inside the PCM, because the solid layer insulates the still molten wax from the cooling surface. This gives an indication of the potential of using heat pipes as well as finned surfaces in PCS systems, where all the heat may be extracted across a small temperature range and within a reasonable period of time. The insulating effect of the wax was overcome to a large degree by the insertion of the fins, and improved heat transfer was realised to and from the PCM. It is recommended that the added aluminium material and manufacturing cost to improve heat transfer performance must be weighed against the improved utility on a life cycle cost basis.

The experimental observations of the experimental module without fins, shown in Figure 5.1, indicated the melt front progression during heat-up of a rectangular wax section heated from the side. It was observed that as the size of the liquid layer increases, so too does the convective currents increase, resulting in an enhanced heat transfer rate. Hot liquid wax collects at the top of the solid wax section and it enhances the progression of the melt front by transferring heat to the solid section of wax. On the other hand during the heat removal cycle the insulative effect of the solidified layer of wax forming on the heat removal HP2 results in very slow heat removal times. The convection effect is not prominent during the solidification process and it is exactly this disadvantage that is overcome by adding rectangular fins to further enhance the heat transfer rate to the heat removal HP2.

The experimental analysis of the finned PCS module shed some light on how

the wax melts inside finned compartments and specifically how the expansion occurs during melting and the contraction during solidification. The experiments showed that during heat removal the wax solidifies onto the heat transfer surfaces, contracts and leaves long vertical void crevices. It also indicated that in such a finned container the wax melts uniformly, and all the wax was quickly melted when heat was applied to the heat absorption HP1, and it quickly solidified compared to what happened in the control case which contained no fins in the PCS compartment. The experimental thermal measurements indirectly indicated the onset of melting and the completion of melting by the change in temperature rise gradient when a constant heat source was applied to the PCS system. This is because the wax melts at a close to constant temperature, so the wax heats up quickly initially when it is still cool and the constant heat source is first applied, then it suddenly slows down its increase in temperature until all the wax is melted, after which it increases in rate of temperature rise before finally slowing down to its final thermal equilibrium temperature.

The heat absorption HP1 was successful in transferring heat all along its condenser section length and transfers heat in a uniform manner across its entire condenser section. This enables the wax to form a liquid vertical layer all along its heat transfer surfaces during heat absorption cycle and reduces the pressure that would be exerted on the wax container if it was heated from below and expanded during melting.

The temperature variations in the PCS system in both the vertical z -direction, the horizontal x -direction, as well as the depth variation in the y -direction were measured. Taking only one control volume in the vertical direction into consideration is deemed accurate enough, as well as the assumption of thermal symmetry in the depth of the PCS module. The melting front progresses horizontally and has a vertical shape when the thermocouple readings in the PCS system are compared. Insight into when a segment has completely melted or started to solidify was also determined from the thermocouple readings, and the analysis thereof led to finding the range at which the wax starts to melt and finally completely melts and vice versa during solidification. The assumption in the numerical model that control volumes may be divided into long vertical compartments are justified from the thermocouple readings.

6.3 The contribution of the simulation of the PCS system with HTE fins to the numerical analysis

The numerical analysis indicated that the heat up phenomena may be better described in the light of the temperature rise and the melt fraction. It was shown in Figures 5.8 and 5.9 that the heat is first absorbed sensibly until the first control volumes start to melt, then a melt front progresses from left to right as heat is absorbed, mostly in latent form. Then finally the wax heats up sensibly to the thermal equilibrium point. The opposite happens when heat is removed from the heat removal side of the PCS system. From the power graph in Figure 5.11 it can be seen that the fins act as heat transfer conduits that stop heating up while the wax is melting or solidifying and pass the heat on to the wax control volumes until all the wax is liquefied during the heat absorption phase or solidified during the heat removal phase. The importance of the fins can be deduced from this analysis by assessing how much heat is transferred just through the fins to the wax control volumes, thereby increasing its effective thermal conductivity by creating heat paths throughout the PCS system. The numerical analysis makes it possible to test different fin configurations without requiring the manufacture of many modules and adapting the system to suit a particular application, for example, developing a PCS system that can deliver heat more quickly or using minimal fin material and still yielding reasonable heat removal times. It also opens up the possibility to test the PCS in conjunction with the solar thermal system that absorbs energy from the sun and stores heat in the geyser before it is delivered to the consumer, as discussed in Section 6.5.

6.4 The benefit of comparing the numerical and experimental results to the numerical model validation

During the experimental and numerical analyses the underlying heat transfer phenomena, such as enhanced conduction heat transfer to and from the PCM, were observed regarding the heat absorption and heat removal of a compact thermal PCS module. The numerical results were calculated using the experimentally determined heat transfer coefficients of the heat pipes. From the comparative tests it was found in Section 5.2 that the numerical model of the module does well to calculate the thermal response of the experimental module. It was also found that the heat transfer could be derived, such as the heat transfer coefficients that result during the sensible and latent heat absorption and heat removal cycles. It was found from the numerical

analysis of the temperatures that occur in the PCS system as well as the melt fraction indicated in Figures 5.8 and 5.9 that when fins were used heat was transferred first sensibly, until the onset of melting, and then the whole PCM melted without either the fins or wax heating up significantly, until all the wax was melted, then finally it heated up sensibly to the equilibrium temperature. There were some differences between the discreet measurements of the temperatures with the thermocouples, which are placed close to the centre of the wax compartment, and the control volumes in the numerical analysis which assume one temperature exist inside the whole control volume. It was decided that the thermocouples' temperature measurements can best represent the PCS system by assigning a melt fraction to the temperature of each segment, such that the total energy absorbed or removed correlates with the energy calculations of the entire module. The correlation used for this analysis is given in Equations 5.1 and ???. It is suggested that in future analysis the thermal properties of the PCS material are determined first and then to adapt the numerical model to implement these thermal properties in the numerical calculation.

6.5 The potential of an additional latent heat storage tank in a solar water heating application

The test module that was heated above melting was capable of delivering heat to the water in the heat exchanger, initially at 100 W and the heat delivered decreased linearly to 35 W after an hour. The average heat transferred per kilogram of wax is calculated to be 77 W for an hour to deliver a total of 0.077 kWh. The numerical simulation calculated that more heat should be removed early in the simulation (Starting at 180 W and dropping proportionally to 100 W after 30 min) and less energy was removed later in the simulation between 30 min and 1 h. This is mainly due to the difference between how the wax performs physically and how it is simulated numerically. The numerical analysis assumed that all latent energy is available at 59 °C, which would be the case for a pure crystalline wax, but from the experiments it is deduced that the latent heat stored in the wax is delivered across a range of temperatures between 40 °C and 59 °C. The quality of the energy is recommended to be used as an indication of what the PCS module can deliver at different flow rates. If this module was used exactly as it was used in the experiment, but only in a full scale solar water application, where a total mass of 150 kg of wax is used and exactly the same geometry of the modules, then the phase change system would be able to deliver heat at 11.56 kW for an hour to deliver a total of 11.56 kWh from the PCS system. This would be a more than sufficient heat input to heat up a tank full of water to 46 °C. This means that the PCS system has potential as an additional heat store in solar water heating applications,

but some alterations may still be made such as to use less fin material and still transfer sufficient heat to the geyser.

It is suggested that different configurations be tested and the performance of each geometry quantified. For example, if the collector is enlarged, while keeping the PCS system and geyser the same would result in higher temperatures, but also higher environmental losses. If the PCS tank is enlarged, the time it takes to heat it up takes longer, because of the larger thermal inertia of the solar thermal system. If the geyser is enlarged, then the water in the geyser takes much longer to heat up, but more hot water is available at a time. In the present configuration during days of low solar radiation there may not be enough energy to heat up both the solar collector and the PCS system and during these periods the system will act as a sensible system. It is therefore suggested that the geyser is coupled to a solar collector, and the PCS system then acts as an additional heat source at nighttime.

The numerical results of the chosen PCS system in a SWH application indicated that the PCS system can store heat at a sufficiently high temperature to have the capability to heat up the geyser water from 20 °C to 50 °C which was more than sufficient. It is recommended that more tests be conducted with evacuated tube solar collectors and a higher melting synthetic wax such as the C80 SASOL wax that can withstand very high temperatures and store the heat at a higher quality, which will result in faster geyser heat up periods. For the current set-up it was found that a large 3.6 m² collector with a selective coating can heat up a 150 kg wax storage with 34 kg of fin and heat pipe material and a 150 L geyser on a sunny day in summer. This heat can then be used to deliver hot water at above 50 °C to the consumer at night and again the next morning. This was deemed as sufficient proof for a proof of concept that a PCS system can be incorporated to deliver dispatchable heat and decrease electric backup energy input. Further tests may lead to cheaper systems that are still capable of delivering sufficient heat on a year round basis.

6.6 Main conclusions and contributions of the thesis

In this study a novel PCS system was developed and investigated. It was shown that by using heat pipes and fins as HTEs the heat absorption and heat removal rates in the PCM can be greatly enhanced. This improves the application possibilities of the concept where fast and reliable heat extraction rates may be required from the storage system.

From the experiments conducted on the finned PCS module it was found that the approximation of 2 dimensional heat front as seen from the top is justified

because of the rectangular heat pipes capability to spread the heat uniformly all across its condenser surface during heat absorption phase. In a similar fashion heat could be extracted uniformly by the heat removal heat pipe.

The fins greatly improved the thermal performance of the storage section by increasing the energy removed five fold (250 W vs. 50 W during one hour of heat extraction). The fin material may be reduced to decrease cost, while still achieving good thermal performance

In this thesis a numerical C++ code was developed that solves the explicit energy balance computer algorithm. The numerical model handles each of the PCM control volumes by keeping track of the temperature, melt fraction and density. The phase change was modelled to occur at a constant temperature of 59°C. The control volumes expand in the vertical direction during the expanding melting process. No mass transfer processes were considered, but because of the chosen geometry this phenomenon is regarded as negligible.

The numerical analysis of the PCS module depicted in Figures 5.8 and 5.9 indicates graphically that the PCS system first heats up like a normal sensible system until melting is initiated. Then after melting initiation of the first wax control volume the storage exhibits the characteristic of a storage with a very large thermal inertia. This results in very slow temperature rise of the whole storage until all the wax control volumes have melted. Looking at the numerical analysis during heat absorption the power absorbed decreases proportionally from 85 W to 65 W in 35 min. This system was exposed to a constant temperature heat source. This showcases the steady heat absorption of the storage module during melting at a constant temperature. Similarly during the heat removal phase a steady rate of heat extraction was achieved during solidification. Looking at the numerical analysis during heat removal the power absorbed decreases proportionally from 180 W to 120 W in 25 min. Also from observations and energy calculations it was possible to uniformly melt all the PCM during heat absorption and uniformly solidify all the PCM during heat removal.

In the spearhead modelling of a SWH system that incorporates a PCS system it was found that the system shows promise to improve the hot water utility of a SWH system. The improvement was mainly due to the additional storage being able to heat the geyser during night time without the need to use the electric backup element for early morning hot water use.

Chapter 7

Recommendations for future work

The development and long term testing of the proposed SWH with additional PCS system concept would shed light on the actual savings that could result with such a system. The numerical model of the PCS system can be adapted to simulate different fin materials and PCM depending on the application. For example, in a solar cooking application that needs to store heat for nighttime cooking, the PCM would have a melting temperature between 150 °C for boiling water, and 300 °C for baking and grilling applications. In around the clock solar heating industrial applications additional PCS may improve operating periods in applications such as hot water for washing and steam generation. On the solar side evacuated tubes may be considered for reaching temperatures up to 200 °C. Parabolic troughs or parabolic dishes and central receiver systems may also be used to obtain higher input temperatures in power generation for example. For each application the model needs to be adapted to calculate the solar energy input, the storage of energy of the PCS system, as well as the load conditions that could be expected.

It is suggested that further PCS-SWH tests that use this indirect PCS system that use heat pipes and fins to transfer the heat to the PCM be conducted it with an evacuated tube solar collector and that a higher melting synthetic wax melting at least at 80 °C be used. This could result in even faster heat absorption times between the PCS system and the geyser water because of the hotter wax which would result in a larger temperature difference. From a HTE perspective further tests on inherently safe form stable composites of either clay and wax or polyethylene and wax as tested by Krupa *et al.* (2007) to prohibit the risk of hot molten wax spilling out of the container in the case of the container cracking. In this solid setup the natural convection can not take place and the pure conduction model would predict the system even with a wide variety of fin configurations. It is also suggested that some of the heat absorbed in the solar collector be connected directly to the geyser so that the water may be heated faster during the day. Then when the geyser is hot enough the heat could be redirected to heat the PCS system.

It is also recommended that future analysis of such solar heating applications that use PCM as storage material to combine the first law of thermodynamics analysis, such as energy balances on each control volume, but also to have a strong focus on second law of thermodynamics analysis that quantifies the loss in quality of energy from the high quality, high temperature solar input to the

lower temperature and thereby lower quality PCS system and finally to the energy delivered to heat water to above 40 °C and thereby to low quality heat, or to bake food, or to produce steam or to generate electricity.

Appendix A

Calibration and error analysis of the thermocouples used in the experiments

The calibration of the thermocouples was conducted using a calibration machine that can be accurately set to any temperature between -20°C and 180°C . The temperatures that were measured during testing was between 10°C and 100°C . The tests were conducted in temperature steps of 10°C from 0°C to 150°C to capture whether the temperatures deviate from the readings of the resistance thermometer. During each step the temperatures were allowed to reach thermal equilibrium before a reading was taken from the resistance thermometer. The calibration test set-up is shown in Figure A.1. The thermocouples were placed inside the temperature controller with the resistance thermocouple. The thermocouples were connected to temperature channels which measure the voltages that result from temperature changes. The thermocouple channel readings were then converted to temperature readings by the National Instruments software and these temperature readings were stored in the memory of the laptop.

Two calibration tests are shown in Figure A.2 and it indicates a very close correlation between the different thermocouples and similar readings compared to the resistance thermometer. In Figure ?? the difference between the thermocouple readings at thermal equilibrium and the reading from the resistance thermometer is calculated between 0°C and 100°C . The error of the readings are within 0.9°C of the resistance thermometer. The experiments measured values between 20°C and 100°C . A 0.9°C error does not significantly introduce inaccuracies to the analysis of the experiments. The error between two channels are very small (in the order of 0.1°C). By choosing two thermocouples (T_{S12} and T_{S15}) that have a very similar response curve to measure the temperature difference across the heat exchanger the system error is minimised to within 0.02°C . By ensuring that the flow rate through the heat exchanger is such that there exist a 3°C temperature difference the relative error is limited to 0.66% as calculated in Equation A.1. The calculated heat absorbed by the water passing through the heat exchanger could vary within 0.66% .

$$\frac{0.02\text{ }^{\circ}\text{C}}{3\text{ }^{\circ}\text{C}} = 0.66\% \quad (\text{A.1})$$

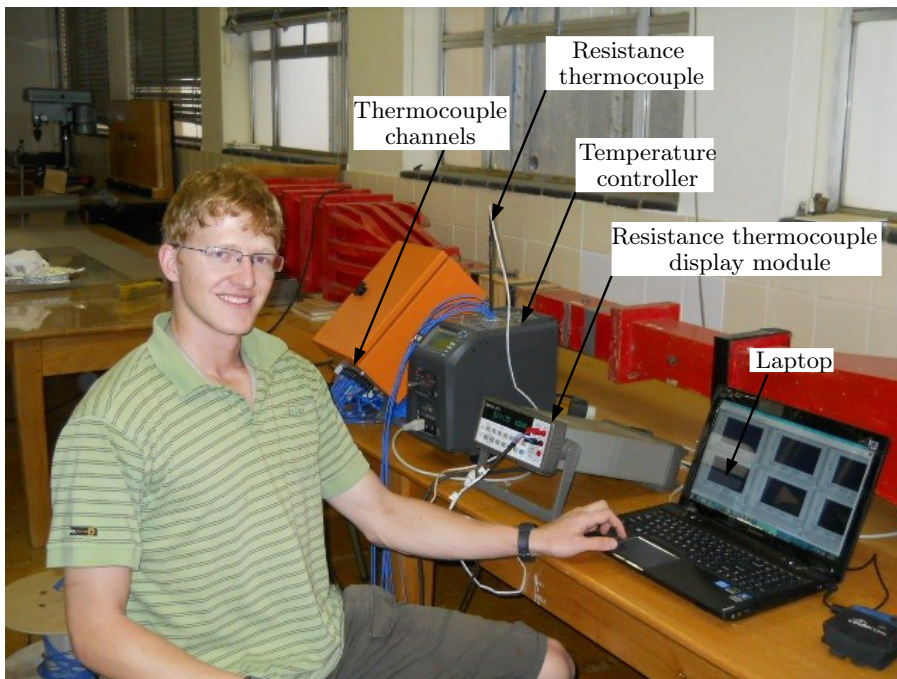


Figure A.1. The calibration test set-up of 9 thermocouple wires with a resistance thermometer.

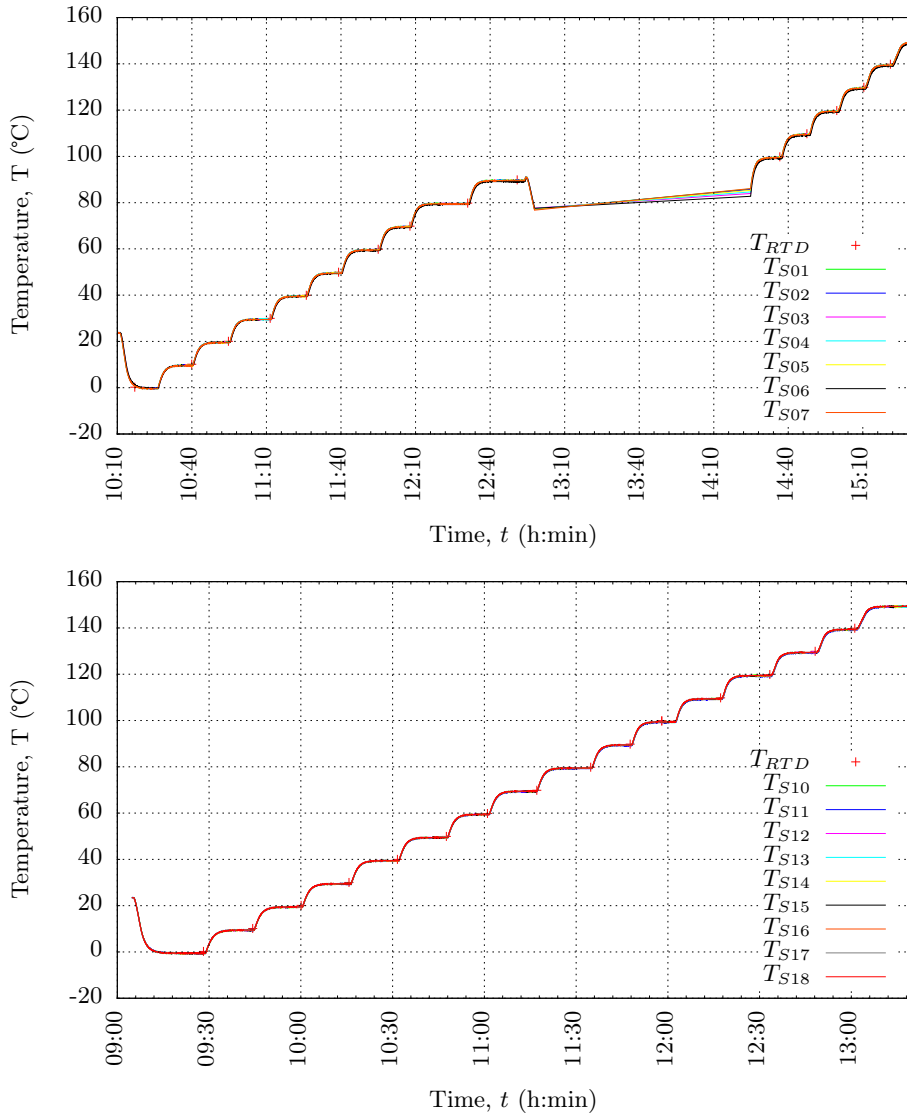


Figure A.2. The calibration of the thermocouples in the range of 0°C to 150°C.

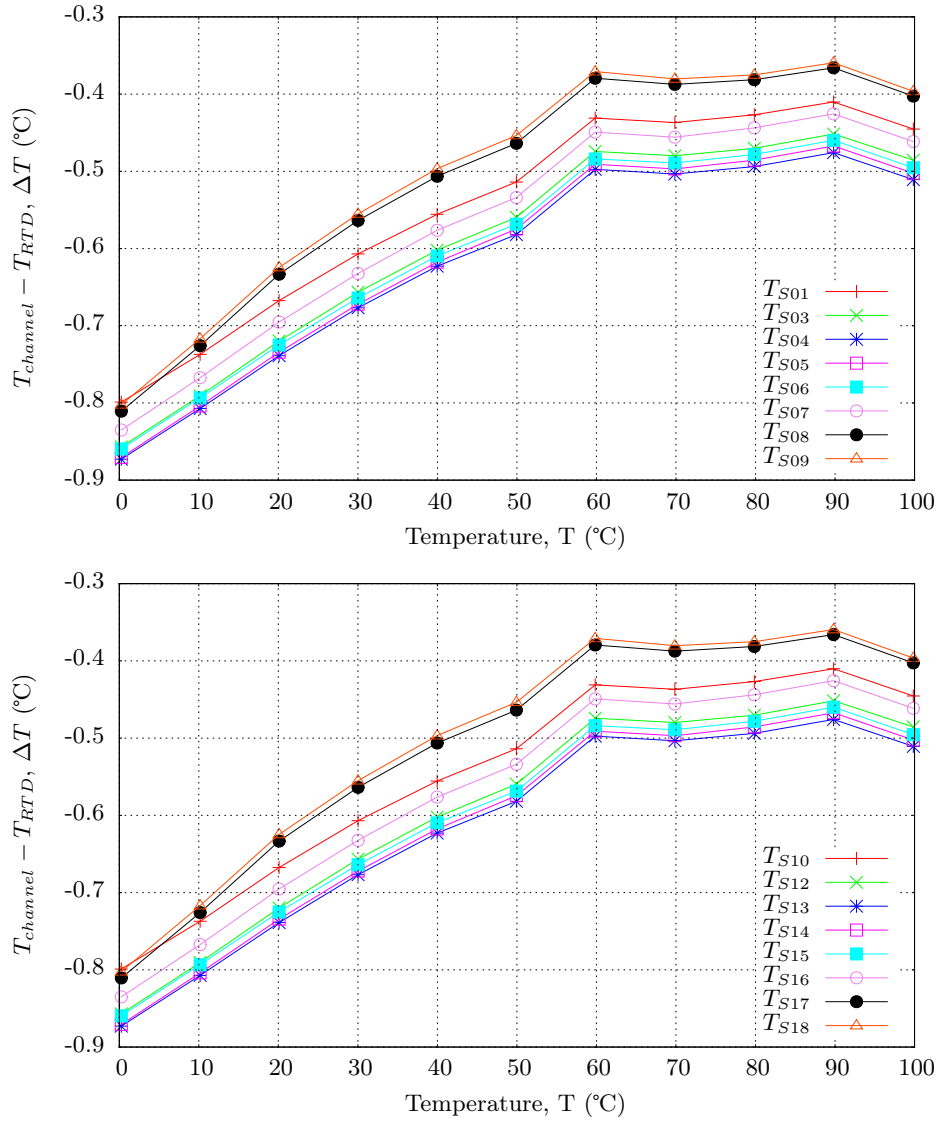


Figure A.3. The error of the thermocouples when compared to the resistance thermometer in the range of 0 °C to 100 °C.

Appendix B

In depth experimental results

The experimental results aid in understanding the operation of the heat pipes, as well as the wax and fins PCS module. The heat pipe characteristic experiments were conducted to capture its heat transfer response during varied temperature differences. The full experimental set-up of the two heat pipes sandwiched between the PCS system included 27 thermocouples. These measurements are analysed from a temperature response point of view, as well as calculating heat flow to and from the PCS module as well as the energy absorption in the PCS module. The temperature difference between the inlet and outlet of the heat exchanger, as well as the flow rate are used to determine how much heat is transferred from the PCS module to the water in the heat exchanger.

B.1 Analysis of the heat flow characteristics conducted for the kettle and the heat pipe

To accurately model the total system consisting of the kettle, the heat absorption HP1, the thermal PCS system, the heat removal HP2 and the heat exchanger the components are first tested separately. From these tests correlations for the kettle as it cools down to the environment and the heat pipe operating under various temperature differences to transfer heat from the bottom evaporator section to the top condenser section are determined.

B.1.1 The heat pipe characteristic test

In Figure B.1 on page 102 three characteristic tests are plotted together. The procedure followed during each of these tests was to heat the kettle while the evaporator side of the heat pipe was immersed in the water of the kettle. Most of the heat absorbed in the kettle by the heat pipe was transferred to the heat exchanger at the condenser at the top of the heat pipe. The heat transfer rate into the cooling water is calculated from the measured temperature difference between the inlet and outlet of the heat exchanger and the mass flow rate from the following equation:

$$\dot{Q}_{extracted} = \dot{m}_w c_{p(w)} (T_{c(out)} - T_{c(in)}) \quad (B.1)$$

The cooling results are much more uniform than the heating up results, but this may be because of electronic interference of the measuring equipment between the kettle and the thermocouples during the heat up mode. The cool down tests are deemed to be much more accurate because the kettle is switched off during the cooling down of the kettle water. The heat pipe's response during the three cool down tests and two of the heat up tests can be divided into three distinct zones. The first zone is a linear response where the power transferred increases as the temperature difference increases. This follows the equation of:

$$\dot{Q}_w = 3.3406 \left(T_{h(avg)} - \frac{T_{c(in)} + T_{c(out)}}{2} \right) - 5.530 \quad (\text{B.2})$$

This correlation is followed up until the transition phase where the heat pipe stops following the linear relationship and reaches a limit of the highest rate of heat transfer. The highest rate measured was during test three where the linear relationship was followed up until 150 W. This test was conducted at a slow, but constant flow rate of cold water through the heat exchanger and it also gave the most uniform curve (see the blue bottom blue plot of Figure B.1). After the transition phase the correlation changes to a constant limit of $\dot{Q}_w = \gamma$ where γ varies between a value of 100 W for a slow flow rate at the heat exchanger to 80 W at a faster flow rate. In the tests with the two heat pipes and the PCS system sandwiched in between the two, the aim with the PCS modules is to operate in the linear zone. The two heat pipes' temperature difference will be checked to ensure that the maximum limit is not reached during operation of heating and cooling tests.

B.1.2 The kettle characteristic test

In the kettle cool down test the kettle was first heated up to a maximum temperature, and then the kettle's element was switched off and left to cool down. The floats were placed on the surface of the water during all tests with the kettle to inhibit evaporation on the surface. The kettle cools down quite slowly when not heating up the PCS system, and this can be attributed to the kettle being well insulated and the floats sufficiently suppressing evaporation of the kettle water. The resulting temperatures of the kettle as it cools down to the cool environment are then averaged over 400 seconds to average out the small fluctuations in the kettle water temperature readings. From these values a correlation of the energy loss from the kettle to the environment for each kettle temperature is calculated.

The cool down of the kettle was measured on 06/10/2013 and the average values over 400 seconds of cooling were used in the calculation of each of the averaged temperature loss during cool down of the insulated kettle. The

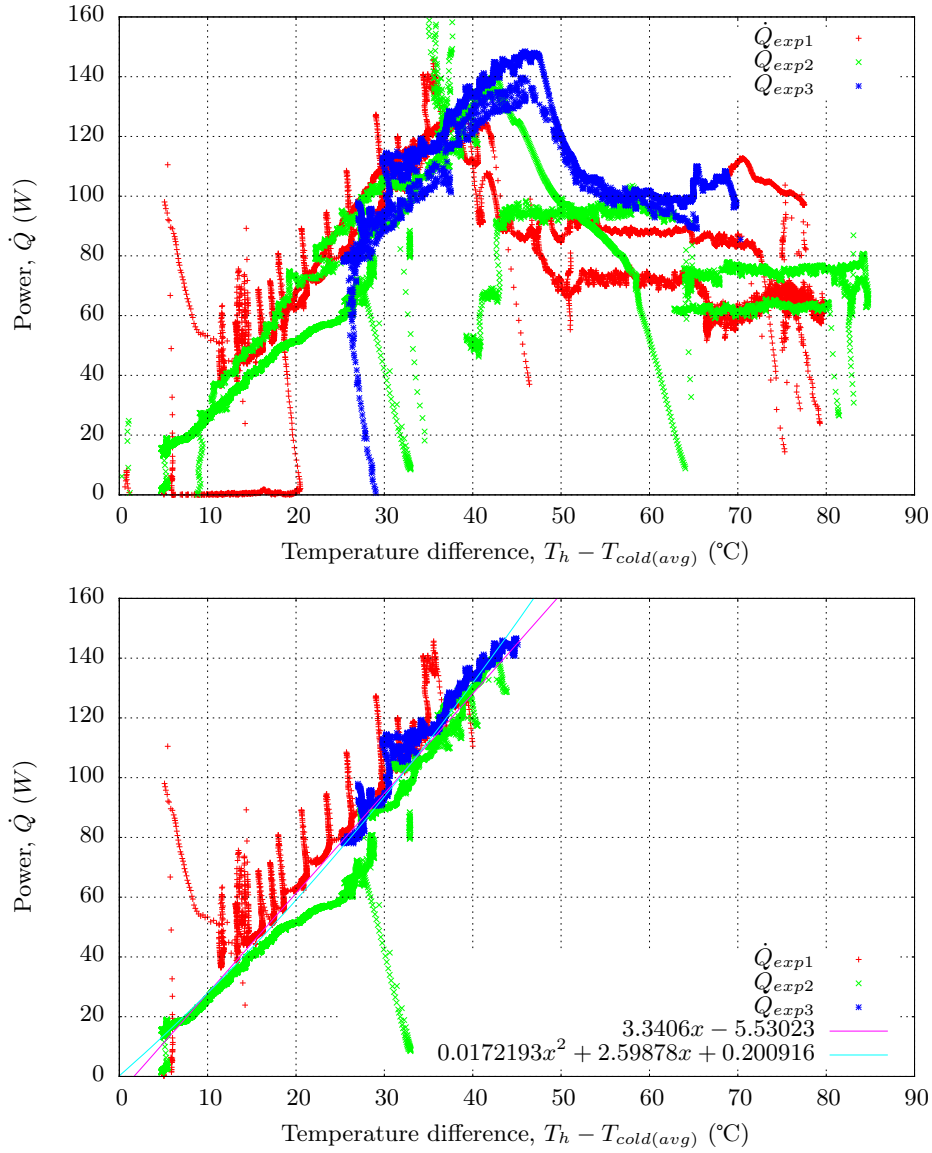


Figure B.1. a)The characteristic of heat transfer rates of the heat pipe for various $T_h - T_{cold(avg)}$ temperatures, and b)the least squares regression fits through the initial mode of heat transfer rates.

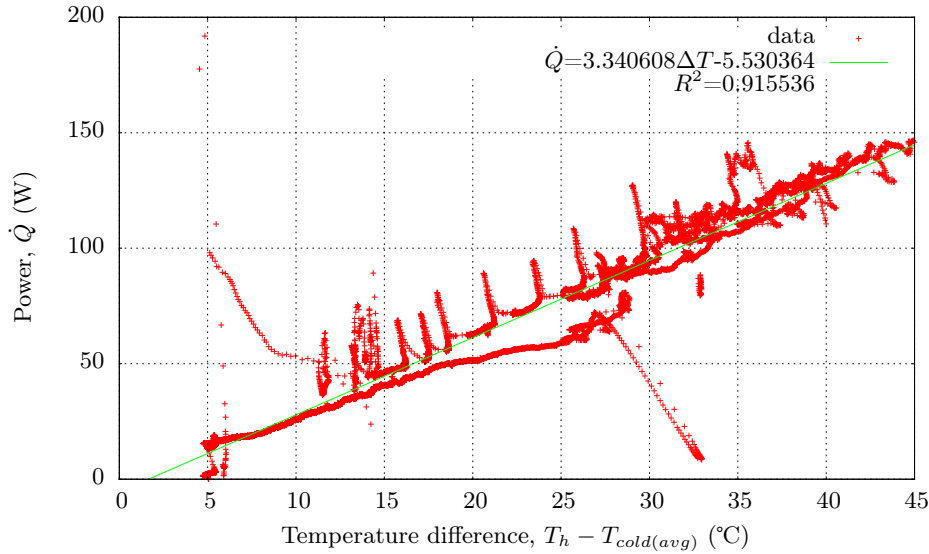


Figure B.2. The initial mode of the characteristic heat pipe heat transfer performance with a linear curve fit.

regression fits yielded a close resemblance between the linear and the quadratic fit. The function used in consecutive tests used the linear relation given in Equation B.3.

$$\dot{Q}_{kettle(loss)} = -0.477721(\Delta T) + 2.67464 \quad (\text{B.3})$$

B.2 Analysis of the PCS module with HTE fins

During the heat up test conducted on the 15th of June 2013 the kettle was turned on at the full power of 1850 W. The water then heated up quickly and started to boil, when this high temperature was reached the kettle was turned off. The kettle was turned on and then off for four cycle periods during the wax heat up test. The total energy entering the system of the kettle and the PCS system is the rating of the element times the amount of time in which it was switched on.

B.2.1 The temperature variations in the PCS system

In the following description the thermocouples readings are compared. These thermocouples are placed according to that depicted in Figure 4.2 In the central plot of Figure B.5 the top of HP1 is indicated in red. This gives a good indication of when the kettle is on, and when it is off. The kettle is on when the gradient is positive. The rest of the temperature readings always have a positive gradient during heat up, because of the large difference

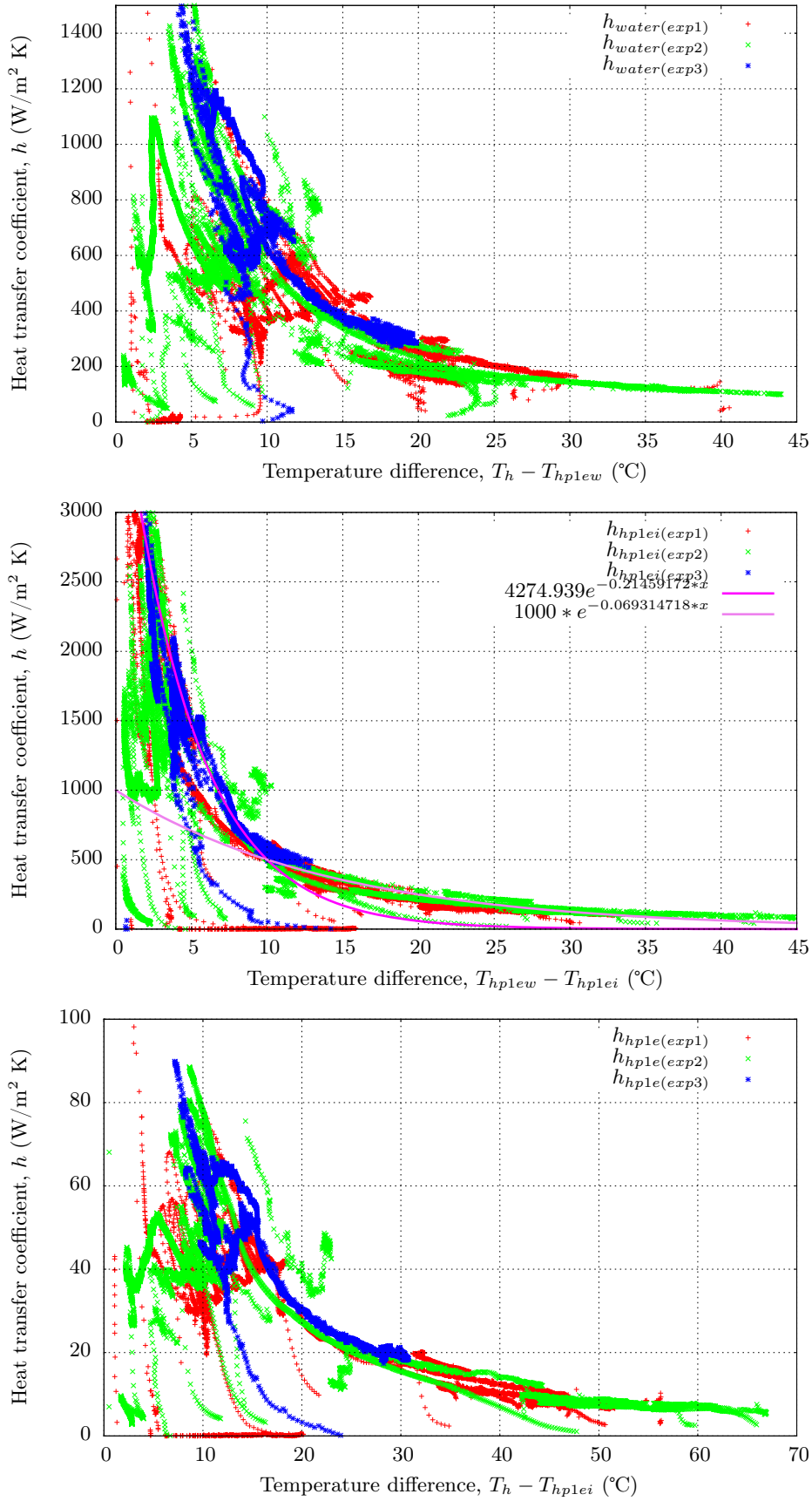


Figure B.3. The heat transfer coefficient of the evaporator side of the heat pipe during characteristic test.

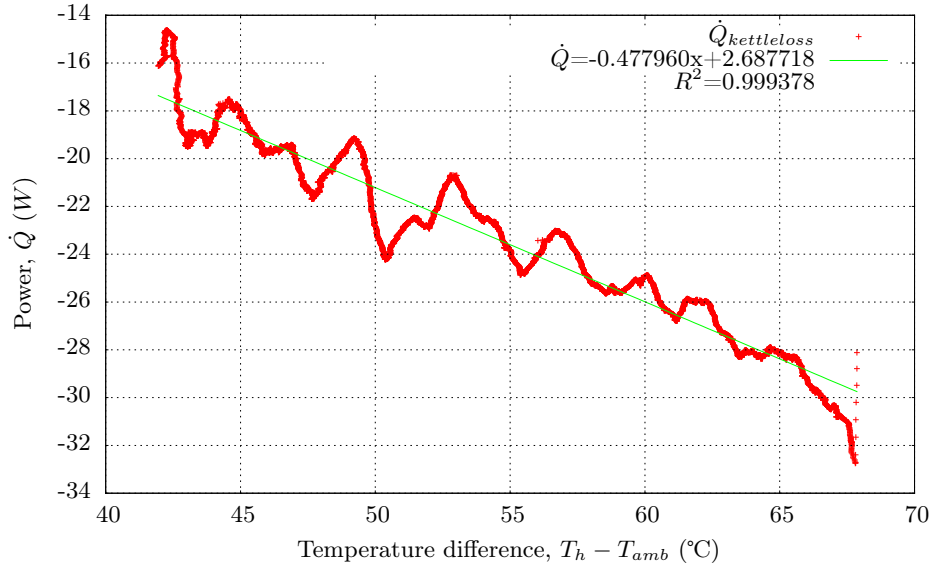


Figure B.4. The loss to the environment from the kettle averaged over 400 seconds and a linear regression fit

in temperature between the kettle water and the heat absorption HP1. The thermocouple at point T_{S10} is the top left edge of the PCS system and measures about three degrees lower than in its central counterpart indicating some temperature difference at the left top side between the middle and the side. The T_{S11} thermocouple on the side of the container is similar to its central counterpart T_{S05} . This indicates that as the heat front progresses it is more and more uniform in the y -direction. The temperature variation between the leftmost and the rightmost temperatures stay about the same until melting at 59°C is reached when the temperature variation becomes less and less as it converges at a point of thermal equilibrium. It is also observed that the temperature variation between the leftmost and rightmost temperature points are largest at the top at about 6°C and the bottom variation of about 3°C . This may be because of stratification between the top and the bottom, and this is further analysed with the vertical thermocouple comparison in Figure B.7 for the heat up mode and in Figure B.8 for the heat removal test. The temperatures in the vertical direction are very close to each other throughout both the heat absorption and the heat removal mode. This validates the assumption that there are not large variations in the vertical or z -direction. A final note on the rate of change of the temperatures with respect to time, or in other words the gradient. The gradient suddenly increases when the temperatures reach the melting point. This may be because of convection of hotter fluid that is transported over the thermocouple reading point, or it may be because of faster heat transfer of the molten wax when the wax medium is solidified.

The horizontal thermocouple measurements are indicated Figure B.6. The rightmost thermocouple cools down first and then the middle and finally the leftmost thermocouples follow suit. The temperatures during cool down first drop quickly in temperature, and then flatten out when the solidification temperatures are reached. The flattening out indicates that more energy is now extracted through the solidification process and less through sensible cooling down of the wax. Finally when all the wax has solidified the gradient becomes steeper even though less and less energy is extracted by the heat exchanger (see Figure B.13 on page 115.). This is because all the latent heat has been extracted from the PCS system and it is quickly depleted of its last bit of sensible energy.

B.2.2 The power transferred through the heat pipes during heat absorption and heat removal modes

Two different rates of heat transfer occur in the heat absorption HP1. The red line in Figure B.9 indicates the rate when the kettle is switched on. The calculation of the criteria whether the dominant heat transfer mode is forced or mixed or natural convection, indicated a value of $Gr/Re^2 = 0.12$ which gives rise to mixed convection. The red line shows the rate of heat transfer when the kettle is switched off and when natural convection is the main mode of heat transfer. It is noted that the temperature difference across the heat pipe stays small throughout the heat up test and that the heat is thus effectively absorbed in the PCS system.

During the cool down of the finned PCS system the temperature difference across the heat pipe is much larger. This may be because of the low temperature of the cooling water in the heat exchanger. The extracting heat pipe operates in the first zone of heat transfer, where the first zone is a region of operation in which the heat transfer varies linearly with respect to the temperature difference across the heat pipe. The heat pipe only enters the transition phase for a short period of time as indicated in Figure B.10. The results indicated in the graph is calculated from the temperature difference between the thermocouple at the bottom of the second heat pipe T_{hp2b} and the average water temperature in the heat exchanger T_{bhe} which stands for the bulk temperature. A linear and a quadratic curve are fitted using the least squares regression method through the $Q_{extracted}$ data set and it is found that the quadratic function fits the data better across the entire range of operation that the heat removal HP2 experiences.

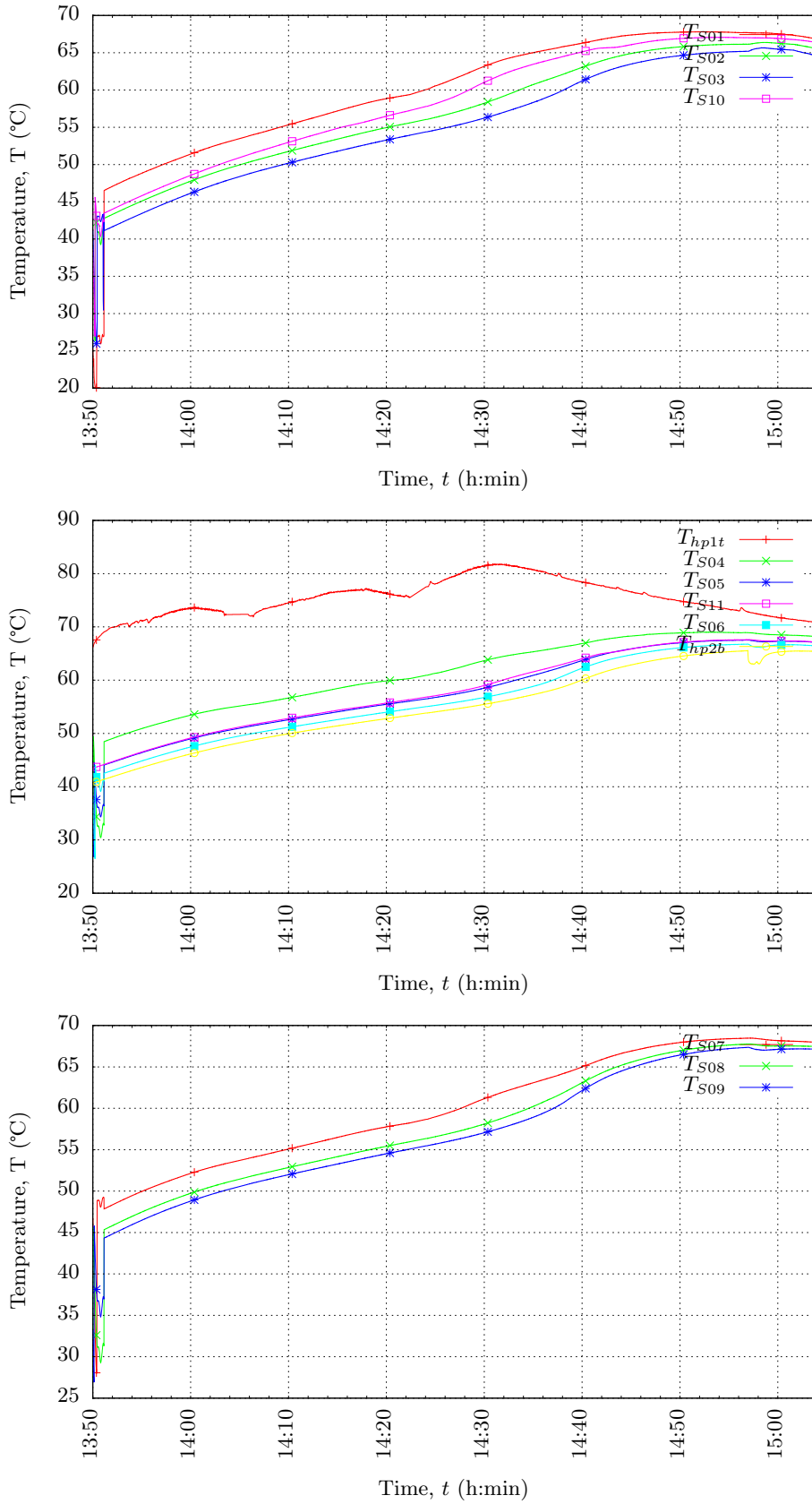


Figure B.5. The temperatures measured at the top of the PCS system, the middle of the PCS system and the bottom of the PCS system and the heat pipes during the heat up test

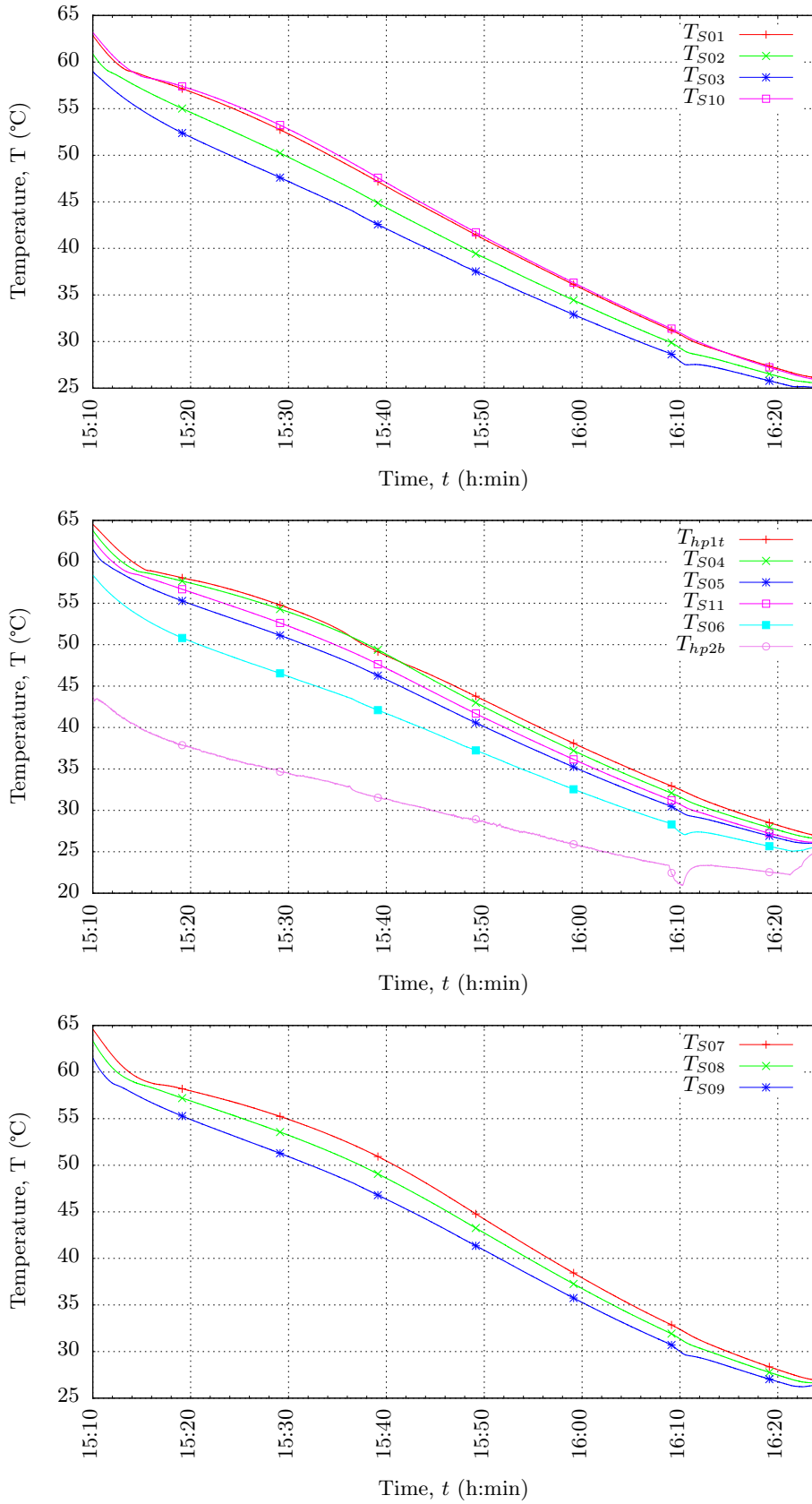


Figure B.6. The temperatures measured at the top of the PCS system, the middle of the PCS system and the bottom of the PCS system and the heat pipes during the cool down test

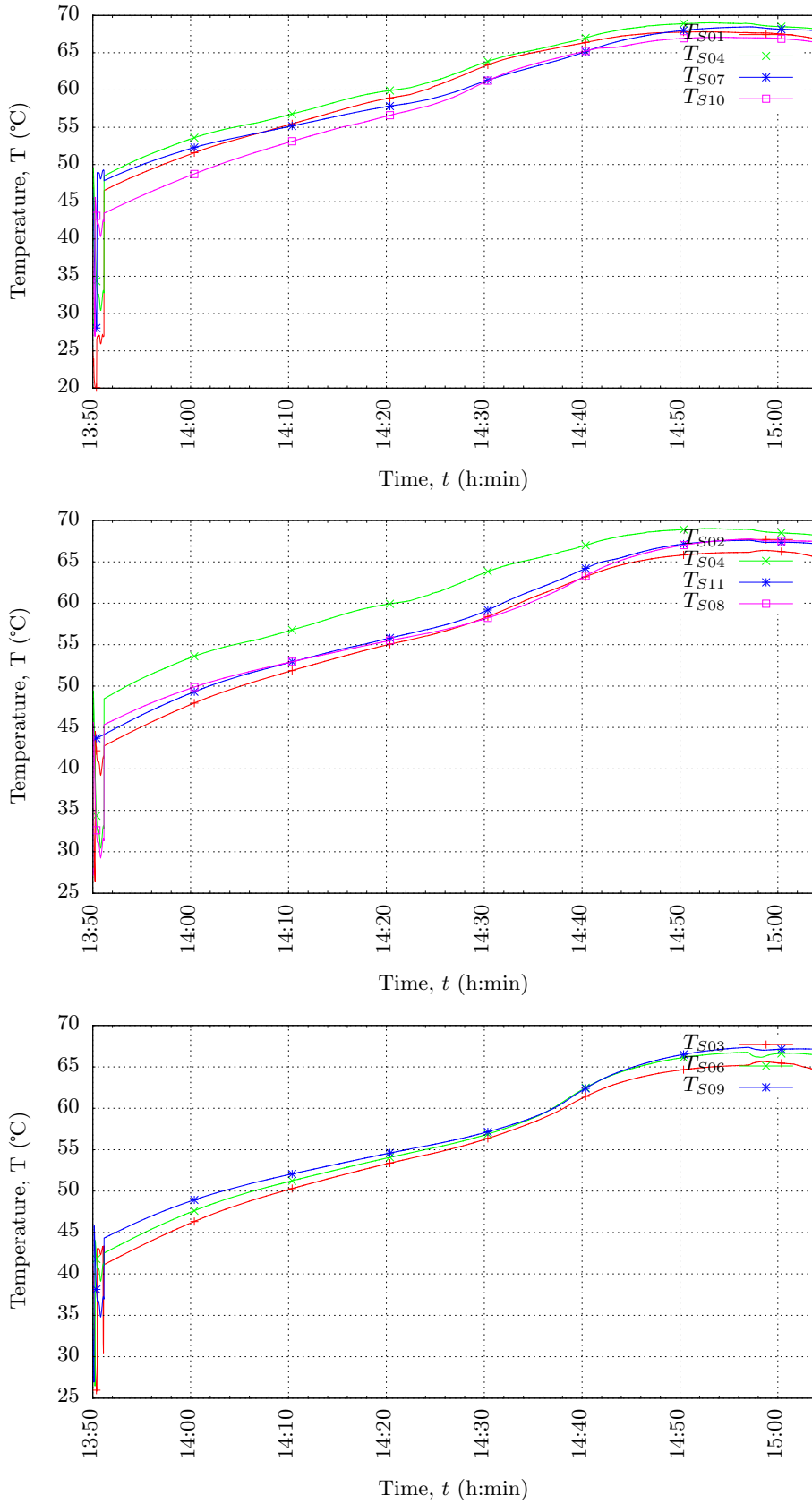


Figure B.7. The temperatures measured at the left, the middle and the right side of the PCS system during the heat up test.

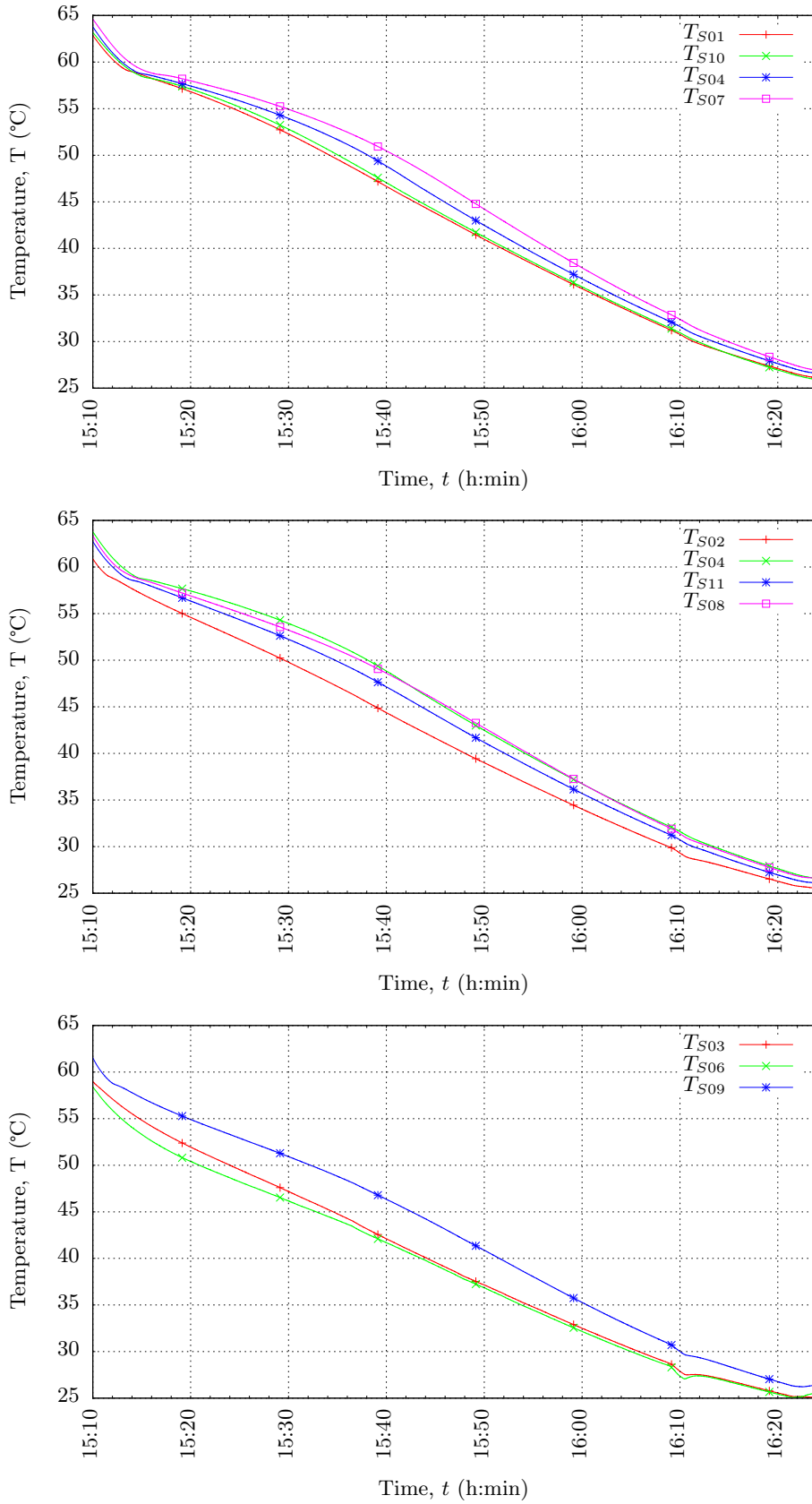


Figure B.8. The temperatures measured at the left, the middle and the right side of the PCS system during the cool down test.

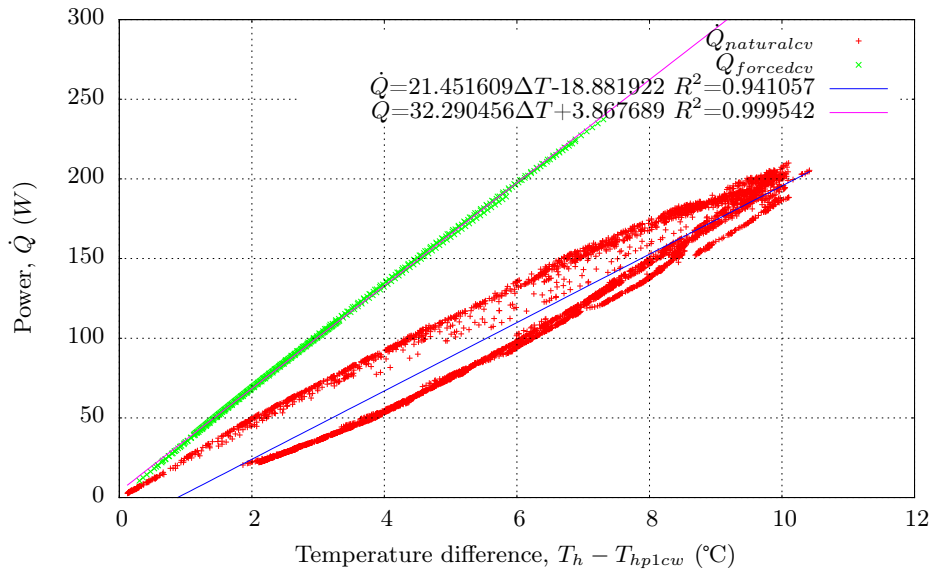


Figure B.9. The power transferred through the heat absorption HP1 during the heat absorption cycle.

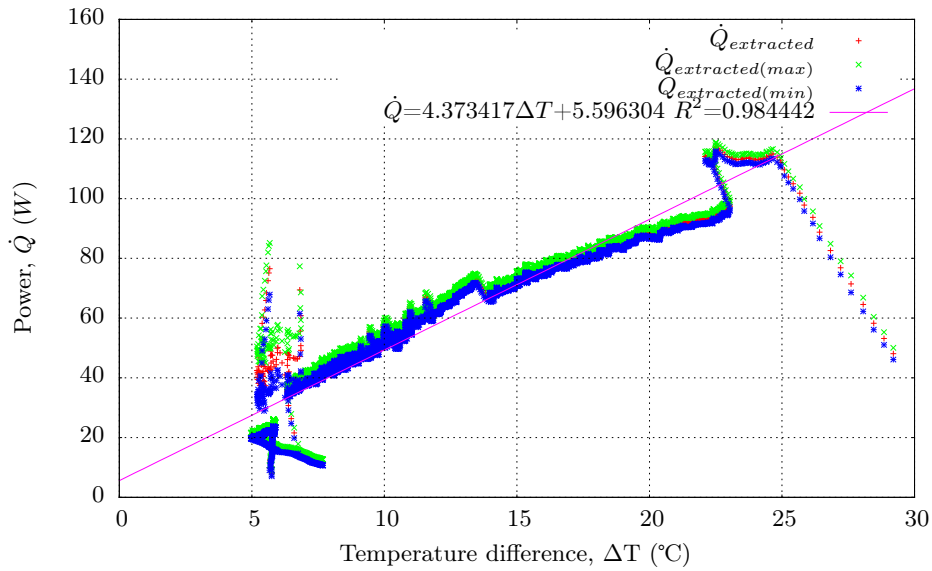


Figure B.10. The power transferred through the heat removal HP2 during heat removal.

B.2.3 The total energy and power absorbed and extracted during a heat up and a cool down test

During the test conducted on 15/06/2013 the total energy entering the system is 860 kJ as can be seen in Figure B.11. The loss to the environment from the hot kettle is then calculated to be a total of 180 kJ, or 21% of the total energy entering the system was lost to the environment. This is according to the cool down test of the kettle done in Section B.1.2. A total of 38% of this nett energy entering the system is ultimately extracted into the heat exchanger water. Where does the 62% that is left go to? It seems that most of it is left behind and not absorbed in the wax in the first place. It is deduced that the steam escaping during boiling during the heat up phase may be the place where the excess energy escapes from the PCS system. The kettle cool down test only considers hot water that is cooling down, not boiling water that is heating up. In consecutive tests the variac was used to limit the power which enters the system. The total energy absorbed in the wax totals about 280 kJ. Of this value a total of 260 kJ is extracted into the cooling water. A minimal amount of 20 kJ is either left in the PCS module or lost to the environment. Most of the stored energy is transferred to the water that is passed through the heat exchanger, but the quality of the energy decreases significantly from hot kettle water at 90 °C to cool water in the heat exchanger at 23 °C.

According to Figure B.12 on page 113 the power absorbed in the wax starts off at a high rate of 100 W. This is because of the large temperature difference that exists between the wax and the kettle water. The rate then

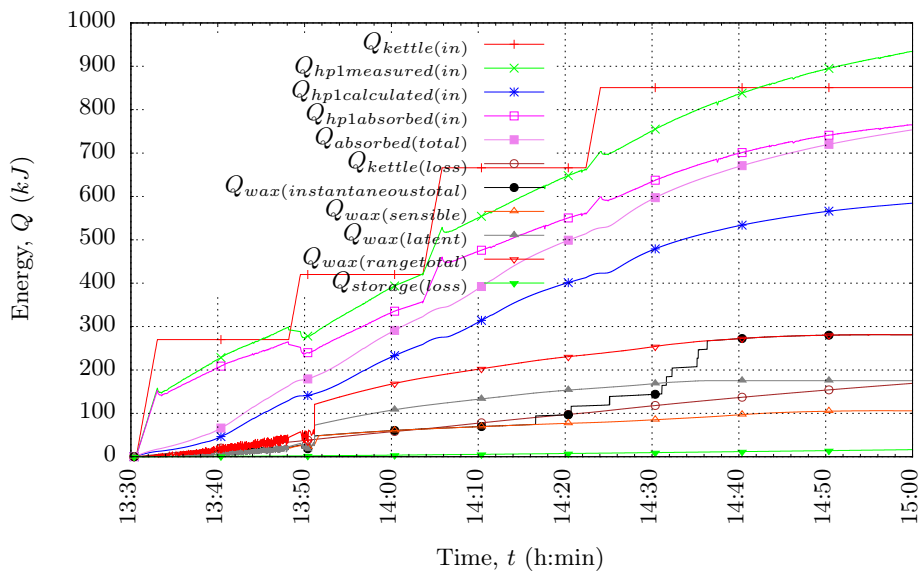


Figure B.11. The total energy in the kettle and the total energy flows into and out of the kettle measured and calculated

slowly decreases until a plateau is reached. This indicates the onset of melting. After all the wax has melted the rate decreases until thermal equilibrium is reached and no more energy is absorbed in the wax.

In the cool down test the power transferred gradually decreases as the test progresses and as the wax cools down. This is shown in Figure B.13 on page 115. The power transferred is measured from the flow rate and the temperature difference between the inlet and outlet of the heat exchanger. From the four thermocouples that measured the temperature difference the total difference between the minimum and maximum energy transferred during the whole test is 2.6% which is negligibly small and is due to measurement differences in the insufficiently mixed water, and measurement errors. Maximum heat transfer from the PCS system takes place when it is at its hottest and less and less heat is transferred as the PCS system cools down. The flow rate was close to constant during heat removal for most of the experiment and the heat extracted does not deviate much in any short span of time. From the mass of the wax in the PCS module (0.876 kg) and using a latent heat of fusion of $h_{sl} = 200 \text{ kJ/kg}$, it is calculated that 67% of the heat absorbed in the wax is latent energy. The solidifying of the wax and efficient transfer from the PCS system to the heat removal HP2 also gives rise to the steady rate of heat transfer during the solidification of the PCS system.

The extracting heat pipe operates in the first zone of heat transfer, where the first zone is a region of operation where the heat transfer varies proportionally with respect to the temperature difference across the heat pipe. The heat

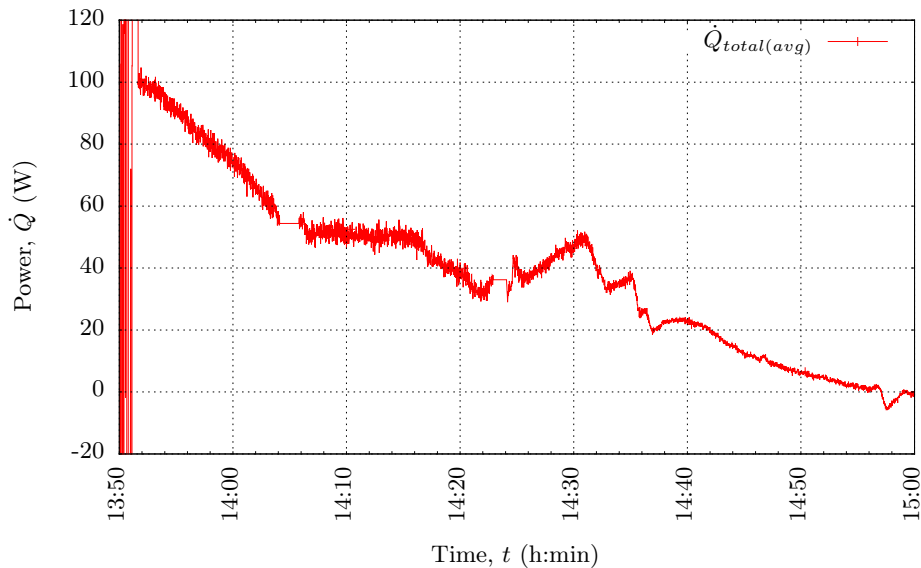


Figure B.12. The power absorbed in the wax during heat up according to measurements

pipe only enters the transition phase for a short period of time. The graph is calculated from the temperature difference between the thermocouple at the bottom of the second heat pipe, T_{hp2b} , and the average water temperature in the heat exchanger.

B.2.4 The total energy in each segment of the PCS system

As can be seen in Figure B.14 on Page 116 complete melting during the heat up test takes place as follows. First control volume T_{S04} starts to melt, then T_{S01} , then T_{S07} , which is first the middle then the top and then the bottom of the leftmost measuring points. Then later the middle group melts very shortly after each other first T_{S05} , then T_{S02} , then T_{S08} , and finally the furthest group T_{S09} , T_{S06} , and then T_{S03} . Each of the last two groups melt so shortly after each other that it can safely be said that the melt front during melting progresses horizontally in the x -direction and the melt front has a vertical shape.

During solidification the solidification front does not develop in the same way as the melting front does. During melting it was observed that the fluid filled up the voids, but during solidification large elongated voids formed in the vertical z -direction. First T_{S06} solidifies, then T_{S03} , which is first the middle and then the top of the rightmost measuring points. Then T_{S09} and T_{S02} solidifies and shortly after T_{S05} , then later the middle-top and middle-middle points melt very shortly after each other first T_{S01} , T_{S04} , T_{S08} , then finally T_{S07} . The solidification front progresses horizontally in the $-x$ -direction and the bottom layer solidifies last. The reason may be because of voids forming, but most likely the hot wax is trapped at the bottom after the top solidifies into solid form.

The total loss to the environment is mostly the loss to the left of heat pipe and the loss on the right, which is about a half that on the left. The three side control volumes are very close to each other and the temperature distribution is closely coupled to the energy loss to the environment. The total loss to the environment is however negligibly small in comparison to the total energy absorbed in the wax.

During the heat up of the wax control volumes it is observed that the gradient increases suddenly when the temperature reaches the melting temperature. The temperature of the wax rises to about 65 °C before flattening out again. In the bottom graph of Figure B.17 the change in temperature and a 30 seconds moving average of the data is taken. It is observed that the change in temperature in time starts at $\Delta T = 0.01^\circ\text{C}/\text{s}$ and after some time lowers

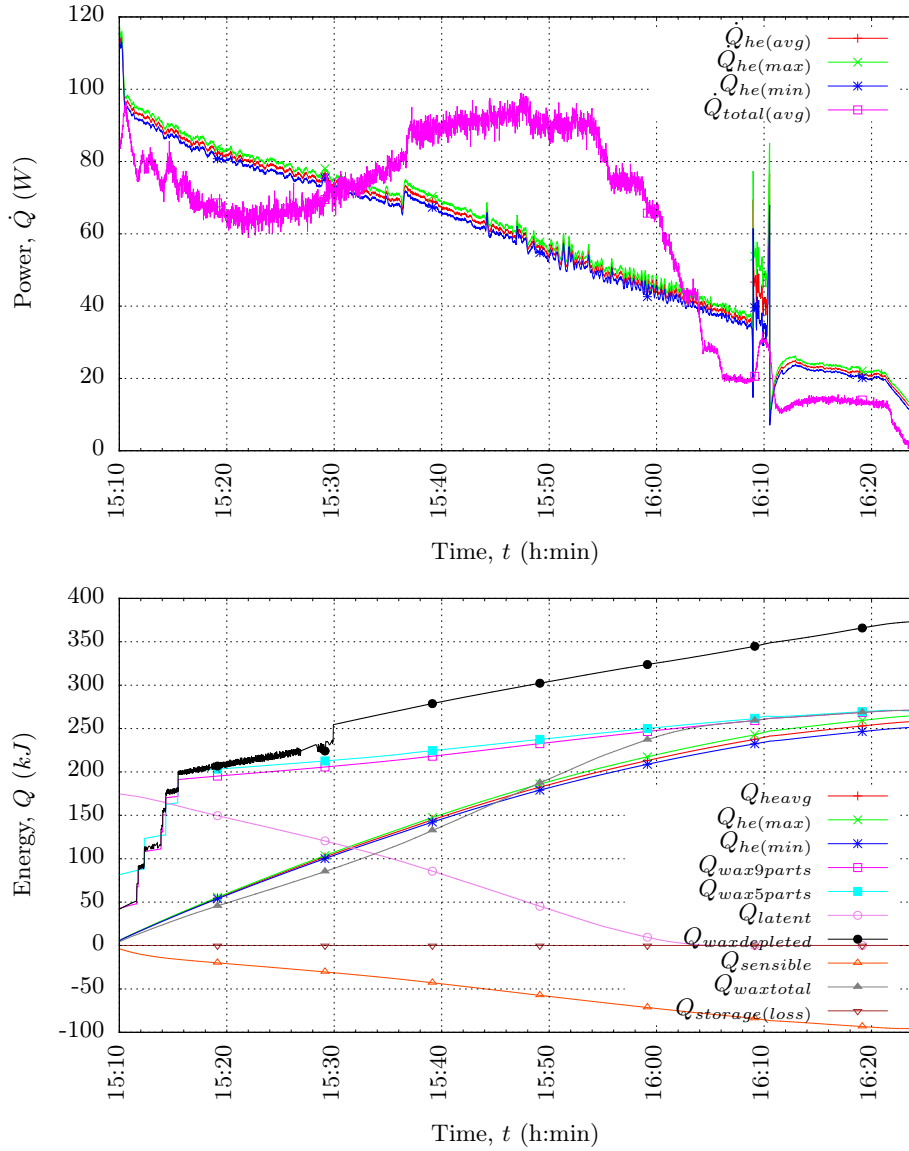


Figure B.13. The power transferred into the water of the heat exchanger from the heat removal HP2 and the total energy absorbed in the water and removed from the PCS module.

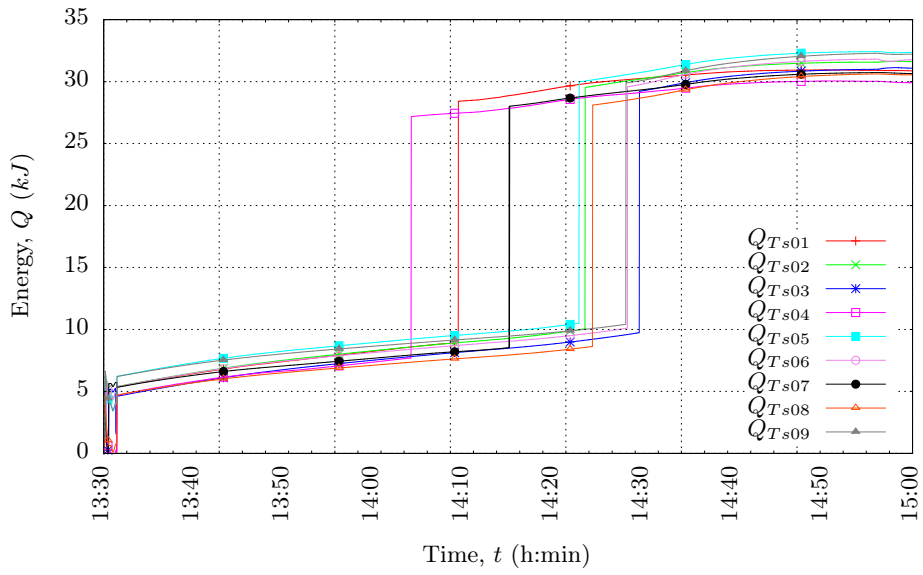


Figure B.14. The total energy in each segment of wax during heat up indicating instantaneous melting in the measuring point

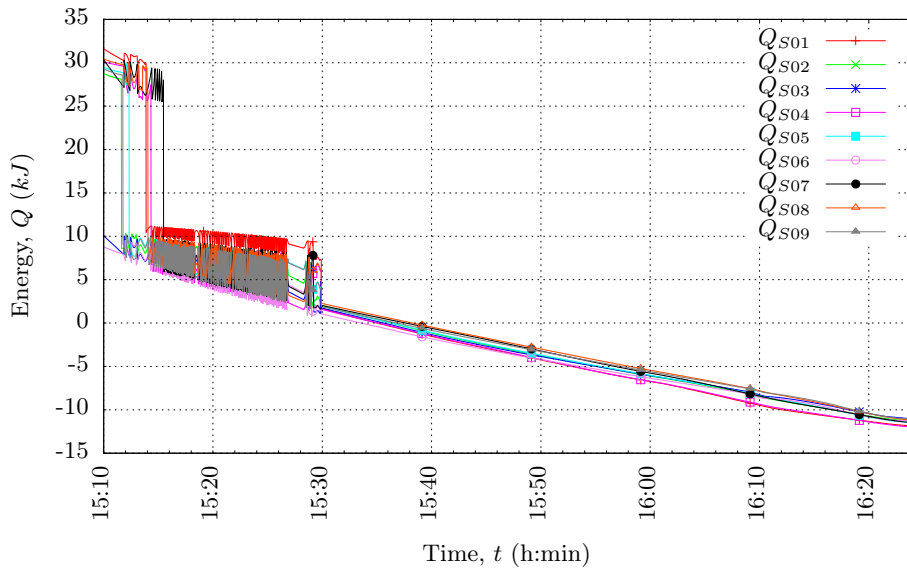


Figure B.15. The total energy in each segment of wax during cool down indicating instantaneous solidification in the measuring point

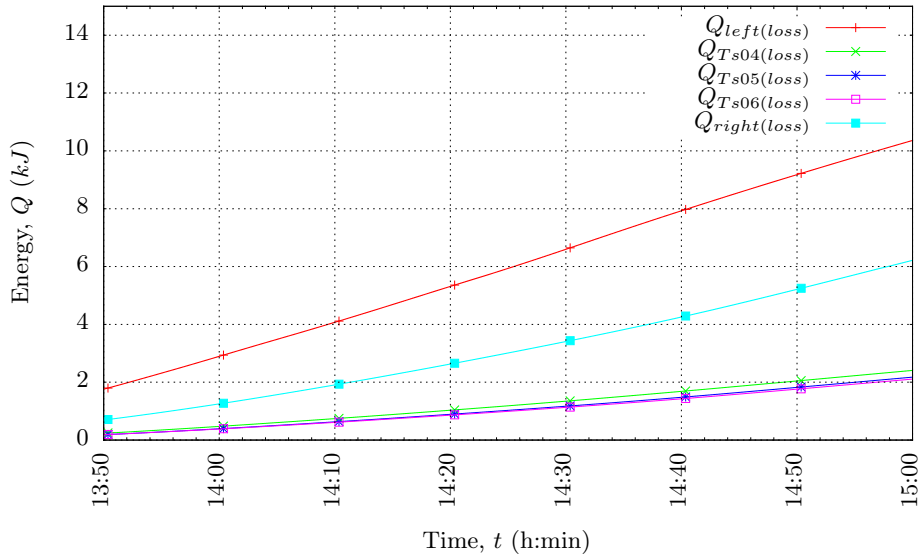


Figure B.16. The total energy loss to the environment calculated from the energy PCS system sides

gradually to about $\Delta T = 0.005^\circ\text{C}/\text{s}$ when it reaches a minimum at 55°C . It then gradually increases until it reaches a peak of $\Delta T = 0.013^\circ\text{C}/\text{s}$ at about 61°C . Finally it gradually decreases until thermal equilibrium is reached. From the graph it can be noted that in spite of high heatup temperatures the thermal inertia of the wax during melting is high. In other words the wax takes a long time to heat up from 40°C to 59°C . This is because the wax starts to melt between 40°C and 59°C and it only heats up to 65°C when all the wax in the control volume has melted. The melting range of the control volume is the relatively flat heating up part when it measures between 45°C and 59°C . The peak is then an indication of the time at which all the material in the control volume has completely melted.

In Figure B.18 on page 119 four horizontal points are indicated. Again the scale of the change in temperature is used to indicate the times at which only small temperature gains are achieved, which gives an indication when melting is initiated and when it is completed. A quick increase in temperature even though a more or less constant heating up condition exists, indicates that melting is completed in this section. Figure B.18 depicts the change in temperature of four thermocouples during a constant temperature heating experiment, it can be seen that the leftmost control volume melts first, because it heats up more quickly after 35 min of the test, then the central and finally the rightmost control volume completes its melting phase and all the wax is now completely melted. The same criteria is used on Figure B.18 where the three peaks indicate the time at which the leftmost, the central and finally the rightmost control volumes complete the melting phase.

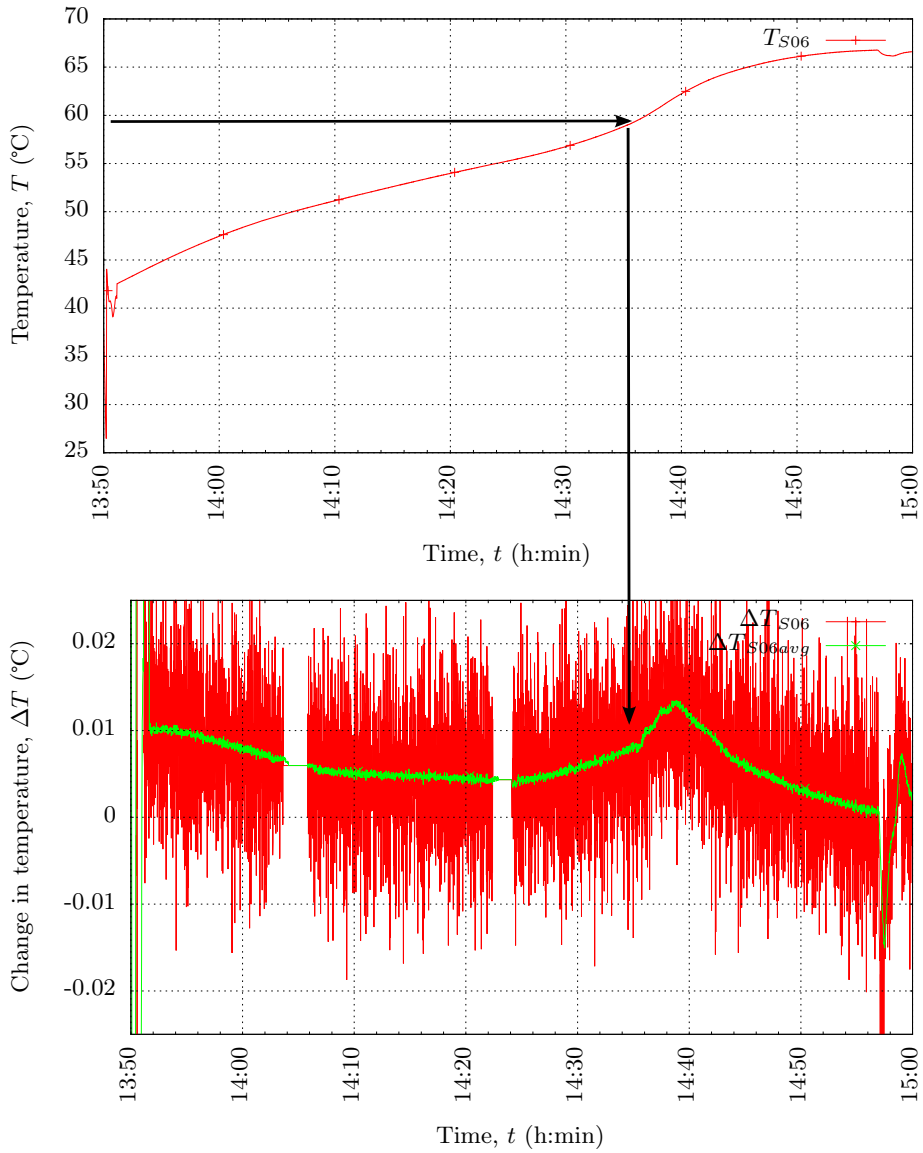


Figure B.17. The temperature of the wax during a heat up test and the instantaneous rate of temperature change as well as the average rate during the test.

As can be seen in Figure B.19 on page 120, the power variations in each wax control volume during heat up starts at a high rate of about 12 W according to . The heat absorption rate then drops down gradually until it reaches a minimum value of about 4 W before it gradually increases again until it finally drops off to zero. The final quick increase in heat absorption rate may be because of the melting that is initiated in the PCS control volumes which increases the rate of heat absorption of the wax.

During the solidification of the wax control volumes the heat transfer rate starts off at a high rate of heat removal that is absorbed by the cooling water. This is because of the high temperature difference between the hot melted wax and the cold cooling water passing through the heat exchanger. The rate of heat removal then drops off to 10 W and stays at this rate of heat removal until all the wax is solidified. Then the rate of heat removal drops off to zero. At this point all the wax control volumes are completely solidified and at a low temperature. In other words the PCS module is now completely cooled.

The heat transfer coefficients resulting from the heat pipe experimental analysis were found to be quite high at about 3000 W/m K in the evaporator and condenser of the heat removal HP2 for example. This enabled high heat transfer rates that was uniformly transferred to and from the PCS system.

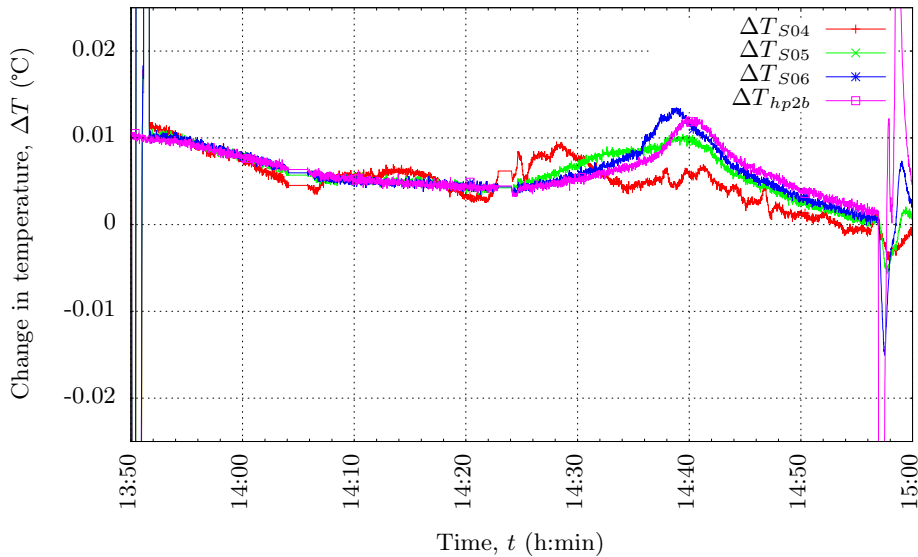


Figure B.18. The averaged rates of temperature change for the middle horizontal level of thermocouples during heat absorption mode.

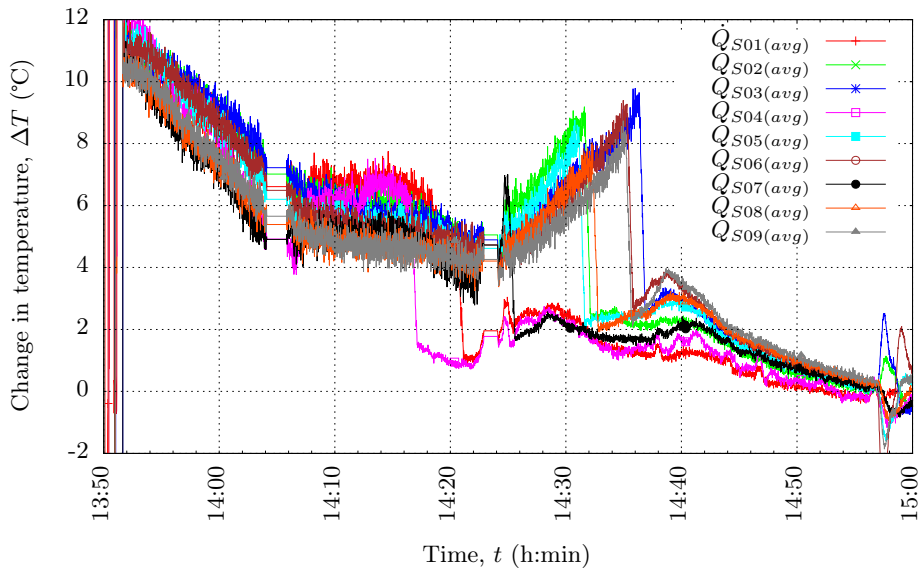


Figure B.19. The averaged rates of temperature change for the 9 sections during heat absorption mode.

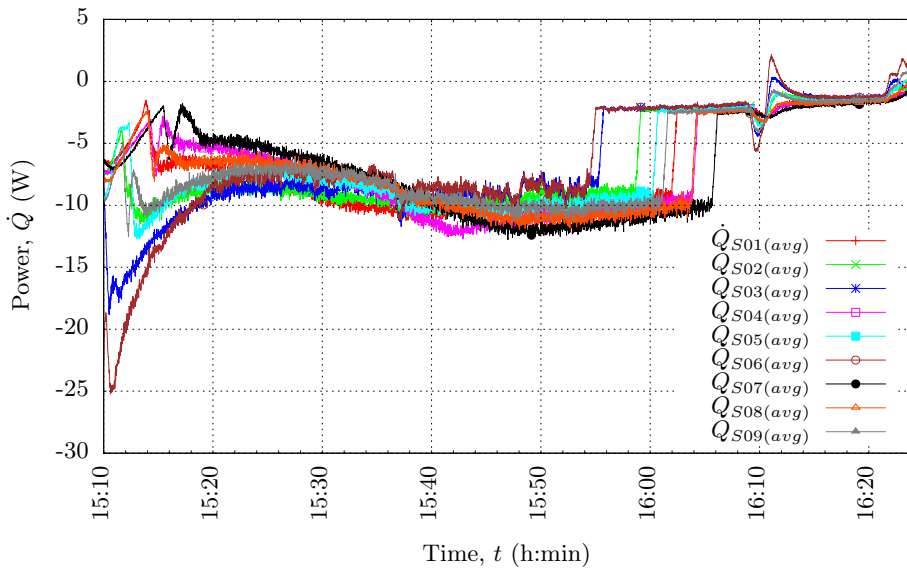


Figure B.20. The averaged rates of temperature change for the middle horizontal level of thermocouples during heat removal mode.

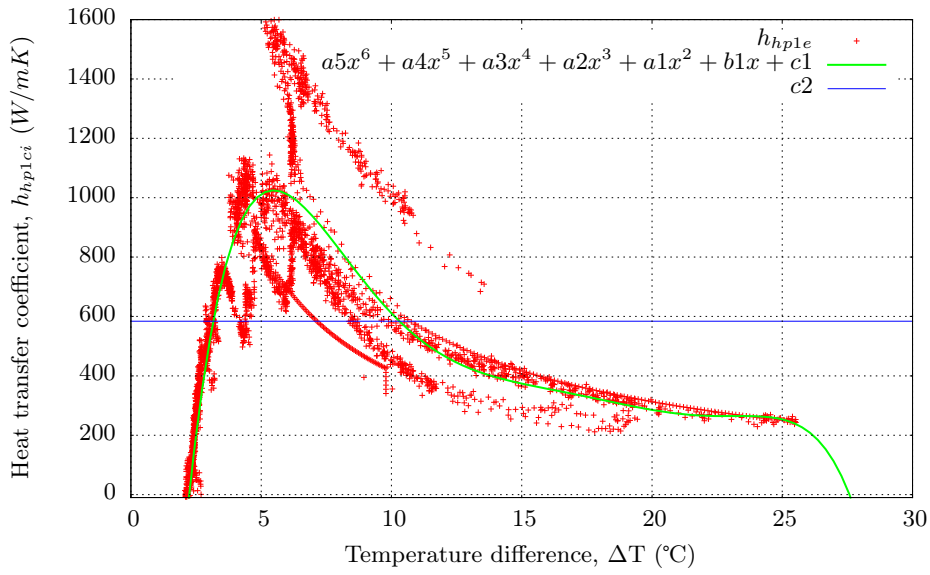


Figure B.21. The heat transfer coefficient of the heat absorption HP1 evaporator section.

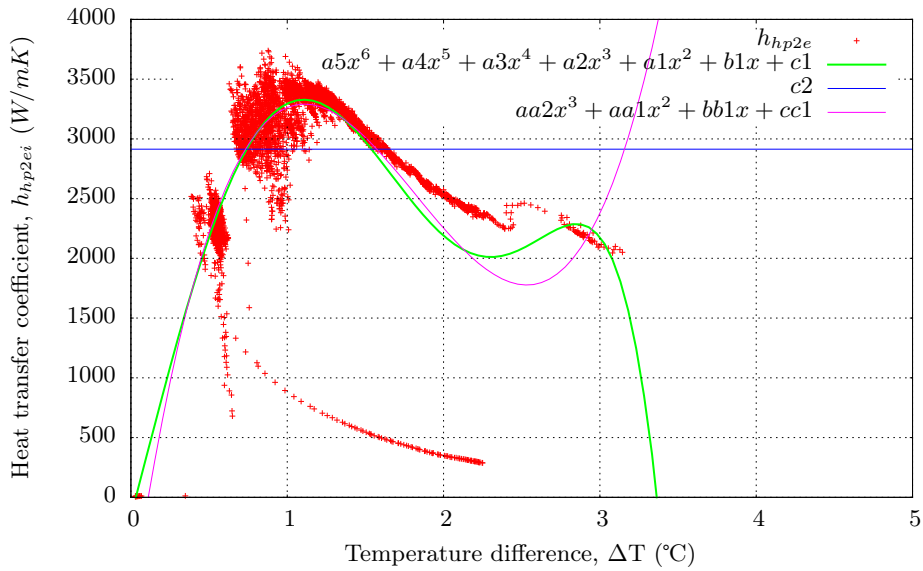


Figure B.22. The heat transfer coefficient of the heat removal HP2 evaporator section.

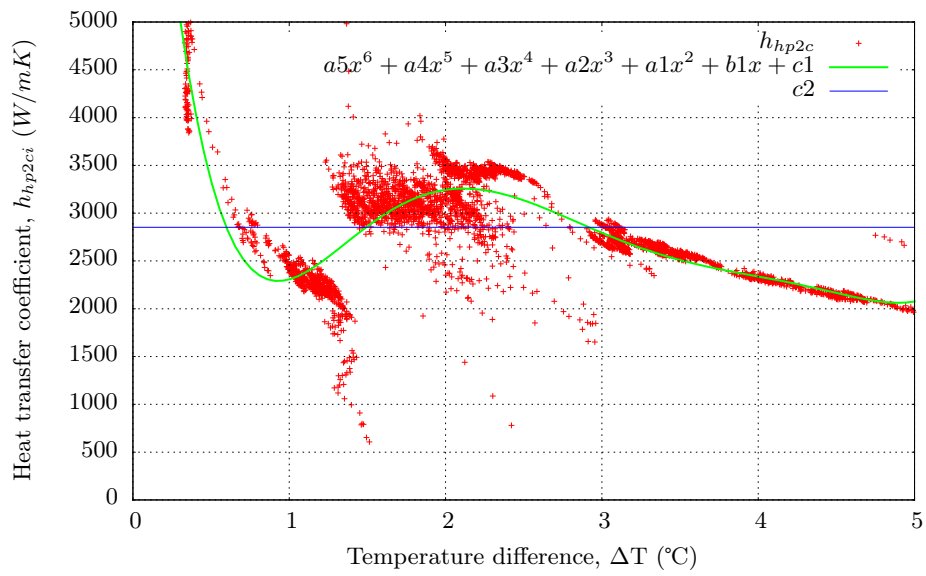


Figure B.23. The heat transfer coefficient of the heat removal HP2 condenser section.

Appendix C

Solar angle calculation and heat transfer coefficients determination for the SWH system.

The angle of the sun's rays in respect to a solar collector determines the intensity of the incident rays on the solar collector. This angle depends on the geographic position (longitude λ , latitude σ and orientation γ_{sc}) and tilt angle β_{sc} of the solar collector, the time of day, and the day of the year.

The heat transfer coefficients are dependent on the wind speed V_w , the temperature difference between the glazing T_g and the ambient temperature T_{amb} as well as the temperature difference between the glazing and the sky temperature.

C.1 Calculation of the solar angles.

The input variables need to be initialised to set up the particular system simulation. This includes the geometry of the system and its position and orientation, as well as the time at which simulation starts taking place. As the time of simulation increases with each time step, so the variables that are dependent on time, such as the solar angle and solar irradiance intensity change. The temperatures of the system change during operation, so also do the heat transfer rates from the system to the surroundings.

Calculate for each time step the solar angles and solar irradiance. Also calculate the number of seconds that the simulation has been conducted: $seconds = f(seconds_i, \Delta t)$ The day of the year that the simulation takes place is taken into consideration in the calculation of B . Adapt the local time to solar time the day of the year is used to calculate the value of B :

$$B = \frac{360}{365.242}(yearday - 1) \quad (C.1)$$

The equation of time is calculated according to the day of the year.

Table C.1. The input conditions for the PCS SWH system analysis.

Date and time Input:
Day of the year: $yearday_i$
Start hour: $hour_i$
Start minute: $minute_i$
Start second: $second_i$
Geographic location input of Stellenbosch:
Latitude angle
$\sigma = -33.9301^\circ$
Longitude angle
$\lambda = 18.8647^\circ$
Height above sea level
$h_{sea} = 136$ m
Atmospheric pressure
$P_{atm} = 98$ kPa,
GMT=2.0 (South Africa is in the second meridian)
Position of the solar collector
$\beta_{sc} = 45^\circ$,
$\gamma_{sc} = 0^\circ$.

$$EoT = 0.258\cos(B) - 7.416\sin(B) - 3.648\cos(2B) - 9.228\sin(2B) \quad (C.2)$$

The local solar time median is calculated from the GMT value:

$$LSTM = 15^\circ GMT \quad (C.3)$$

The time correction in minutes is determined from the longitude, the local solar time median and the equation of time:

$$TC = 4(\lambda - LSTM) + EoT \quad (C.4)$$

The local solar time in hours is calculated from the local time and the time correction value. If the value is smaller than zero then 24 hours is added to the LST value.

$$LST = hour + \frac{minute}{60} + \frac{second}{3600} + \frac{TC}{60} \quad (C.5)$$

The hour angle in degrees is then calculated from the local solar time.

$$\omega = 15(LST - 12) \quad (C.6)$$

The declination angle at which the earth is tilted is calculated with B which is dependent on the day of the year

$$\delta = asin(sin(23.45)sin(B)) \quad (C.7)$$

The altitude angle at which the sun is relative to the horizon of the earth is calculated with the different solar angles

$$\alpha = asin\left(sin(\delta)sin(\sigma) + cos(\delta)cos(\sigma)cos(\omega)\right) \quad (C.8)$$

The zenith angle θ_z can now be calculated as the angle that the sun is relative to the vertical.

$$\theta_z = 90 - \alpha \quad (C.9)$$

The azimuth angle γ is the angle of the sun's position relative to North = 0° .

$$\gamma = acos\left(\frac{sin(\delta)cos(\sigma) - cos(\delta)sin(\sigma)cos(\omega)}{cos(\alpha)}\right) \quad (C.10)$$

At solar noon the local solar time $LST = 12$. At this time the sun is north of the object and the azimuth angle γ must be corrected to be west facing by using the following relation.

$$\gamma_c = 2\pi - \gamma \quad (C.11)$$

These are all the important solar angles that characterises where the sun will be at any time of the year relative to the solar collector position, except the incident angle that the solar collector makes with the sun which is calculated in Equation C.18. The intensity of the solar irradiance is also an important parameter and is determined with the following relation:

$$I_a = 1367 \left(1 + 0.034 \cos\left(\frac{360 \text{ year day}}{365.25}\right) \right) \quad (\text{C.12})$$

The coefficients that are used for clear sky analysis are the following:

$$a_0 = 0.4237 - 0.00821 \left(6 - \frac{h_{sea}}{1000} \right)^2 \quad (\text{C.13})$$

$$a_1 = 0.5055 + 0.00595 \left(6.5 - \frac{h_{sea}}{1000} \right)^2 \quad (\text{C.14})$$

$$a_2 = 0.2711 + 0.01858 \left(2.5 - \frac{h_{sea}}{1000} \right)^2 \quad (\text{C.15})$$

The direct normal irradiation is calculated from these coefficients

$$I_n = I_a \left(a_0 + a_1 e^{\frac{-a_2}{\cos(\theta_z)}} \right) \quad (\text{C.16})$$

The diffuse solar irradiation can also be calculated from these coefficients and the total solar irradiation.

$$I_d = I_a \cos(\theta_z) \left(0.271 - 0.2939(a_0 + a_1 e^{-a_2 \cos(\theta_z)}) \right) \quad (\text{C.17})$$

The angle at which the solar radiation acts on the solar collector is described by the incident angle ι .

$$\iota = a \cos \left(\sin(\alpha) \cos(\beta_{sc}) + \cos(\alpha) \sin(\beta_{sc}) \cos(\gamma_{sc} - \gamma_c) \right) \quad (\text{C.18})$$

The solar angles are plotted in Figure C.1. The hour angle ω which varies from -180° at the start of the solar day to 180° at the end of the solar day. The altitude angle α which crosses the horizon or 0° line during sunrise and sunset is also shown. The zenith angle θ_{sc} is the angle that the sun makes with the vertical and it crosses the 90° line during sunset and sunrise. The corrected azimuth angle γ_c is the angle of the sun relative to true North. The angle is 0° just before solar noon and 360° just after solar noon. The incident angle indicates whether sunlight is incident on the tilted solar collector, when the angle is smaller than 90° , then solar irradiance is incident upon the solar collector.

$$I_t = I_n \sin(\alpha) + I_d \quad (\text{C.19})$$

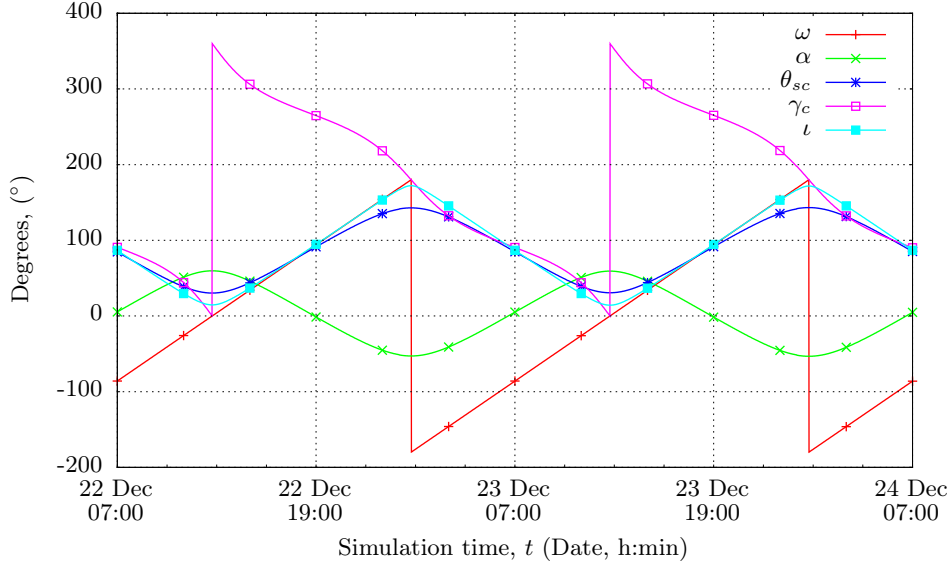


Figure C.1. The solar angles for two consecutive days that relates to the solar irradiance intensity determination.

The total incident solar irradiation upon the solar collector is described by the following relation:

$$\dot{G}_{sc} = I_n \cos(\iota) + I_d \left(1 + \frac{\cos(\beta_{sc})}{2}\right) + \rho_{surr} I_t \left(1 - \frac{\cos(\beta_{sc})}{2}\right) \quad (C.20)$$

The components of the solar radiation incident on the solar collector is plotted in Figure C.2. The total normal irradiation on a horizontal surface I_n , as well as the diffuse component on a clear day I_d is plotted, along with the total direct and diffuse solar irradiation on a horizontal surface and finally the total incident solar irradiation that includes the reflection from the surroundings \dot{G}_{sc} that is used as input condition to the solar collector.

C.2 Calculation of the ambient air and the sky temperature.

The temperature of the ambient air in degrees Celsius is derived from solar data during summer.

$$T_{amb} = 22.5 + 7.5 \left(-\cos\left(\frac{\pi}{12}(hour_i + seconds/3600)\right) \right) \quad (C.21)$$

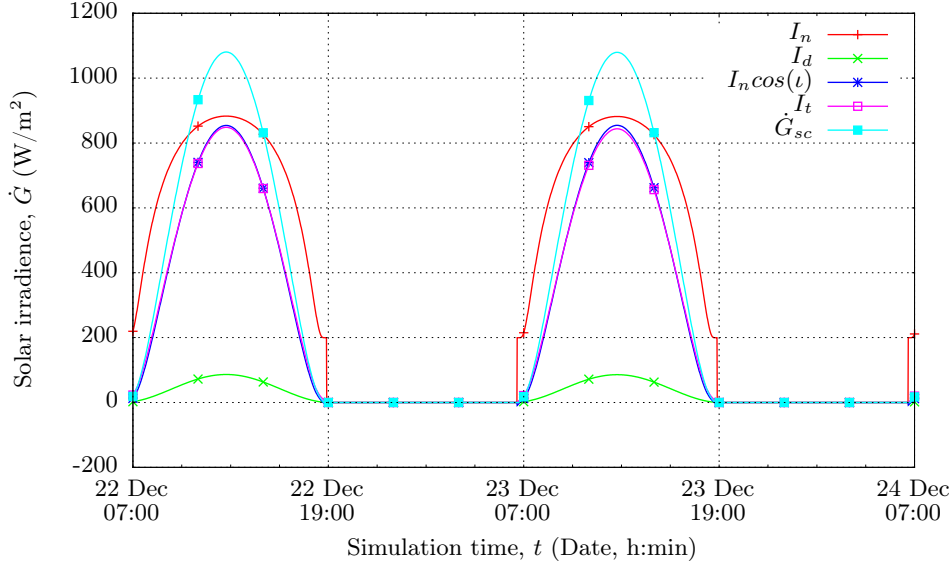


Figure C.2. The solar irradiance components for two consecutive days.

In a similar fashion the relative humidity is determined by fitting a simple sine curve through 5 summer days in Stellenbosch.

$$\omega_{rel} = 0.6 - 0.2 \left(- \cos \left(\frac{\pi}{12} \left(hour_i + \frac{seconds}{3600} \right) \right) \right) \quad (C.22)$$

The vapour pressure is a function of the relative humidity and the tabulated ambient temperatures. An exponential curve is fitted through the data.

$$P_v = \omega_{rel} 647.4073345572 e^{0.0622124839 T_{amb}} \quad (C.23)$$

From this vapour pressure the dew point temperature may be determined:

$$T_{dp} = \frac{\log \left(\frac{P_v}{647.4073345572} \right)}{0.0622124839} \quad (C.24)$$

In the case where $\theta_z < 90^\circ$ the sun is above the horizon relative to the solar collector and, the daytime sky temperatures are calculated according to the following relation:

$$\epsilon_{sky} = 0.727 + 0.006 T_{dp} \quad (C.25)$$

But in the case where $\theta_z \geq 90^\circ$ the nighttime radiation correlations are used.

$$\epsilon_{sky} = 0.741 + 0.0062T_{dp} \quad (C.26)$$

Now the sky temperature may be determined with the aid of the coefficient ϵ_{sky} calculated above.

$$T_{sky} = (\epsilon_{sky}(T_{amb} + 273.15)^4)^{0.25} - 273.15 \quad (C.27)$$

The surrounding ambient and sky temperatures are calculated and it is used to determine the heat losses to the environment. The heat transfer coefficients need to be determined for each time step to fully quantify both the convective and radiation losses of each component of the PCS SWH. For both these losses the surface temperature needs to be determined and in the case of the convective losses the film temperature needs to be determined to determine the fluid properties at these temperatures. The heat transfer coefficients form part of the resistances that are used to set up the thermal resistance network. With this network in place the heat transfer rates are determined and finally the new temperatures for the new time step are determined for the numerical thermal resistance model. The solar radiation input heats up the collector, the PCS and the geyser, and as it is heated up the losses to the environment increase. The heat loss correlations are incorporated into the SWH model that incorporates an additional PCS system.

References

- Bejan, A. (2004). *Convection Heat Transfer, 3rd ed.* John Wiley & Sons, New York.
- Cabeza, L.F., Iba, M. and Sole, C. (2006). Experimentation with a water tank including a PCM module. *Solar Energy Materials and Solar Cells*, vol. 90, pp. 1273–1282.
- Canbazoglu, S., Sahinaslan, A., Ekmekyapar, A., Aksoy, Y.G. and Akarsu, F. (2005). Enhancement of solar thermal energy storage performance using sodium thiosulfate pentahydrate of a conventional solar water-heating system. *Energy and Buildings*, vol. 37, no. 3, pp. 235 – 242. ISSN 0378-7788. Available at: <http://www.sciencedirect.com/science/article/pii/S0378778804001975>
- Çengel, Y.A. and Ghajar, A.J. (2011). *Heat and mass transfer: fundamentals & applications.* New York : McGraw-Hill, New York.
- Cheng, P. and Wu, H.Y. (2006). Mesoscale and Microscale Phase-Change Heat Transfer. *Advances in heat transfer*, vol. 39, no. 06, pp. 461–563.
- Delgado, M., Lá zaro, A., Peñ alosa, C., Mazo, J. and Zalba, B. (2013). Analysis of the physical stability of pcm slurries. *International Journal of Refrigeration*, vol. 36, no. 6, pp. 1648 – 1656. ISSN 0140-7007. Available at: <http://www.sciencedirect.com/science/article/pii/S0140700713001096>
- Eskom (sa). Available at: url = http://www.eskom.co.za/AboutElectricity/FactsFigures/Documents/The_Solar_Water_Heating_SWH_Programme.pdf, urldate = [8 September 2014].
- Hasnain, S. (1998). Review on sustainable thermal energy storage technologies, part i: heat storage materials and techniques. *Energy Conversion and Management*, vol. 39, no. 11, pp. 1127 – 1138. ISSN 0196-8904. Available at: <http://www.sciencedirect.com/science/article/pii/S0196890498000259>
- Krupa, I., Miková, G. and Luyt, A. (2007). Phase change materials based on low-density polyethylene/paraffin wax blends. *European Polymer Journal*,

vol. 43, no. 11, pp. 4695 – 4705. ISSN 0014-3057.

Available at: <http://www.sciencedirect.com/science/article/pii/S0014305707004909>

Laing, D., Bauer, T., Breidenbach, N., Hachmann, B. and Johnson, M. (2013). Development of high temperature phase-change-material storages. *Applied Energy*, vol. 109, no. 0, pp. 497 – 504. ISSN 0306-2619.
Available at: <http://www.sciencedirect.com/science/article/pii/S0306261912008689>

Laing, D., Bauer, T., Steinmann, W. and Lehmann, D. (2009). Advanced high temperature latent heat storage system - design and test results. In: *The 11th International Conference on Thermal Energy Storage*.

Li, P., Lew, J.V., Chan, C., Karaki, W., Stephens, J. and Brien, J.E.O. (2012). Similarity and generalized analysis of efficiencies of thermal energy storage systems. *Renewable Energy*, vol. 39, no. 1, pp. 388–402. ISSN 0960-1481.
Available at: <http://dx.doi.org/10.1016/j.renene.2011.08.032>

Liu, Z., Wang, Z. and Ma, C. (2006a). An experimental study on heat transfer characteristics of heat pipe heat exchanger with latent heat storage . Part I : Charging only and discharging only modes. *Energy Conversion and Management*, vol. 47, pp. 944–966.

Liu, Z., Wang, Z. and Ma, C. (2006b). An experimental study on the heat transfer characteristics of a heat pipe heat exchanger with latent heat storage . Part II : Simultaneous charging / discharging modes. *Energy Conversion and Management*, vol. 47, pp. 967–991.

Mettawee, E.-b.S. and Assassa, G.M.R. (2006). Experimental study of a compact PCM solar collector. *Energy*, vol. 31, pp. 2958–2968.

Mhike, W., Focke, W.W., Mofokeng, J.P. and Luyt, a.S. (2012). Thermally conductive phase-change materials for energy storage based on low-density polyethylene, soft Fischer-Tropsch wax and graphite. *Thermochimica Acta*, vol. 527, pp. 75–82.
Available at: <http://dx.doi.org/10.1016/j.tca.2011.10.008>

Rausch, A., Andresen, L., Crow, A. and Saloner, D. (2011). Stored Energy Solar Cookstove for Rajasthan India. Tech. Rep..

Riffat, S.B. and Zhao, X. (2004). A novel hybrid heat pipe solar collector / CHP system - Part 1 : System design and construction. *Renewable energy*, vol. 29, pp. 2217–2233.

Robak, C.W., Bergman, T.L. and Faghri, A. (2011a). Economic evaluation of latent heat thermal energy storage using embedded thermosyphons for concentrating solar power applications. *Solar Energy*, vol. 85, no. 10, pp.

2461–2473. ISSN 0038-092X.

Available at: <http://dx.doi.org/10.1016/j.solener.2011.07.006>

Robak, C.W., Bergman, T.L. and Faghri, A. (2011*b*). Enhancement of latent heat energy storage using embedded heat pipes. *International Journal of Heat and Mass Transfer*, vol. 54, no. 15-16, pp. 3476–3484. ISSN 0017-9310. Available at: <http://dx.doi.org/10.1016/j.ijheatmasstransfer.2011.03.038>

Sari, A. and Karaipekli, A. (2007). Thermal conductivity and latent heat thermal energy storage characteristics of paraffin / expanded graphite composite as phase change material. *Applied Thermal Engineering*, vol. 27, pp. 1271–1277.

Saving Energy (sa). Available at: url = <http://savingenergy.co.za/energy-saving-shower-heads>, urldate = [3 November 2014].

Shabgard, H., Bergman, T.L., Sharifi, N. and Faghri, A. (2010). High temperature latent heat thermal energy storage using heat pipes. *International Journal of Heat and Mass Transfer*, vol. 53, no. 15-16, pp. 2979–2988. ISSN 0017-9310. Available at: <http://dx.doi.org/10.1016/j.ijheatmasstransfer.2010.03.035>

Shabgard, H., Robak, C.W., Bergman, T.L. and Faghri, A. (2012 March). Heat transfer and exergy analysis of cascaded latent heat storage with gravity-assisted heat pipes for concentrating solar power applications. *Solar Energy*, vol. 86, no. 3, pp. 816–830. ISSN 0038092X. Available at: <http://linkinghub.elsevier.com/retrieve/pii/S0038092X11004385>

Sharifi, N., Bergman, T.L. and Faghri, A. (2011). Enhancement of PCM melting in enclosures with horizontally-finned internal surfaces. *International Journal of Heat and Mass Transfer*, vol. 54, no. 19-20, pp. 4182–4192. ISSN 0017-9310. Available at: <http://dx.doi.org/10.1016/j.ijheatmasstransfer.2011.05.027>

Sharifi, N., Wang, S., Bergman, T.L. and Faghri, A. (2012). Heat pipe-assisted melting of a phase change material. *International Journal of Heat and Mass Transfer*, vol. 55, no. 13-14, pp. 3458–3469. ISSN 0017-9310. Available at: <http://dx.doi.org/10.1016/j.ijheatmasstransfer.2012.03.023>

Sharma, A., Tyagi, V.V., Chen, C.R. and Buddhi, D. (2009). Review on thermal energy storage with phase change materials and applications. *Renewable and Sustainable Energy Reviews*, vol. 13, pp. 318–345.

- Sharma, S.D. (2005). Thermal performance of a solar cooker based on an evacuated tube solar collector with a PCM storage unit. *Solar Energy*, vol. 78, pp. 416–426.
- Shatikian, V., Ziskind, G. and Letan, R. (2005 August). Numerical investigation of a PCM-based heat sink with internal fins. *International Journal of Heat and Mass Transfer*, vol. 48, no. 17, pp. 3689–3706. ISSN 00179310.
Available at: <http://linkinghub.elsevier.com/retrieve/pii/S0017931005002115>
- Shatikian, V., Ziskind, G. and Letan, R. (2008 March). Numerical investigation of a PCM-based heat sink with internal fins: Constant heat flux. *International Journal of Heat and Mass Transfer*, vol. 51, no. 5-6, pp. 1488–1493. ISSN 00179310.
Available at: <http://linkinghub.elsevier.com/retrieve/pii/S001793100700717X>
- Shukla, A., Buddhi, D. and Sawhney, R.L. (2009). Solar water heaters with phase change material thermal energy storage medium : A review. *Renewable and Sustainable Energy Reviews*, vol. 13, pp. 2119–2125.
- Stumpf, P., Balzar, A., Eisenmann, W., Wendt, S., Ackermann, H. and Vajen, K. (2001). Comparative measurements and theoretical modelling of single- and double-stage heat pipe coupled solar cooking systems for high temperatures. *Solar Energy*, vol. 71, no. 1, pp. 1 – 10. ISSN 0038-092X.
Available at: <http://www.sciencedirect.com/science/article/pii/S0038092X01000263>
- Tay, N., Bruno, F. and Belusko, M. (2013). Experimental investigation of dynamic melting in a tube-in-tank {PCM} system. *Applied Energy*, vol. 104, no. 0, pp. 137 – 148. ISSN 0306-2619.
Available at: <http://www.sciencedirect.com/science/article/pii/S0306261912008288>
- Trp, A. (2005 December). An experimental and numerical investigation of heat transfer during technical grade paraffin melting and solidification in a shell-and-tube latent thermal energy storage unit. *Solar Energy*, vol. 79, no. 6, pp. 648–660. ISSN 0038092X.
Available at: <http://linkinghub.elsevier.com/retrieve/pii/S0038092X05001337>
- Vadwala, P.H. (2011). *Thermal Energy Storage in Copper Foams filled with Paraffin Wax*. Ph.D. thesis, University of Toronto.
- van Dorp, J., Schmitz, A. and van Paassen, A. (2004). PCM thermal properties in one-dimensional heat transfer experiment. Tech. Rep..

- Velraj, R., Seeniraj, R.V., Hafner, B., Faber, C. and Schwarzer, K. (1999). Heat transfer enhancement in a latent heat storage system. *Solar Energy*, vol. 65, no. 3, pp. 171–180.
- Verma, P. and Singal, S. (2008 May). Review of mathematical modeling on latent heat thermal energy storage systems using phase-change material. *Renewable and Sustainable Energy Reviews*, vol. 12, no. 4, pp. 999–1031. ISSN 13640321.
Available at: <http://linkinghub.elsevier.com/retrieve/pii/S1364032106001651>
- Wang, S., Faghri, A. and Bergman, T.L. (2010). A comprehensive numerical model for melting with natural convection. *International Journal of Heat and Mass Transfer*, vol. 53, no. 9-10, pp. 1986–2000. ISSN 0017-9310.
Available at: <http://dx.doi.org/10.1016/j.ijheatmasstransfer.2009.12.057>
- Zhang, J., Zhang, X., Wan, Y., Mei, D. and Zhang, B. (2012 May). Preparation and thermal energy properties of paraffin/halloysite nanotube composite as form-stable phase change material. *Solar Energy*, vol. 86, no. 5, pp. 1142–1148. ISSN 0038092X.
Available at: <http://linkinghub.elsevier.com/retrieve/pii/S0038092X12000187>
- Zhao, C.Y. and Wu, Z.G. (2011). Solar Energy Materials & Solar Cells Heat transfer enhancement of high temperature thermal energy storage using metal foams and expanded graphite. *Solar Energy Materials and Solar Cells*, vol. 95, pp. 636–643.
- Zipf, V., Neuhäuser, A., Willert, D., Nitz, P., Gschwander, S. and Platzler, W. (2013). High temperature latent heat storage with a screw heat exchanger: Design of prototype. *Applied Energy*, vol. 109, no. 0, pp. 462 – 469. ISSN 0306-2619.
Available at: <http://www.sciencedirect.com/science/article/pii/S0306261912008471>